A TRANSESOPHAGEAL PHASED ARRAY TRANSDUCER FOR ULTRASONIC IMAGING OF THE HEART

A TRANSESOPHAGEAL PHASED ARRAY TRANSDUCER FOR ULTRASONIC IMAGING OF THE HEART

Een phased array slokdarm scanner voor echografie van het hart

PROEFSCHRIFT

TER VERKRIJGING VAN DE GRAAD VAN DOCTOR

AAN DE ERASMUS UNIVERSITEIT ROTTERDAM

OP GEZAG VAN DE RECTOR MAGNIFICUS
PROF. DR A.H.G. RINNOOY KAN

EN VOLGENS BESLUIT VAN HET COLLEGE VAN DEKANEN.

DE OPENBARE VERDEDIGING ZAL PLAATSVINDEN
OP DONDERDAG 25 JUNI 1987 om 15.00 UUR

DOOR

CHARLES THEODOOR LANCEE

GEBOREN TE HAARLEM

PROMOTIECOMMISSIE

PROMOTOR: PROF. DR IR N. BOM
PROMOTOR: PROF. DR J.R.T.C. ROELANDT

OVERIGE LEDEN:

PROF. DR IR A.J. BERKHOUT
PROF. DRS J. STEKETEE

The clinical data have been obtained in the Thoraxcenter within the framework of Project 8 of the Interuniversity Cardiology Institute of the Netherlands.

Financial support by the Netherlands Heart Foundation for the publication of this thesis is gratefully acknowledged.

Printing of this book has been sponsored by the Oldelft Company of Delft, the Netherlands.

Typesetting by Hoi Studio Rotterdam, the Netherlands.

Printing by 2L Produkties Rotterdam, the Netherlands.

'Progress depends on accurate extrapolation from known phenomena. In order to extrapolate from past data, a mathematical formulation or 'mathematical model' must be built, founded upon basic physical laws and past data.

It can be misleading to formulate a model upon past data alone. This is the method of 'curve fitting', for finding a mathematical expression which generates a curve that matches experimental data to an acceptable degree of accuracy. Such a model is satisfactory for interpolation, but not for extrapolation.

The more difficult, but more satisfying approach is to build the mathematical model from the basic physical laws which govern the phenomenon, including minute effects. Experimentation is then to be directed toward finding the numerical values of the coefficients of the mathematical model. Failure of experimental data to satisfy the model (or vice versa) indicates that the model is incomplete and that intense cerebration is needed to identify the physical effect which was omitted from the model. The model must then be corrected. Mathematical models of this sort tend to be more complex, but they are more accurate in describing the situation which exists, and they permit reliable mathematical investigation of the effects of changes of parameters (extrapolation) without tedious and expensive experimentation.

It seems to me that if more applied mathematicians were to become interested in the medical field, particularly to the field of blood flow dynamics, considerable progress could be made in the understanding of the phenomena observed.'

(Paul Senstad in IRE Trans Med Electr ME-6: 203, 1959).

TABLE OF CONTENTS

PREFACE / ACKNOWLEDGEMENTS

The development of a novel type of transducer together with its clinical evaluation as described in this thesis could only have been realized in a multidisciplinary center. Right from the start of the Thoraxcenter in 1968 its policy has always been to combine a great many of disciplines, thank to the foresight of its founders, Paul Hugenholtz and Jan Nauta.

The department of experimental echocardiography was founded by Klaas Bom in those early days. Under his stimulating guidance we started our research towards real-time cardiac imaging. When the first real-time linear array prototype was launched (and patented) a period of industrial sponsoring of the department was started, the first sponsor being Organon Teknika. Shortly thereafter the Interuniversity Cardiology Institute (ICI) decided to support our work.

In the meantime the clinical introduction of echocardiology was realized by Jos Roelandt and the department of clinical echocardiology was established. Thank to his eagerness for technological innovations, the continuous interaction between the two departments resulted in a series or projects, the development of the transesophageal phased array being just one of these. In 1982 Pie Medical and Oldelft became our industrial partners, Pie Medical sponsoring our instrumentation efforts, while Oldelft participated in our ongoing research in transducer technology. The transesophageal phased array transducer in particular has been sponsored to a large extent by Oldelft, and subsequently introduced by them as a commercial product.

All along this period of time we have been assisted by the Delft University of Technology department of Acoustics of Guus Berkhout. Within the scope of this collaboration graduating students were enabled to work at our laboratory. It is next to impossible to completely acknowledge the contributions of all individual students to the realization of the subjects dealt with in this thesis. However, remaining grateful for the work of all those unmentioned, I like to express my special gratitude to a few colleagues in particular.

- Klaas Bom, who never failed to stimulate my work, including this thesis. I am proud of the fact that he is now acting as my promotor.

- The members of the original team: Jan Honkoop, Frans van Egmond and Gerard van Zwieten, who succeeded in solving an enormous amount of technological problems.

- Jan Vogel and Nico de Jong, for their innovative contributions in the field of transducer technology.

- Cees Ligtvoet, later on assisted by Stef Mientki, who accomplished the development of a variety of instruments and their adaptation to the clincical needs.

- Hans Rijsterborgh and Elma Gussenhoven, both from the ICI. Hans for his healthy criticism and Elma for her enthousiasm to incorporate new developments into clinical use at the earliest possible time.

- Jos Roelandt for acting as co-promotor, but not in the least for creating, with an open mind for research activities, a clinical department of echocardiology.

- Wim Vletter and Jacky McGhie for their continuous co-operation in the evaluation of prototypes.

- Meindert Taams who became only recently involved in the transesophageal project, for this enthousiasm.

- Leo Bekkering, Arie den Ouden en Ruud Niesing from the Central Research Workshop. Leo for his creativity in producing all our transducers from the very beginning up till now. Arie and Ruud for their designs for the development of new technologies in the field of transducer manufacturing.

- The (co-)authors of the original papers on which some of the chapters of this thesis are based.

- The team of Oldelft for taking up the challenge to develop our original prototype design into a commercial product.

- The team of the Audio Visual Center of the Erasmus University Rotterdam who account for all the illustrations used in this thesis.

The author is particularly indebted to our secretary, Corrie Eefting, for her never-ending patience in the preparation of the manuscripts and cheerfully retyping revision after revision, in the meantime keeping a keen eye on syntax errors and inconsistencies.

CHAPTER I - INTRODUCTION

ECHOCARDIOLOGY IN A HISTORICAL PERSPECTIVE

The very first application of ultrasound in the cardiovascular area was reported by Edler and Hertz: 'The use of ultrasonic reflectroscope for the continuous recording of movements of heart walls' (1). This was the first event in an explosive development. Until then only few articles had been published on the subject of application of reflected ultrasound in medicine, the majority of them covering the diagnostic use in neurology

From the Cumulative Bibliography of the World Literature up to 1978 edited by White and co-workers (2), and subsequent publications in 'Ultrasound in Medicine & Biology', the relative position of ultrasound in various disciplines, and in particular in cardiovascular areas, may be assessed from the number of scientific papers in various disciplines as shown in Diagram I-1.

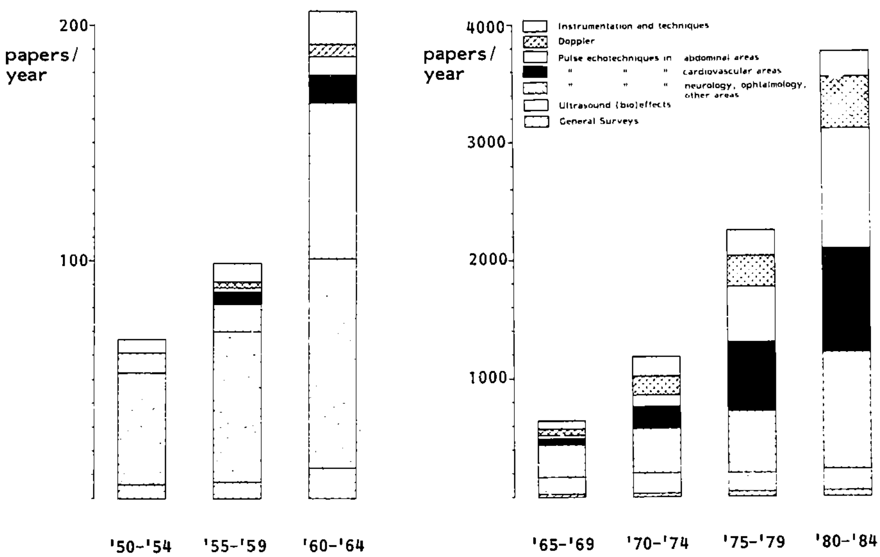

Diagram I-1. Publications in the field of medical ultrasound over the last decades.

EARLY ECHOCARDIOLOGY

Earlier than 1950, 23 papers are listed as general surveys, among these the pioneer work of Richardson of 1912 in the SONAR area and of Sokolov introducing NDT (Non Destructive Testing) techniques in 1929. Thereafter, no less than 107 papers covering the area of ultrasound effects in biology and (bio)-chemistry were published, starting in 1927 (Wood and Loomis: 'Physical and biological effects of high frequency sound waves of great intensity') (3), followed by the first reference to cardiac work by Harvey in 1929 'The effect of high frequency sound waves on heart muscle and other irritable tissues' (4). Starting at 1942, 7 papers appeared on the diagnostic value of ultrasound in neurology using both transmission and reflection techniques. The first entry in abdominal applications dated 1949.

The original paper by C. Doppler 'Ueber das farbige Licht der Doppelsterne und einiger andere Gestirne des Himmels' (5) dates back to 1842 and concerns lightwaves. Buys Ballot (6) described the effect in soundwaves. In the quoted litterature survey there were no ultrasound Doppler entries prior to 1950. Twenty-two papers on instrumentation and techniques were published, among these the pioneer work of the Curie's reporting the discovery of piezoelectricity in 1880 'Développement par pression d'électricité polaire dans les cristaux hémiédres à faces inclinées' (7). Finally it should be mentioned that the one entry listed under other techniques was the historical paper of Gabor in 1948 'A new microscopic principle' (8), which established the foundation of the holographic techniques, later on used in abdominal scanning.

ECHOCARDIOGRAPHIC HISTORY WITH EMPHASIS ON MINIATURIZED TRANSDUCERS

From Diagram I it can be concluded that up till the end of the sixties the amount of papers on (bio)effects of ultrasound outnumbered by far the contributions in the various medical disciplines.

It is also apparent that the applications in neurology, starting several years earlier, peaked around 1970, while later on they gave way to all other possible applications. This may be explained by the fact that interference between skull bone and ultrasonic waves blocked the progress in echoencephalography. All other applications, however, show a continuously increasing progress.

As for the cardiovascular applications of ultrasound several researchers started to look into ways to obtain more and better diagnostic information from the heart. In 1956 Rushmer (9) used two diametrically placed transducers to record the dynamic behaviour of the left ventricular short axis in open-chested dogs. In 1957

Wild and Reid (10) experimented with excised canine hearts and obtained tomograms.

In the same period ultrasonic detection of blood velocity was investigated. Based on the pioneer work of Kalmus in 1954 (11), Herrick (12) reported in 1957 on the application of transmission techniques for measurement of blood velocities in exposed blood vessels, using two transducers in continuous wave mode. The phase shift due to the moving blood was an indication for the effective blood velocity. This technique required two transducers placed diametrically over the blood vessel under investigation. Another application of this technique was mentioned by Franklin (13) in 1959, using pulsed ultrasound transmitted through the vessel of interest, requiring a challenging resolution of 100 psec in the travelling time measurement. Meanwhile, in 1956, Satomura (14) was the first to formulate the application of Doppler frequency shifts for moving cardiac structures, which later on proved to be also applicable for moving blood cells (15).

In that period, say from 1954 till early 1960, transducer technology, electronics and theoretical fundaments were in an early state of development. The instrumentation lacked both sophistication and sensitivity. These facts, combined with the limited accessibility of the heart from the precordium due to anatomical constraints, led several investigators to believe that other gateways to the heart had to be found. Already in 1960 Cieszynski (16, 17) obtained echoes from within the heart with a single catheter-mounted transducer introduced via the jugular vein in dogs.

After their first initial report in 1963 (18), Omoto and Kimoto published their experiences with an intravenous probe (19). They were able to delineate the size of an atrial septal defect in patients with congenital heart disease. Tomograms were obtained by rotation and withdrawal of the probe that was introduced in the right atrium via the femoral vein or the external jugular vein. In a later paper, in 1967 (20), they considered the intravenous method of obtaining B-scan or C-scan tomograms even superior to those to be obtained by means of transesophageal scanning! They therefore never pursued the esophageal approach. The carrier of the probe consisted of a stainless steel tube with a 1.2 mm outside diameter and a wall thickness of .2 mm. Since transducer displacement was necessarily slow, tomograms were obtained using E.C.G. triggered echo acquisition.

However, in the meantime real-time imaging of two-dimensional cross-sections emerged. In 1963 Olofson (21) described an ingenious though bulky scanning system, operating with rotating mirrors, with which tomograms could be obtained precordially at a frame rate of $7\,s^{-1}$.

In 1968 Somer (22) described an adaptation of the electronical phased array technique from SONAR into medical (neurology) use. The first moving images of the heart were obtained with the linear array principle as described by Bom et al (23). For cardiac application, the first mechanical sector scanner that yielded useful results was described by Griffith and Henry (24) in 1974. In the same year that Thurstone (25) described an electronic sector scanning device for use in cardiology, based on the principle described earlier by Somer (22). Still the intracavitary approach stimulated much work. In 1968 Carleton (26) described a catheter-mounted omnidirectional single element. Dimensions of a cavity had to be reconstructed from echo arrival times. In 1970 Eggleton (27) described a catheter system with four elements spaced 90° apart. Slow rotation of the catheter (8 s frame acquisition time) combined with computer reconstruction techniques provided intracardiac tomograms. The long acquisition time required E.C.G. triggering. The catheter was introduced into the heart via the left common carotid, and exhibited an excursion of several mm during the heart cycle. It therefore required some sort of tracking means in order to maintain the possibility of computer reconstructed tomograms.

Our laboratory developed in 1972 the first real-time intracardiac scanner (28). Using state-of-the-art technology we constructed a 32-element circular array with an outer diameter of 3.2 mm mounted at the tip of a No. 9 French catheter (See Figure I.1). Although the frame-rate (over 100 s^{-1}) no longer imposed any limita-

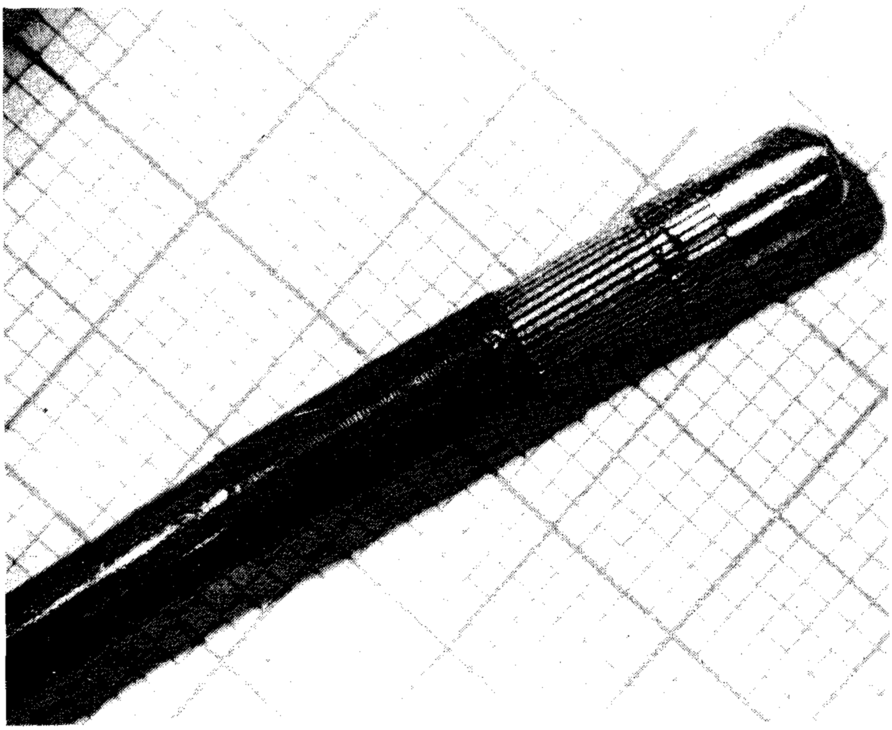

Figure I-1. Prototype of the 32-element intracardiac catheter as built in 1972 and photographed over a millimeter grid.

tions, we experienced two major complications during in vivo experiments in pigs. Excessive motion of the catheter tip during the cardiac cycle rendered the real-time cross-section difficult to interpret. The second complication, however, outweighted the first by far and originated from the grating lobes in the directivity pattern. As pointed out in the original paper (28), the array design had to be a compromise between the optimal design and the limitations imposed by technological constraints. The final design was chosen to operate at 5.6 MHz with a narrow main beam at the cost of a pronounced grating lobe at +/− 56°. As a consequence the resulting display of an intracardiac scan was made up of three components: an image of echoes generated within the main beam and two superimposed images of reduced intensity from grating lobe echoes, but rotated over plus and minus 56°. The net result proved to be too ambiguous to be of much clinical value (See Figure I.2). In Figure I.3 the position and strength of the grating lobe of this particular array is shown as a function of frequency. The project was temporized to allow us to concentrate in refining our major project: the precordial linear array real-time scanner which had been introduced one year earlier, in 1971 (23).

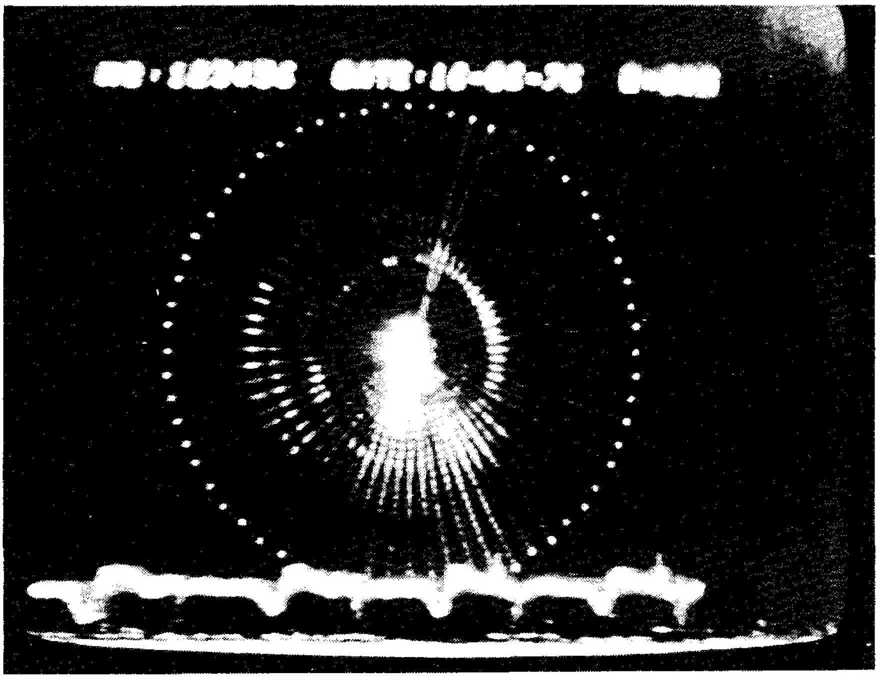

Figure I-2. Typical cross-sectional image as obtained with the described catheter in an animal experiment.

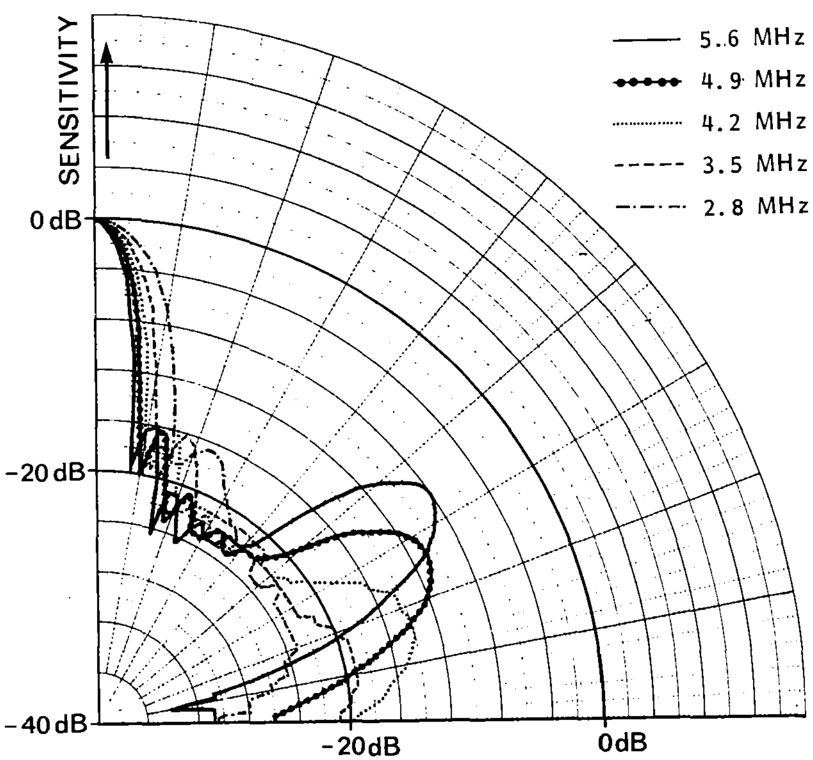

Figure I-3. The far-field directivity pattern of a subgroup of 8 phase-corrected elements from a 32-element circular array at different frequencies. The simulation was performed using narrow-band modelling.

Back again as far as 1967, in a report by Stegall (29) on the use of a Doppler velocity meter in man, a cathetertip-mounted transducer was mentioned. In 1974 the same author (30) described a catheter system with two transducers. When the catheter was curved in a loop inside a cavity (for instance, a ventricle), the transducers would face each other at opposite sides of the cavity. This procedure would allow for dynamic recording of intra-cavitary dimensions.

Because of the increasing success of transthoracic diagnosis due to a wide variety of real-time scanners and scanning principles, the urge for invasive transducer applications disappeared. The esophageal approach remained unexplored until 1971, when Side (31) published the results of a continuous wave Doppler method with the transducer located in the esophagus. In 1975 Daigle (32) introduced the transesophageal pulsed Doppler technique as described earlier by Baker (33) in

1970. In 1976 Frazin (34) established the fundamentals for transesophageal M-mode diagnosis. The first real-time transesophageal transducer was introduced in 1977 by Hisanaga et al (35) in the form of a rotating element in an oil-filled compartment providing sector scan images. Bertini (36) described a similar system in 1984.

Hisanaga also developed a linear mechanical scanner which was described in 1978 (37). A single element was moved parallel to the long axis of the tube, yielding 8-20 images per second. In 1980 Di Magno (38) described the clinical use of a real-time 10 MHz linear array mounted on an endoscope. Inherent to its principle, the field of view is limited but resolution is extremely high. An important development took place in 1982 when Namekawa (39) formulated the basis for a two-dimensional Doppler mapping technique using a velocity colour coding within a sector scan image.

Finally, to end this historical survey, it should be mentioned that, in 1982, Souquet et al (40) introduced the first transesophageal electronic sector scanner. First clinical results were reported by Hanrath (41). All esophageal instruments of the last decade profited from the availability of endoscopes with steerable tips yielding control over the position of the transducer. With this technique it is possible to ensure good acoustic coupling as well as the selection of different scanning planes. For a clinical breakthrough it seemed necessary to study and optimize all relevant paramters in order to obtain high image quality.

PURPOSE OF THIS STUDY

Our aim has been to develop and optimize a diagnostic ultrasound method for cardiological applications, based on a transesophageal electronic sector scan technique.

In this study the actual design and the design criteria of a transesophageal phased array will be discussed together with clinical applications. After the introductory chapter a review of the current situation of cardiac transducers will be given in Chapter II. In Chapter III the design aspects of basic piezoelectric materials will be discussed. In Chapter IV the actual construction and design criteria of a transesophageal probe will be discussed. In Chapters V and VI the influence of amplitude and phase errors of an electronic phased array will be treated. In Chapter VII the possible monitoring function of a transesophageal probe is analysed. In Chapter VIII the clinical results of a prototype transesophageal phased array transducer will be illustrated, highlighting two-dimensional applications and possible use with Doppler velocity measurement. In Chapter IX two clinical case examples are described.

REFERENCES

1. *Edler I and Hertz CH (1954) The use of ultrasonic reflectroscope for the continuous recording of movements of heart walls. K Fysiogr Sallsk Lund Forh 24:1-19.*
2. *White D, Clark G, Carson J, White E (eds) (1982) Ultrasound in Biomedicine. Cumulative Bibliography of the World Literature to 1978. Oxford / New York / Toronto / Sydney / Paris / Frankfurt, Pergamon Press.*
3. *Wood R, Loomis AL (1927) Physical and biological effects of high frequency sound waves of great intensity. Phys Rev 29:273.*
4. *Harvey EN (1929) The effect of high frequency sound waves on heart muscle and other irritable tissues. Am J Physiol 91:284-290.*
5. *Doppler C (1842) Ueber das farbige Licht der Doppelsterne und einiger anderer Gestirne des Himmels. Abh K Bohm Ges Wissensch 2:465-482.*
6. *Buys Ballot CMD (1845) Akustische Versuche auf der niederländischen Eisenbahn nebst gelegentlichen Bemerkungen zur Theorie des Hrn. Prof. Doppler. Pogg Ann B 66:321.*
7. *Curie J, Curie P (1880) Développement par pression d'électricité polaire dans les cristaux hémiédres à faces inclinées. C R Acad Sc Paris 91:294-295.*
8. *Gabor D (1948) A new microscopic principle. Nature 161:777-778.*
9. *Rushmer RF, Franklin DL, Ellis RM (1956) Left ventricular dimensions recorded by sonocardiometry. Circ Res 4:684-688.*
10. *Wild JJ, Reid JM (1957) Progress in the techniques of soft tissues examination by 15 Mc pulsed ultrasound. In: Ultrasound in Biol and Med (Kelly E, ed) Inst of Biol Sci, Washington DC: 30-48.*
11. *Kalmus HP (1954) Electronic flowmeter system. Rev Sci Instrum 25:201-206.*
12. *Herrick JF, Anderson JA, Essex HE (1957) Ultrasonic flowmeter: experimental tests of reliability. Physiologist 1:40.*
13. *Franklin DL, Baker DS, Ellis RM, Rushmer RF (1959) A pulsed ultrasonic flowmeter. IRE Trans Med Elect ME-6:204-206.*
14. *Satomura S (1956) A study of examining the heart with ultrasonics I. Principle. II. Instrument. Jpn Circ J 20:228.*
15. *Satomura S, Kaneko Z (1960) Ultrasonic blood rheograph. Proc 3rd Int Conf Med Electronics, London:254-258.*
16. *Cieszynski T (1960) Intracardiac method for the investigation of structure of the heart with the aid of ultrasonics. Arch Immun Ter Dosw 8:551-557.*
17. *Cieszynski T (1961) Intracardiac method of ultrasound heartstructure investigation. Polsk Przeglad Chirurg 33:1071.*
18. *Omoto R, Atsumi K, Suma K, Toyoda T, Sakurai Y, Muroi T, Fujimori Y, Idezuki Y, Tsunemoto M, Sugiwura M, Saugusa M (1963) Ultrasonic intravenous sonde – 2nd report. Med Ultrason (Jpn) 1:11.*
19. *Kimoto S, Omoto R, Tsunemoto M, Muroi T, Atsumi K, Uchida R (1964)*

Ultrasonic tomography of the liver and detection of heart atrial septal defect with the aid of ultrasonic intravenous probes. Ultrasonics 2:82-86.
20. *Omoto R (1967) Ultrasonic tomography of the heart: an intracardiac scan method. Ultrasonics:80-83.*
21. *Olofsson S (1963) An ultrasonic optical mirror system. Acustica 13:361-367.*
22. *Somer JC (1968) Electronic sector scanning for ultrasonic diagnosis. Ultrasonics 6:153-159.*
23. *Bom N, Lancée CT, Honkoop J, Hugenholtz PG (1971) Ultrasonic viewer for cross-sectional analyses of moving cardiac structures. Biomed Eng 6:500-503 and 508.*
24. *Griffith JM and Henry WL (1974) A sector scanner for real time two-dimensional echocardiography. Circulation XLIX: 1147-1152.*
25. *Thurstone FL, Von Ramm OT (1974) Electronic beam scanning for ultrasonic imaging. In: Ultrasonics in Medicine, De Vlieger M, White DN, McCready VR, (eds). Amsterdam, Excerpta Medica: 43-48.*
26. *Carleton RA, Clark JG (1968) Measurement of left ventricular diameter in the dog by cardiac catheterization. Validation and physiologic meaningfulness of an ultrasonic technique. Circ Res 22:545-548.*
27. *Eggleton RC, Townsend C, Herrick J, Templeton G, Mitchell JH (1970) Ultrasonic visualization of left ventricular dynamics. Ultrasonics 17:143-153.*
28. *Bom N, Lancée CT, Van Egmond FC (1972) An ultrasonic intracardiac scanner. Ultrasonics 10:72-76.*
29. *Stegall HF, Stone HL, Bishop VS, Laenger C (1967) A catheter tip pressure and velocity sensor. Proc Conf Engn Med Biol 9:27.*
30. *Stegall HF (1974) Ultrasonic measurement of organ dimensions. In: Cardiovascular applications of ultrasound (Reneman R, ed). Amsterdam, Exerpta Medica: 150-161.*
31. *Side CG, Gosling RG (1971) Non-surgical assessment of cardiac function. Nature 232:335.*
32. *Daigle RE, Miller CW, Histand MB, McLeod FD, Hokanson DE (1975) Non-traumatic aortic bloodflow sensing using an ultrasonic esophageal probe. J Appl Physiology 38:6.*
33. *Baker DW (1970) Pulsed ultrasonic Doppler flowmeter biological and engineering applications. IEEE Trans Sonics Ultrason SU-17:65.*
34. *Frazin L, Talano JV, Stephanides L, Loeb HS, Kopel L, Gunnar RM (1976) Esophageal echocardiography. Circulation 54:102.*
35. *Hisanaga K, Hisanaga A, Nagata K, Yoshida S (1977) A new transesophageal real-time two-dimensional echocardiographic system using a flexible tube and its clinical application. Proc Jpn Soc of Ultrasonics in Med 32:43-44.*
36. *Bertini A, Masotti L, Zuppiroli A, Cecchi F (1984) Rotating probe for trans-oesophageal echocardiography. J Nucl Med All Sci 28:115-121.*
37. *Hisanaga K, Hisanaga A, Ichie Y (1978) A new transesophageal real-time linear*

scanner and initial clinical results. Proc Jpn Soc of Ultrasonics in Med 35:115-116.

38. *DiMagno EP, Buxton JL, Regan PT, Hattery RR, Wilson DA, Suarez JR, Green PS (1980) Ultrasonic endoscope. Lancet I:629.*
39. *Namekawa K, Kasai C. Tsukamato M, Konjeno A (1982) Imaging of bloodflow using autocorrelation. Ultrasound Med Biol 8:138.*
40. *Souquet J, Hanrath P, Zitelli L et al (1982) Transesophageal phased array for imaging the heart. IEEE Trans Biomed Eng 29:707.*
41. *Hanrath P, Kremer P, Langenstein BA, Matsumoto M, Bleifeld W (1981) Transösophageale Echokardiographie. Dtsch Med Wschr 106: 523.*

CHAPTER II

TRANSDUCER APPLICATIONS IN ECHOCARDIOLOGY

C.T. Lancée, R. Daigle, D.J. Sahn and J.M. Thijssen

Abstract

A comparison is made between phased arrays and mechanical sector scanners in transcutaneous echocardiographic applications. Aspects such as contact area, beam control, side lobes, grating lobes and image quality are discussed in the context of transducer frequency. The incorporation of simultaneous acquisition of Doppler velocity information and display of M-mode signals is considered.

Transesophageal and intra-operative scanning systems for cadiology are also compared, in particular linear arrays, phased arrays and mechanical scanners, and their advantages and disadvantages in relation to the abovementioned aspects are discussed.

The general conclusion is that the electronic sector scanners may have a considerably improved cost/benefit ratio in the near future and thereby will become the leading systems for echocardiography.

Published in Ultrasonics 23: 199-205, 1985.

INTRODUCTION

The history of echocardiography started with the use of a single element transducer to produce an A-mode on a normal cathode ray tube. Afterwards progress in technology allowed the M-mode to become the exclusive diagnostic procedure in echocardiology. Starting at the mid-sixties real-time 2-D imaging began to develop. During the first years ingenious mechanical scanning devices were constructed, followed by the linear array, after which the phased array, earlier already applied in neurology, completed the scanning possibilities for practical applications in cardiology (1, 2, 3, 4, 5).

Current real-time scanning procedures may be divided into transcutaneous, transesophageal and (relatively new) intra-operative scanning. Scanning techniques currently used are either mechanical or electronic. In the following chapter the different scanning systems in relation to their clinical application are compared.

In the first part of this chapter the transcutaneous transducer applications will be discussed. In the second part other applications, such as transesophageal and intra-operative contact scanning are treated.

TRANSCUTANEOUS SCANNING

Transducer systems for transcutaneous scanning can be divided into two different categories, each containing 3 types.

Mechanical scanners may be composed of a rotating set of transducers, a single transducer driven by a mechanical or magnetic force or a stationary transducer (single element or annular array) combined with a moving mirror. The electronic scanners are either the phased array sectorscanner, the linear array or a combination of these techniques.

Of the mechanical scanners the moving mirror principle has found little application in transcutaneous echocardiology and will be omitted in the discussion. Of the electronic scanning systems, linear arrays have been overtaken by phased array sector scanners in cardiology applications and will therefore not be treated in this discussion. A schematic illustration of the current echocardiographic scanning principles is shown in Figure II-1.

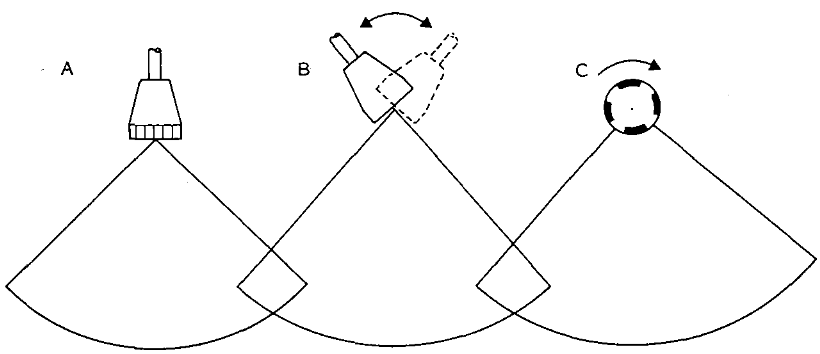

Figure II-1. Basic scanning principles. A - electronic sector scan; B - oscillating element ('wobbler'); C - rotating multiple element.

Table II-1. General comparison of mechanical vs electronic scanning systems. Transcutaneous applications.

	mechanical	electronic
System costs	low	high
System complexity	low	high
Contact area	medium	small
Transducer size	large	small
Image quality	equivalent	
Beam control	fixed	variable
Side lobes	low	high
Scanning artifacts	present	absent
Beam agility	low	high
Frequency range	large	limited
Simultaneous Doppler	impossible*	possible
Simultaneous M-mode	impossible*	possible
Transducer maintenance	required	absent

* Unless complicated additional transducer assemblies are incorporated.

A qualitative comparison of the parameters of the scanning principles is listed in Table II-1 and is discussed in detail below.

System costs/complexity

The mechanically driven transducers require some sort of miniaturized motor. This yields a rather complicated transducer assembly, while the system electronics can be kept fairly simple. The beamsteered phased array, on the contrary, requires a large amount of electronics, while the transducer assembly may be considered as solid state. The transducer construction, however, requires a high level of technology.

Contact area

A mechanical scanning device operates with a beam that is swept over the area of interest. Since the virtual point of deflection usually does not coincide with the contact surface, the area of acoustical contact needs to be larger than the element aperture. The phased array requires a contact area which equals the size of the array itself, while the apex of the sector is within the aperture boundaries.

Transducer size

Of the two mechanical scanning principles the rotary set of transducers requires a large volume due to the combination of a motor and a rotating mounting wheel for the transducers. The smallest mechanical scanners use a single pivoting element driven by a magnetic field, where volume is occupied only by the magnetic force (or similar) generator and the trajectory of the element within a fluid-filled space. The phased array, on the contrary, requires only enough volume to accommodate a backing volume, a connection area between the array elements and a multi conductor cable. This assembly may reach subminiature dimensions, as has been demonstrated by Souquet in the form of a chip transducer.

Image quality and beam control

Image quality will be a function of axial and lateral resolution, dynamic range and spatial sampling amongst other parameters. Of these variables, axial resolution and dynamic range can be optimized regardless of the scanning technique used. Mechanical scanning will impose different design limits on both lateral resolution and spatial sampling from those imposed by phased array scanning.

Since mechanical scanners employ circular elements, the resulting beam profile will be rotationally symmetrical, and the mainlobe to sidelobe ratio is defined by a Bessel function. Focussing of the beam can be achieved by using a fixed-foxus lens or a concave element.

The frame rate will be limited since the receiving aperture is continuously changing orientation, which results in the so-called firehose effect discussed below. The rather low scanning speed, however, enables a high scan line density. Non-rotating mechanical scanners will tend to vibrate at high speed due to forces developed at motion reversal, which causes another upper limit in frame rate.

The rotating multiple transducer assembly has the possibility of sequencing fixed-focus transducers differently, yielding a so-called zone focussing. The frame rate will then be considerably lower, due to the limited rotational speed combined with the sequential use of the circumferential elements. For all mechanical scanners the sequence of scanning is a rigid one, because of the inertia of the scanning system. Common to all systems is the constant resolution and constant sensitivity at different scan angles.

The beam of an electronic sector scanner is asymmetrical. The width of the scanning volume is, in general, controlled by a fixed-focus cylindrical lens. The angular resolution in the scanning plane is controlled by electronic phasing of the array elements in addition to the phasing required for the beam steering. Most scanners are able to switch from one setting to the other in times of the order of micro-seconds, allowing for almost instantaneous focussing and beamsteering. Therefore the upper limit for frame rate and line density is only imposed by the sound propagation velocity.

The angular resolution is not constant. Optimal resolution is obtained at zero deflection, while at large deflection angles the effective aperture decreases and consequently the beamwidth increases. Also, at large scan angles the sensitivity of the array is decreased, owing to the directivity of the individual array elements. This effect, however, can be corrected for within the limits of the dynamic range of the electronic circuitry. The directivity of a typical array element is illustrated in Figure II-2.

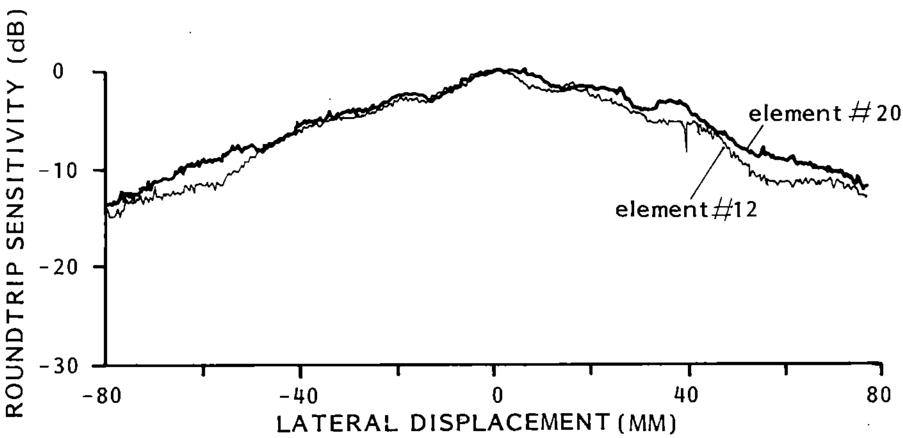

Figure II-2. Round-trip sensitivity of two typical phased array elements (No. 12 and No. 20) at axial distance of 80 mm. $F_0 = 3.1$ MHz. Lateral displacement of $\pm$ 80 mm corresponds to $\pm$ 45°.

The firehose effect

A mechanically deflected beam has an angular velocity depending on frame rate and sector angle. For example, a 90° sector with a frame rate of 30 frames per second yields an angular velocity of the transducer of 2700° per second (or 15π radian per second). A reflector at a given depth R will produce an echo signal on the transducer after a time delay T. During that time the axis of the transducer is rotated over 2700 x T degrees. For instance, when R = 80 mm the corresponding time T = 100 μs. The transducer is rotated over 2700 x 10^{-4} degrees (0.27°) during that time interval. The result will be a decrease in sensitivity and a discrepancy in the echo location on the screen (see Figure II-3). This phenomenon, sometimes called the firehose effect, is responsible for an upper limit of the rotation speed of a mechanical sector scanner. This holds in particular for oscillating transducers, where the effect will be different for each change in scan direction.

Side lobes

Mechanical sector scanners with circular elements have a reasonably low side

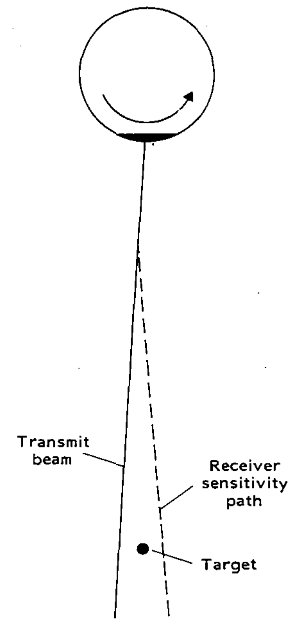

Figure II-3. Schematic geometry to illustrate the 'firehose effect'. Note the curvature of the receiver sensitivity path.

lobe level defined by a Bessel function and the beam is rotationally symmetrical.

Electronic sector scanners have a completely different beam structure. As mentioned above, the beam is asymmetrical. Perpendicular to the scanning plane the beam is defined by the height of the array and a cylindrical lens, yielding a fixed sinc function. Within the scanning plane, theoretically, each point can be electronically focussed yielding another sinc function for the pressure distribution. An example is given in Figure II-4. Compared to the Bessel function the sinc function exhibits a higher side lobe level, which may cause the electronic sector scan images to appear somewhat noisier. On top of that is the effect of the grating lobe. Only those arrays with an interelement spacing below 1/2 λ_m (where λ_m is the wavelength corresponding to the highest frequency component in the spectrum of the transmitted pulse) will exhibit no grating lobes at large deflection angles ($\pm$ 45°) (see note on grating lobes below).

Grating lobes

The requirement that the element spacing should preferably be less than half the wavelength of the maximum frequency component is not easy to meet. Given a realistic spectrum of 2-4 MHz, the determining wave length λ_m is 0.385 mm; 1/2 λ_m = .19 mm. Even with 64 elements at a spacing of 0.19 mm the effective aperture

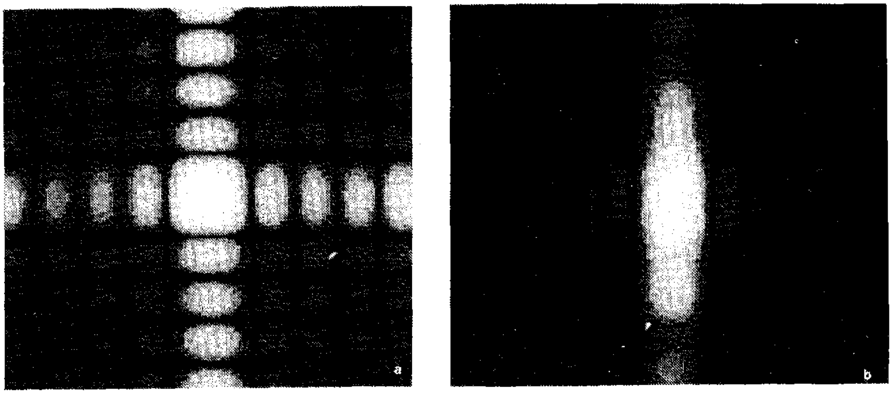

Figure II-4. a, Far field pressure distribution of a square aperture in a plane perpendicular to the propagation direction (C-plane). b, Pressure distribution of a rectangular sector scan aperture, with strong focussing along the horizontal axis and weak focussing along the vertical axis (C-plane).

will be no more than 12.2 mm. This example illustrates the designer's dilemma: he has to trade element width (technology), number of elements (costs) and total aperture (resolution) against each other, while keeping the resulting grating lobe level (image distortion) below an acceptable level (7). In Chapter IV grating lobes will be dealt with in more detail.

Scanning artefacts

All mechanical scanning systems have moving parts separated from the patient by a coupling medium and a membrane. This introduces the possibility of a reverberation effect between the transducer surface and the membrane-patient interface (see Figure II-5). Furthermore, there will be (decaying) sound energy within the transducer enclosure, increasing the background noise level.

In the case of direct contact scanners, such as the electronic phased array, the only possible sources of reverberation and background noise are in the lens medium and the backing of the array respectively. Both can be designed in such a way that the resulting effects are well below practical limits.

High frequency limit

There is virtually no limit for the maximum frequency of discrete piezoelectric transducers. For practical transcutaneous cardiac scanning, however, the limit appears to be in the 5-10 MHz range, because of the increase in attenuation as a function of frequency. Mechanical scanners meet no restrictions in implementing

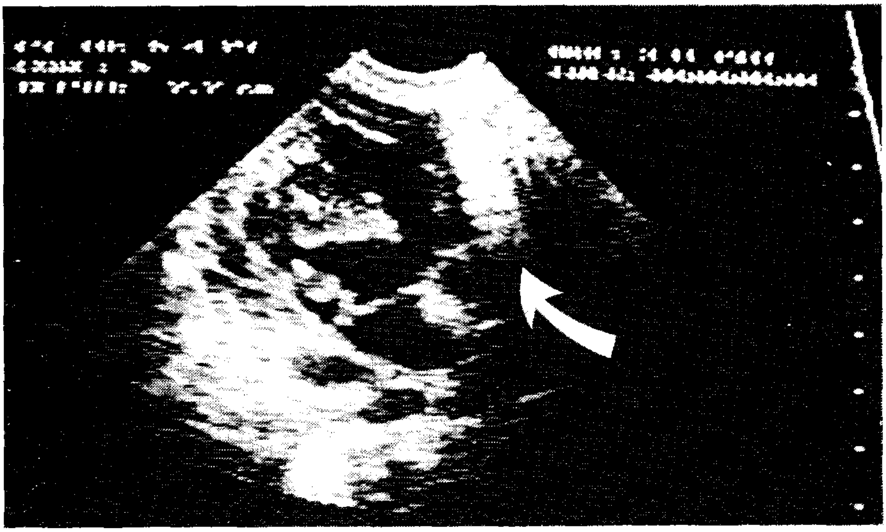

Figure II-5. Long axis cross-section of the left ventricle in the left part of the image. Strong reverberation due to loss of contact in the right part of the image (arrow).

such frequencies. For the electronic phased array, the technological requirements for the production of extremely small element widths become increasingly difficult to meet at frequencies of 5 MHz and above.

Simultaneous Doppler

The trend in modern echocardiography is to derive as much clinical information as possible from each investigation. One of those information sources is the Doppler signal derived from an area identified within the two-dimensional image. Since the Doppler signal sampling in pulsed systems requires a very high repetition frequency, one should be able to sequence, at maximum speed, 2D image formation and Doppler signal acquisition in a specific region. Mechanical scanning systems do not have the flexibility to manoeuvre the beam in such a way as to accomplish this. On the contrary, the electronic scanners are by definition able to generate beams on demand and therefore are able to provide a scanning scheme enabling simultaneous 2D imaging (at a reduced frame rate) and high repetition rate Doppler sampling.

Short-range Doppler investigation at maximum repetition frequency results in increased transducer heat dissipation. The mechanical scanner has a rather high heat capacity because of the large volume of the transducer assembly together with the coupling liquid.

In a miniaturized phased array assembly the increased transducer dissipation will yield an increased temperature at the scanning surface. The temperature has to be kept below 41°C (the safety limit), thus imposing an upper limit on electrical input power in these applications. Normal phased arrays, however, can easily be designed to incorporate adequate heat flow away from the scanning surface.

Simultaneous M-mode

The same arguments as for simultaneous Doppler apply for simultaneous M-mode, although the repetition frequency may be considerably less. A standard feature on all electronic sector scanners is now the provision of at least one M-mode in a preselected direction simultaneously with a 2D image. For most mechanical scanners the 2D image formation has to be halted to get one M-mode registration from a direction chosen within the image field.

Transducer maintenance

The electronic sector scan transducer has the advantage of being a solid state device. Although susceptible to shock, the array and its associated multiconductor cable are one permanent structure, requiring no further attention. Almost all mechanical scanners incorporate moving parts in a space filled with an acoustical coupling medium of a fluid type which should remain free from gas. Therefore periodical degassing is a standard procedure for most mechanical scanners. Furthermore, since there is some sort of a drive mechanism, mechanical wear is a source of transducer ageing and ultimately of replacement.

Transcutaneous scanning - conclusion

Although for transcutaneous scanning in cardiology both mechanical and electronic scanning methods have their own advantages, it is our opinion that in the near future electronic sector scanning will become the leading method. There are several reasons for this statement:

- The cost/performance ratio can be improved. Costs may be lowered by the increasing use of VLSI (very large scale integration) electronic circuits, while the performance can be improved by careful array design.
- Diagnostic needs in echocardiology will increasingly cause demand for optimal M-mode and Doppler (both pulsed and continuous) incorporation in the transducer as well as in the mainframe.
- Operational advantages of the electronic sectorscan transducers will exceed the mechanical scanners in terms of costs, contact area, size, weight.
- The technologically imposed high frequency limit of phased array has no

practical consequences for transcutaneous scanning, since because of chestwall conditions in most patients a frequency limit of about 5 MHz will be imposed by the patients themselves.

TRANSESOPHAGEAL AND INTRAOPERATIVE TRANSDUCERS

Special attention in transducer development is presently directed towards intra-operative contact scanning and transesophageal (monitoring) scanning. Linear array electronic scanning is now included in the discussion, since its applications in high resolution, high frequency contact scanning are highly relevant.

The general features of the high frequency linear array are listed in Table II-2.

Table II-2. General features of a high frequency linear array compared with other scanning systems.

System costs/complexity	low
Image quality	fair
Beam control	limited
Spurious lobes	medium
Scanning artifacts	low
Beam agility	high
Simultaneous Doppler/M-mode	possible

For specific use in intraoperative contact scanning and transesophageal scanning, Table II-3 compares the mechanical scanners, the linear array and the phased array.

Table II-3. Qualitative comparison of different scanning transducers in intra-operative and transesophageal applications.

Parameter	Mechanical	Linear array	Phased array
Contact area	medium	medium	small
Size	large	small	small
High frequency limit	high	high	medium
Sterility	poor	good	good
Special formats	impossible	variable	variable
Maintenance	required	absent	absent
Electrical isolation	good	fair	fair

Transesophageal transducers

The first applications of this special technique were reported in Japan. They were based on a rotating single element in an oil-filled balloon. Inherent to this principle the size of the transducer was considerable. Recently, electronic scanners mounted at the tips of standard gastroscopes have been introduced, using the electronic phased array (6, 8) and linear array (9).

The size of a solid state transducer can be kept within such limits that the overall dimensions of a transesophageal scanhead will be the same as the gastroscope tube diameter. Here the phased array has the advantage of a small contact area combined with a large (90°) angle of view, resulting in an adequate coverage of heart structures some distance away from the esophagus. The rectilinear scanning format of a linear array needs a considerable length to cover the same area, which results in an endoscope with a long rigid tip. This hinders the overall acoustic coupling.

Mounting a very high frequency linear array with the dimensions of a normal phased array on a gastroscope provides a highly detailed cross-section of posterior cardiac structures only.

It is our opinion that transesophageal scanning will find increasing use as a cardiac monitoring technique during high risk surgery. The routine clinical use of this type of investigation will remain limited, mainly because of the special precautions required by the application of a gastroscope. Precautions must be taken to ensure sufficient electrical isolation and, particularly in the case of the phased array, to control the temperature increase of the transducer.

In Figure II-6 an experimental transducer assembly is shown consisting of a 32-element sector scan array with a central frequency of 3.1 MHz mounted on an Olympus XP gastroscope with a tube diameter of 7.9 mm.

In Figure II-7 the tip of this assembly is shown, on the right, during manufacturing. The actual array can be seen as a light square area, which measures 10 x 10 mm^2. The overall thickness of ceramic and backing is just 6 mm. It is placed in the bottom part of a mold together with the wiring before final casting. Positioning pins assure correct placement in the mould after it is closed by putting the top part (shown on the left) and the bottom part together.

Intraoperative transducers

In cardiac applications of intraoperative transducers the scanning procedure is constrained by a number of factors. In open-chested patients the working area is rather small, which means that only miniaturized transducers will enable the operator to access the heart from sites other than just the anterior area.

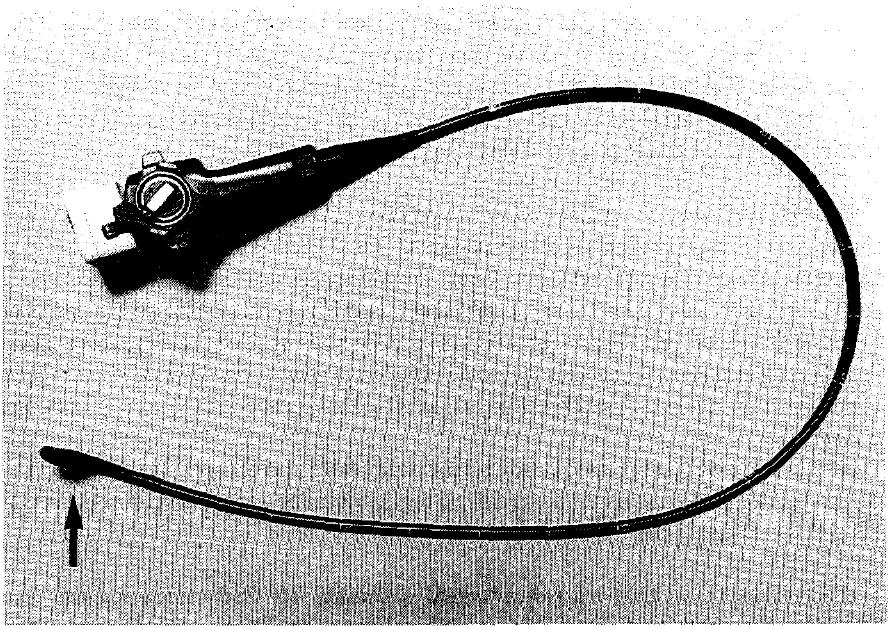

Figure II-6. A prototype transesophageal sector scan transducer 3.1 MHz mounted on an Olympus XP tube (diameter 7.9 mm). The scanhead (arrow) itself measures approximately 24 mm x 13 mm x 10 mm (length x width x height) and the scanning plane is perpendicular to the long axis of the endoscope.

Furthermore, when the heart is beating freely, it is difficult to maintain a stable contact position in order to study specific structures during the cardiac cycle. Last but not least the transducer and its connecting cable are in a sterile environment and precautions are required to exclude possible contact with non-sterile parts.

Use of intraoperative scanners will serve two major objectives: the study of overall cardiac anatomy and the provision of highly detailed information on superficial structures (coronary arteries and (infarcted) wall segments).

Two different types of contact scanners may be applied, electronic scanners and mechanical scanners.

The electronic scanners may be subdivided in two categories: the linear array with a rectilinear scanning format and the phased array, with a sector-scanning format. The mechanical scanners may also be subdivided in two categories: the rotating/oscillating transducers, with a sector-scanning format originating near to the contact area, and the waterpath scanners with a variety of scanning formats while the transducer is fixed, the beam being deflected by a multifaced mirror rotating in a fluid-filled compartment (9).

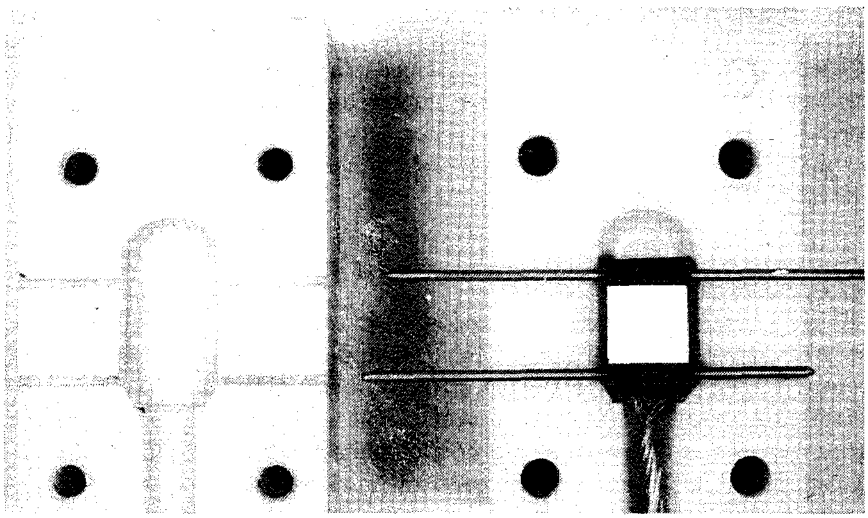

Figure II-7. The prototype of Fig. II-6 during manufacturing.

In the remainder of this section a qualitative comparison is made of the various scanning systems (see Table II-3).

Contact area

The phased array requires the smallest possible contact area of all scanning systems. In general it can be stated that currently used systems operating at 3-5 MHz require an area of 15 x 15 mm or less.

The linear array, when applied as a high frequency (7-15 MHz) small-parts scanner, can be designed to cover just the area required for adequate investigation. The length of the array will define the image boundaries (typical length will be of the order of 20 mm or more), while the height of the array defines the resolution in the elevation plane and depends on the frequency used (typical value will be 10 mm or less).

The various mechanical scanners require different contact areas. The rotating type will need the largest area of all, because of the circumferential trajectory of the scanning transducers. The oscillating type ('wobbler') requires a smaller area. The waterpath scanners will require a contact area comparable to that of the linear array.

Transducer size

To enable the operator to manoeuvre the probe freely in the open-chested patient, the transducer should be small and easy to handle. As mentioned before this requirement is met by the electronic scanners. It is, however, extremely difficult to miniaturize the mechanical scanners, in particular the waterpath type with its additional volume. Souquet (6) reported on the construction of a chip transducer for an electronic sector scanner, to be placed underneath the heart during surgery. Transducer dissipation and the associated temperature rise seem to be the limiting factors.

High frequency limit

Most applications of cardiac intraoperative scanning will lie in the field of high resolution imaging of structures. High resolution requires a high ultrasound frequency. The penetration of high frequency ultrasound will now be determined by the frequency-dependent absorption of cardiac tissue alone, allowing for much higher frequencies than in the case of transcutaneous scanning (5-15 MHz as against 2-5 MHz). The electronic sector scanner will be the only scanning system that imposes technological limitations on reaching this frequency range.

Sterility

Using a contact scanner intraoperatively demands a sterile transducer assembly. Since most piezoelectric materials and plastics cannot withstand high temperatures, a commonly used sterilization technique is ethylene oxide or cold gas sterilization. In order to remove the toxic gas residues this procedure requires a prolonged period in a vacuum.

The solid state character of the electronic scanners will, in principle, be compatible with this procedure. The mechanical scanners containing a fluid-filled compartment will suffer from a low pressure environment, and special care should be taken in the design to prevent leakage. The application of non-sterile scanners can be accomplished by using a sterile covering sheet.

In a paper of Wells et al (10) the sterility and electrical safety considerations are discussed in more detail.

CONCLUSION

Each scanning system has its own merits in relation to imaging possibilities.

The electronic phased array will provide the operator with a wide angle of view but limited resolution because of high frequency restrictions. The near field will remain limited, but simultaneous Doppler or M-mode are possible. The probe size can be made quite small.

The linear array will allow for higher resolution, and simultaneous Doppler or M-mode are also possible. The probe size can be small and near-field imaging capabilities will be improved. The imaging area, however, is limited to the actual length of the array.

Both electronic systems can easily be sterilized.

The rotating and oscillating mechanical scanners suffer from near field clutter, inhibiting the imaging of structures near the contact area. High resolution, high frequency transducers may be applied. The sector scan image allows for a wide angle of view at cardiac structures located at greater depth. Doppler and M-mode studies may be obtained, but the two-dimensional orientation will then be lost.

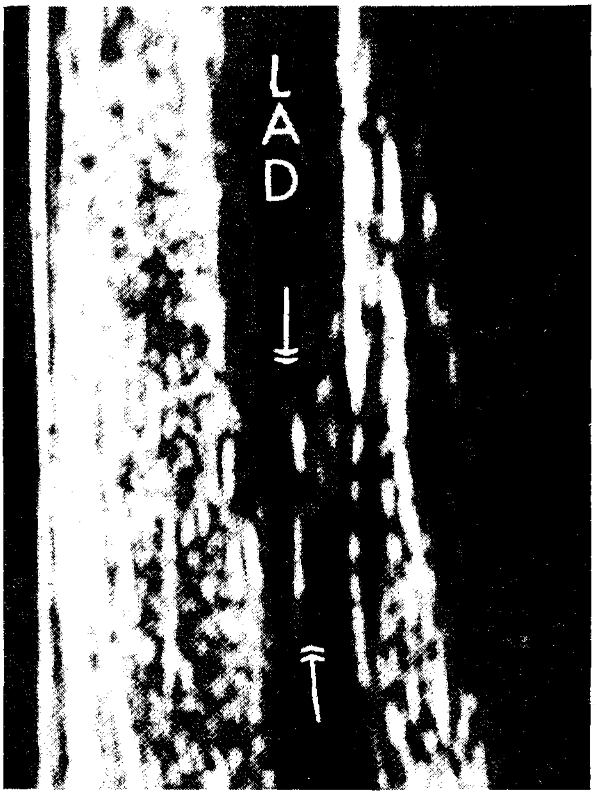

Figure II-8. Image of occluded coronary artery (LAD) obtained with a waterpath system. The obstruction is indicated between the arrows. Note the absence of near field artifacts.

Waterpath scanners allow for a high resolution image of the area of interest starting at the contact area (no near-field problems). Doppler and M-mode scans have to be performed without a 2D-image.

In Figure II-8 a coronary artery is shown as scanned by a waterpath system with a frequency of 10 MHz. The waterpath itself is left out of the image.

It is interesting to note that the advantages of waterpath scanning systems with respect to near-field imaging can also be obtained with other scanners when a suitable stand-off medium is applied. Solid coupling media have recently been introduced and practical experiences may be expected in the near future.

Meanwhile it seems reasonable to forecast an increase in use of intraoperative scanning devices and a possible change in surgical procedures, because of the immediate and on-the-spot information as provided by the ultrasound image, the M-mode tracings and Doppler flow characteristics.

REFERENCES

1. *Somer JC (1968) Ultrasound Diagnosis, Progress Report Institute of Medical Physics TNO: 37.*
2. *Pätzold J, Krause W, Kresse H, Soldner R (1970) Present State of an Ultrasonic Cross-section Procedure with Rapid Image Rate, IEEE Trans Biomed Engng 17: 263.*
3. *Gramiak R, Shah PH (1971) Cardiac Ultrasonography: A Review of Current Applications, Radiol Clin N America 9: 469.*
4. *Thurstone FL, von Ramm OT (1974) A New Ultrasound Imaging Technique Employing Twodimensional Electronic Beam Steering. In: Acoustical Holography 5 (Green PS, ed) Plenum Press, New York: 249.*
5. *Wells PNT (1979) Historical Review of Echo Instrumentation. In: Echocardiology (Lancée CT, ed). Martinus Nijhoff Publishers, The Hague: 361.*
6. *Souquet J (1982) Phased Array Transducer Technology for Transesophageal Imaging of the Heart: Current Status and Future Aspects. In: Cardiovascular Diagnosis by Ultrasound (Hanrath P, Souquet J, eds) Martinus Nijhoff Publishers, The Hague: 251.*
7. *De Jong N, Souquet J, Faber G, Bom N (1985) Vibration Modes, matching layers and grating lobes. Ultrasonics 23: 176-182.*
8. *Lancée CT, Ligtvoet CM, de Jong N (1982) On the Design and Construction of a Transesophageal Scanner. In: Cardiovascular Diagnosis by Ultrasound (Hanrath P, Souquet J, eds) Martinus Nijhoff Publishers, The Hague: 260.*
9. *DiMagno E.P. (1982) Endoscopic Ultrasonography, A New Horizon? in Cardiovascular Diagnosis by Ultrasound (P. Hanrath and J. Souquet, eds) Martinus Nijhoff Publishers, The Hague: 308.*
10. *Wells PNT, De Jong N, Somer J (1986) Transducer Safety. Ultrasonics 24: 230-232.*

CHAPTER III

FERRO-ELECTRIC CERAMICS VERSUS POLYMER PIEZOELECTRIC MATERIALS

C.T. Lancée, J. Souquet, H. Ohigashi, N. Bom

Abstract

A wide variety of transducer shapes and applications exists in the field of diagnostic ultrasound. As basic material ferro-electric ceramics are used almost exclusively, but polymer piezoelectric material seems to be a new alternative. By comparing in a qualitative way the most relevant parameters of these materials, a state of the art judgement may be made about their applicability in diagnostic ultrasound.

Note: The material presented in this Chapter reflects the expert opinions expressed at a Workshop on transducers during the 6th Symposium on Echocardiology held in Rotterdam, June 26-28, 1985.

Published in Ultrasonics 23: 138-142, 1985.

MATERIAL PARAMETERS

In this Chapter a comparison of the parameters of lead zirkonate titanate (PZT) and polyvinyliden fluorid (PVDF) will be discussed. A summary of basic differences between the two materials is listed in Table III-1, where of each parameter a quantitative evaluation is given (high or low) and also a qualitative evaluation is expressed as + or — (+ means advantageous, while — means disadvantageous).

PZT5A is chosen as a typical member of the (large) PZT family. As polymer material PVDF is chosen, while in the last section a qualitative comparison is included between PVDF and P(VDF-TrFE).

Acoustic impedance ρc: $\rho c_{[PZT]} \approx 30 \times 10^6$ kg m^{-2} s^{-1}

$\rho c_{[PVDF]} \approx 4.3 \times 10^6$ kg m^{-2} s^{-1}

Table III-1. Comparison of piezoelectric parameters (ceramic against polymer).

Parameter		Ceramic	Polymer
Relative acoustic impedance	: $\rho c/\rho c_{(water)}$	high (−)	low (+)
Coupling factor	: k_{33}	high (+)	low (−)
Sensitivity for spurious modes	: $k_{spurious}$	high (−)	low (+)
Stress constant	: e_{33}	high (+)	low (−)
Relative dielectric constant	: $\epsilon_{33}{}^{S}/\epsilon_o$	high (−)	low (+)
Mechanical loss factor	: $\tan \delta_m$	low (−)	high (+)
Electrical loss factor	: $\tan \delta_e$	low (+)	high (−)

This means that the acoustical mismatch with soft tissue ($\rho c \approx 1.5 \times 10^6$ kg m^{-2} s^{-1}) is much lower for PVDF. Consequently, optimal matching and power transfer into soft tissue may be more easily obtained with PVDF. Typical quarter-wave matching layer impedance for PZT is in the order of 5×10^6 kg m^{-2} s^{-1} while that for PVDF needs to be in the order of 2×10^6 kg m^{-2} s^{-1}. This yields another advantage of the low acoustic impedance of PVDF since the required matching layer impedance is found in commonly available plastics, while for matching with PZT the matching layer impedance has to be composed of different materials.

Coupling factor k33: $k_{33[PZT]} \approx 0.5 — 0.7$; $k_{33[PVDF]} \approx 0.2$

Although the coupling factor for PVDF has been subject to extensive research it is up to this moment still a rather low value compared to that of PZT. The low value of k_{33} for PVDF indicates that a large amount of electrical energy is needed to provide for the necessary amount of mechanical energy. As will be discussed later the electrical energy has to be supplied to a low but lossy capacitance which requires a high driving voltage combined with high dissipation losses.

Other coupling modes: $k_{spurious}$

One of the interesting characteristics of PVDF is its low sensitivity for vibration modes other than the thickness mode because of its internal structure. Although no specific figures were presented at the Workshop, all experts agreed that the magnitude of spurious vibration modes in PVDF material is considerably lower compared to PZT. PZT needs special precautions such as subdicing (of rectangular elements) to cancel spurious modes. Experience with (large) PVDF circular elements has shown the absence of spurious (radial) modes. Linear arrays with PVDF have been announced.

Piezoelectric stress constant e_{33}:

$$e_{33[PZT]} \approx 15\ \mathrm{C\,m^{-2}};\ e_{33[PVDF]} \approx 0.16\ \mathrm{C\,m^{-2}}$$

There is a significant difference in the value of e_{33} for PZT and PVDF. The effect of this parameter is found in the transformation factor 2α in the equivalent circuit for an air-backed transducer (see Fig. III-1). The acoustical load impedance Z_r is

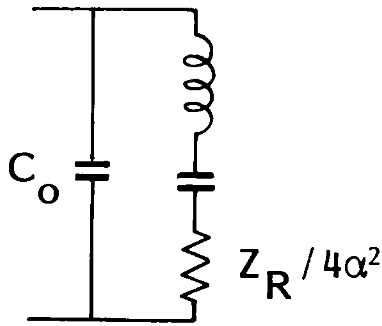

Figure III-1. Simplified equivalent circuit of an air-backed transducer near resonance frequency.

transformed to an equivalent electrical impedance $Z_e = Z_r/4\alpha^2$, where $\alpha = e_{33}A/t$ (A is the transducer area and t is the thickness). For transducers with identical A and t the ratio

$$\frac{Z_{ePVDF}}{Z_{ePZT}} = \frac{(e_{33PZT})^2}{(e_{33PVDF})^2}$$

is in the order of magnitude of 9 x 10^3.

A more realistic comparison is that of transducers with identical area and resonant frequency. The thickness t of the transducers will differ, due to the difference in sound propagation velocity V_3 of PVDF and PZT (2.4 x 10^3 and 4.6 x 10^3 m s^{-1} respectively). Accordingly we obtain a ratio

$$\frac{Z_{ePVDF}}{Z_{ePZT}} = \frac{[e_{33}^2/t^2]_{PZT}}{[e_{33}^2/t^2]_{PVDF}} = \frac{e_{33PZT}}{e_{33PVDF}} \times \frac{V_{3PVDF}}{V_{3PZT}} \approx 2 \times 10^3.$$

This result indicates that the electrical load impedance of a PVDF transducer is 2000 times higher than the load impedance of an identical PZT transducer.

Relative dielectric constant $\epsilon^s_{33}/\epsilon_0$ (ϵ_r):

$$\epsilon_{r[PZT]} \approx 600; \epsilon_{r[PVDF]} \approx 6.$$

This constant determines the capacitance C_0 of a piezoelectric transducer. Comparing transducers with identical area and resonant frequency will provide a ratio for the capacitance

$$\frac{C_{oPVDF}}{C_{oPZT}} = 0.02.$$

This yields a capacitance of a PVDF transducer which is 50 times lower than that of a comparable PZT transducer. Although this effect alone seems to be in favour of PVDF material, it has to be considered in combination with the electrical impedance Z_e (see Note).

Note

The combined effect of the large differences for PVDF and PZT with respect to the load impedance Z_e and the capacitance C_0 may be found in the power factor at resonance:

$$\cos\phi = (1 + \omega_o^2 R_e^2 C_o^2)^{-1/2}$$

This power factor is defined for a lossless half-wave resonant, air-backed transducer at resonant frequency $\omega_o (Z_e \rightarrow R_e)$. ϕ is the phase angle between the current into the transducer terminals and the current through the transformed load resistance R_e. The product $\omega_0 R_e C_0$ has to be less than unity to ensure sufficient power transfer into the load at untuned operation. Comparing PVDF and PZT yields an RC ratio

$$\frac{R_e C_{oPVDF}}{R_e C_{oPZT}} \approx 40.$$

resulting in a considerably lower power factor for PVDF transducers. This indicates that, in spite of its low capacitance, tuning of a PVDF transducer is even more necessary than in the case with PZT transducers.

Mechanical loss tangent $\tan \delta_m$: $\tan \delta_{m[PZT]} \approx 0.004$; $\tan \delta_{m[PVDF]} \approx 0.10$.

PZT's are known to have a low internal damping, and therefore require external backing and matching layers to obtain a short impulse response and a wide bandwidth. Although the higher mechanical loss of PVDF shows an intrinsic shorter impulse response at the cost of transducer efficiency, additional backing and matching layers are still required to obtain sufficient bandwidth for diagnostic ultrasound applications.

Dielectric loss tangent tan δ_e: tan $\delta_{e[PZT]} \approx 0.002$; tan $\delta_{e[PVDF]} \approx 0.15$.

The difference between PVDF and PZT material is very large with respect to dielectric losses. While the loss for PZT material is almost negligible, the loss in PVDF material is high, which will result in an appreciable amount of electric power being dissipated in the transducer itself.

MODEL STUDIES OF PVDF AGAINST PZT

Using the Mason model a more descriptive comparison can be made of the two materials when applied to a simple transducer configuration (1, 2). The test device is a circular single element with a diameter of 13 mm and a resonant frequency of 6.5 MHz.

The used Mason model is shown in Fig. III-2 (2). The losses tan δ_e and tan δ_m are incorporated, but are assumed to be independent of frequency. Furthermore, losses in both backing and front layers are neglected and (especially in the case of PZT) the occurrence of vibration modes other than the thickness mode is also neglected. As a result the higher frequency components of the model output will be somewhat overemphasized.

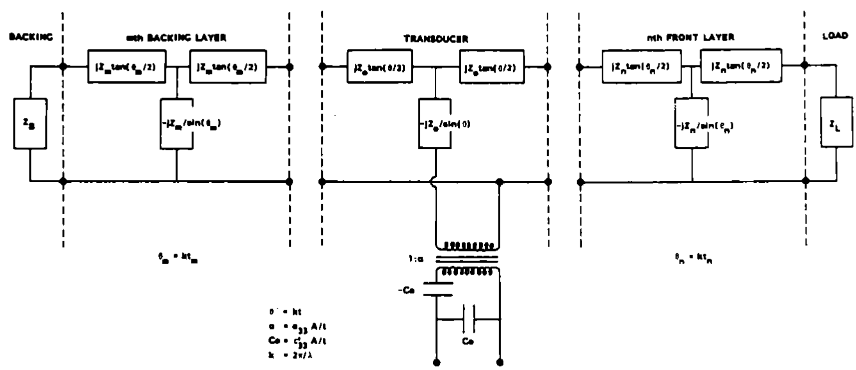

Figure III-2. Equivalent circuit of a piezoelectric transducer according to Mason.

The model is used each time to calculate transmission loss in decibels for two specific source configurations. Transmission loss is defined to be the ratio between the acoustic power transmitted into the loading medium and the available power from an electrical source. In Figs. III-3 to 8 a reference curve is shown, where the source has a complex impedance being the complex conjugate of the transducer impedance over the total frequency range. In this case optimal power transfer into the load medium is obtained for all frequencies considered. This curve is indicated with a solid line.

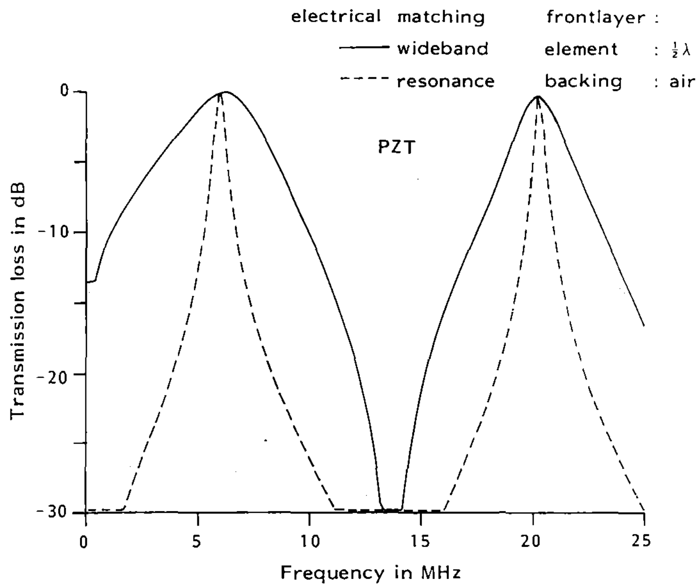

Figure III-3. Frequency dependence of transmission loss for a PZT transducer: 1/2 λ thickness; air-backing; no matching layer; $f_0 = 6.3$ MHz.

A second curve shows the transmission loss when the source is matched to the real part of the series input impedance of the transducer at resonant frequency, while a series tuning matches the capacitive part of the transducer at this frequency. This curve is indicated with a dotted line. Series tuning is chosen because it lowers the response at higher harmonics, thereby improving the impulse response.

In Fig. III-3 the transmission loss as a function of frequency is shown for an air-backed 1/2 λ PZT transducer without matching layer. In Fig. III-4 the transmission loss is shown for a 1/2 λ PVDF transducer with air-backing and without matching layer. The PZT transducer shows, even with series tuning, a pronounced third harmonic, virtually no loss at resonance and a very small bandwidth. The PVDF transducer on the contrary exhibits appreciable loss at resonance, a much reduced third harmonic at series tuning and a moderate bandwidth, while the frequency response shows a Gaussian profile.

The series tuned impulse response in the medium is shown in Figs. III-9 a and b

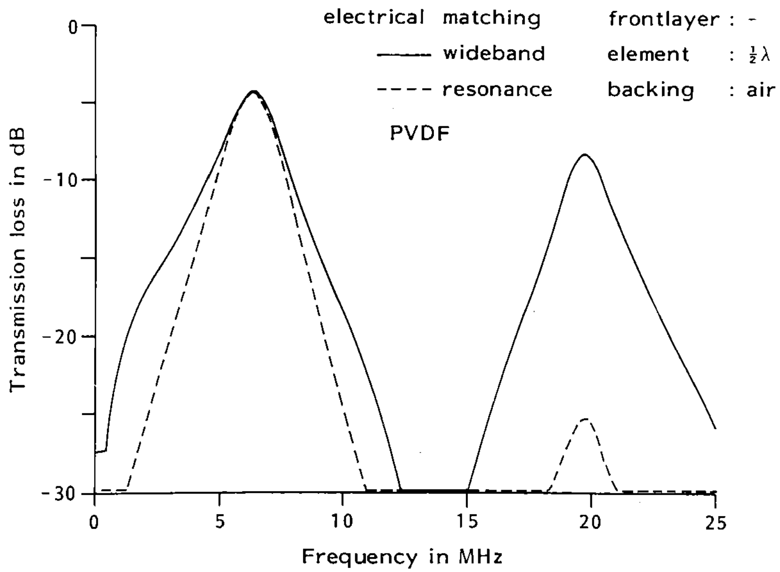

Figure III-4. Transmission loss against frequency of a PVDF transducer: 1/2 λ thickness; air-backing; no matching layer; $f_o = 6.3$ MHz.

respectively. As may be expected the PZT response is poor compared to the PVDF response.

Calculated at resonant frequency the input impedances differ enormously. The PZT transducer at resonance is almost real with a parallel resistance of 2.5 Ω, while the PVDF transducer has a capacitance of 54pF and a parallel resistance of 1200 Ω.

These observations are in good agreement with the discussions of the first part of this Chapter, except for the input impedance. The input impedance of a PVDF transducer is dominated by the parallel loss resistance. With the transducer used in this model study the transformed load resistance is much higher than the dielectric loss resistance. As a result the input impedance is much lower compared to the idealized lossless situation at the cost of transducer efficiency, while the bandwidth is increased because of damping.

In Figs. III-5 and III-6, two practical applications of PZT with a thickness of 1/2 λ are shown. The transducer shown in Fig. III-5 is matched to the load by means of a quarter-wave layer and has a very low impedance backing (air). At resonance there is still almost no loss, while the third harmonic is suppressed with the series tuning. Fractional bandwidth is 60%.

When the low impedance backing is replaced by a backing medium of moderate impedance (2.5 x 10^6 kg $m^{-2}s^{-1}$ as illustrated in Fig. III-6 a small amount of power (≈ 1 dB) is diverted into the backing and the bandwidth increases slightly to 62%.

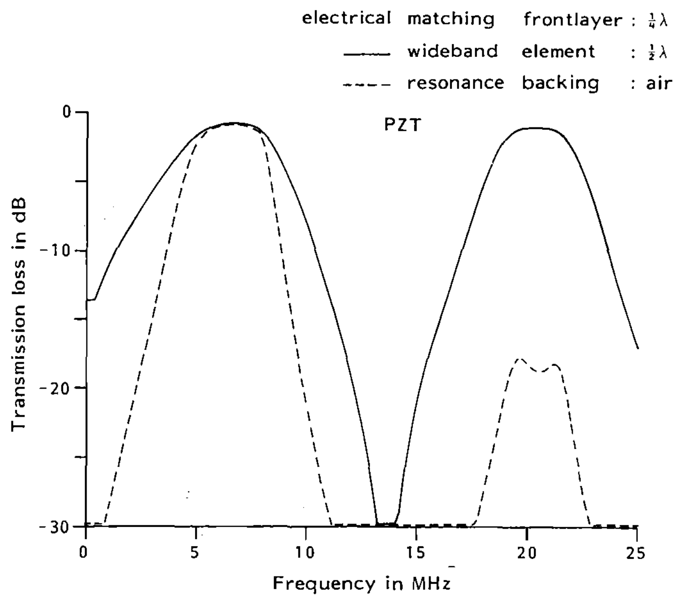

Figure III-5. Transmission loss against frequency of a PZT transducer: 1/2 λ thickness; air-backing: 1/4 λ matching front layer: f_0 = 6.3 MHz.

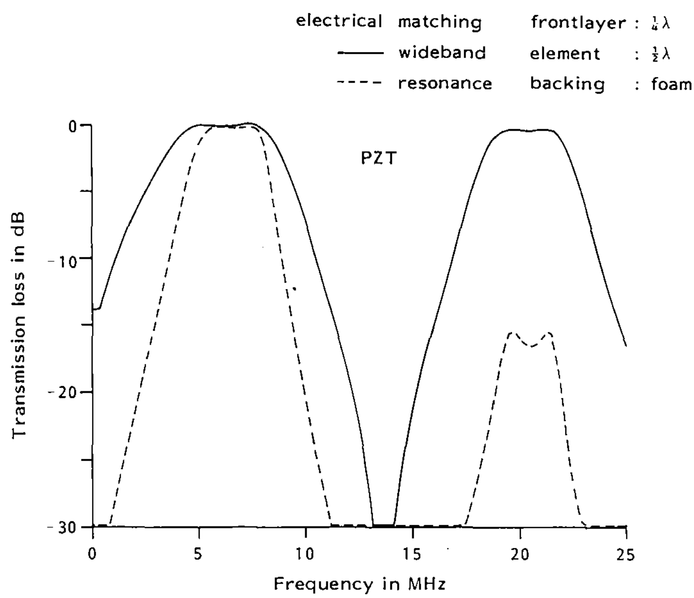

Figure III-6. Transmission loss against frequency of a PZT transducer: 1/2 λ thickness; medium backing (2.5 x 10^6 kg $m^{-2}s^{-1}$); 1/4 λ matching front layer; f_0 = 6.3 MHz.

Series tuned the third harmonic is lower. Input impedance in both cases is in the order of 2400 pF parallel to 15Ω. The corresponding inpulse response in the medium is shown in Fig. III-9c (identical for both configurations).

The application of PVDF as a 1/2 λ resonator is limited. Direct application with airbacking as shown in Fig. III-4 yields a fractional bandwidth of 29%. In order to increase the bandwidth a quarterwave matching layer can be introduced. However, the transducer efficiency will be reduced appreciably due to the increase of the transformed load impedance relative to the parallel loss resistance. The same applies for increase of the backing impedance. Since the impedance of PVDF is rather low, increase of the backing impedance will present increasing loss of power.

When relative to the PVDF acoustic impedance a heavy backing is applied, the resonator becomes stiffness controlled and will resonate only at odd multiples of 1/4 λ thickness. This procedure yields several advantages. First, a reduced thickness will lower the input impedance and second, only a small amount of power will be lost in the backing.

In Fig. III-7 the characteristics of a sandwich transducer as proposed by Ohigashi (3) are shown. The transducer is composed of a 1/4 λ layer of PVDF,

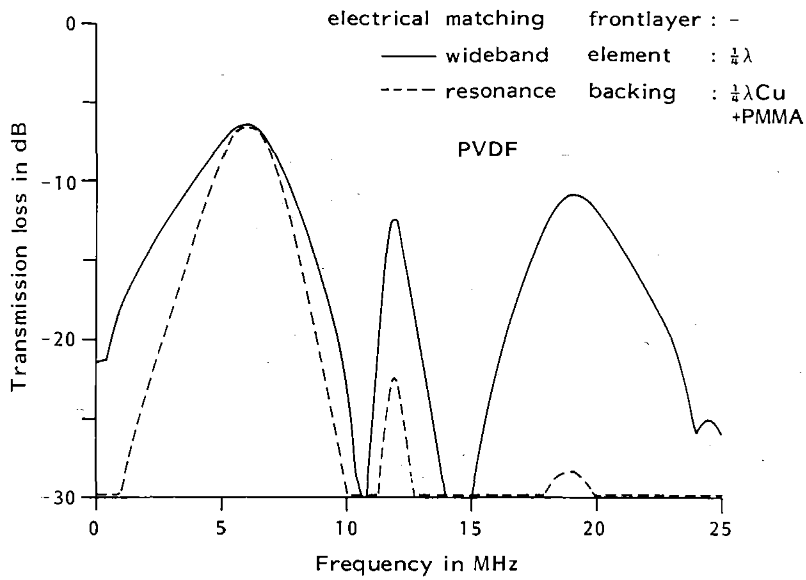

Figure III-7. Transmission loss against frequency of a PVDF sandwich transducer: 1/4 λ thickness; 1/4 λ heavy backing layer (43.5 x 10^6kg $m^{-2}s^{-1}$); medium backing (3 x 10^6kg $m^{-2}s^{-1}$); 10 μm thin front layer (3 x 10^6kg $m^{-2}s^{-1}$); f_0 = 6.3 MHz.

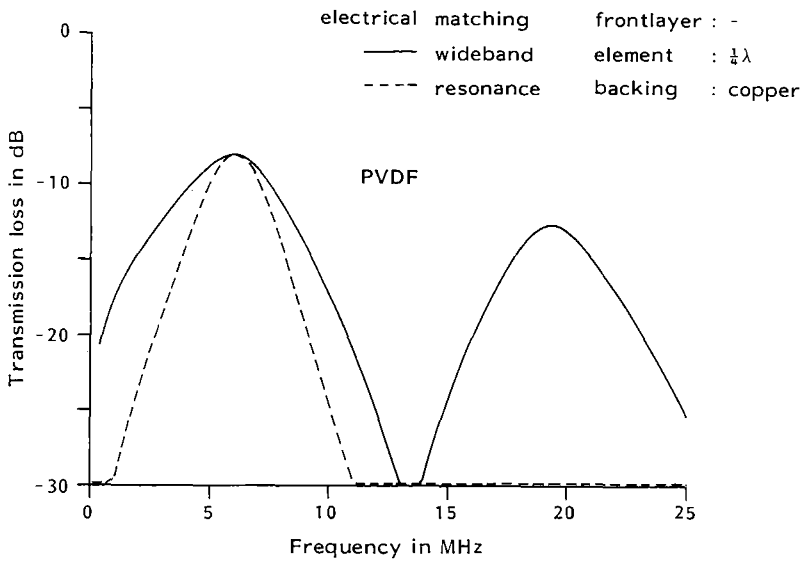

Figure III-8. Transmission loss against frequency of a 1/4 λ PVDF transducer: 1/4 λ thickness; heavy backing layer (43.5 x $10^6 kg\, m^{-2} s^{-1}$); thin front layer (as in Fig. III-7); $f_0 = 6.3$ MHz.

combined with a 1/4 λ layer of copper at the backface, mounted on a backing of Perspex, while at the front a thin layer (10 μm) of plastic isolates the transducer from the patient side.

When tuned in series a fractional bandwidth of 39% is obtained at the cost of a slight decrease in efficiency (compared to Fig. III-4). Input impedance is now reduced to 106 pF parallel to 730 Ω, while the impulse response in the medium is improved as shown in Fig. III-9d.

The typical frequency response shows a second harmonic due to half-wave resonance and the 'normal' third harmonic. Series tuning eliminates most of the contributions of these higher harmonics.

An alternative is illustrated in Fig. III-8. The transducer configuration is a 1/4 λ resonator on a heavy (copper) backing medium. As may be seen from the curve, fractional bandwidth is increased to 43% at the cost of a slight further decrease in efficiency. Input impedance has not been changed much, while furthermore the impulse response in the medium is improved as shown in Fig. III-9e.

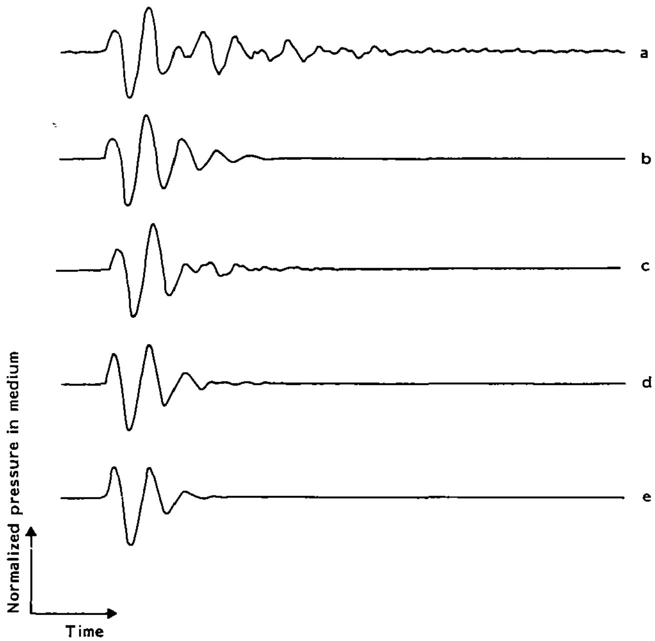

Figure III-9. Normalized pressure impulse responses in the medium (that is, transmission only) of the transducers from Figs. III-3 to 8: a, PZT re Fig. III-3; b, PVDF re Fig- III-4; c, PZT re Figs. III-5 and 6; d, PVDF re Fig. III-7; e, PVDF re Fig. III-8.

DISCUSSION

When used as (large) single elements the high electrical impedance of PVDF transducers need not to be a major disadvantage, since a transformer can be used to lower the impedance within a practical range.

Because of the significant transmission loss, the driving voltage has to be higher compared to PZT in order to develop the same amount of acoustical power in the load. The impulse response of PVDF is much 'cleaner' than that of PZT, because of the Gaussian shape of its frequency response. Unwanted vibration modes can deteriorate even further the pulse shape of a PZT transducer. Spurious response for which the circular PZT transducers with a high radial coupling factor are known, is almost absent in PVDF, resulting in a better defined beam profile. Furthermore the shape of a circular PVDF transducer can be defined at will since the construction consists of flexible layers. A focal point can be easily obtained by pressing the assembly into the required concave shape. PZT material needs to be machined to obtain a similar shape, which in addition requires special care for the 1/4 λ matching layer. Most PZT transducers use a separate lens medium in front of a flat transducer surface. The introduction of P(VDF-TrFE) allows for the construction of more efficient transducers because of its superior performance as compared to PVDF (3). The basic differences are given in Table III-2.

Table III-2.

	PVDF	P(VDF-TrFE)
k_{33}	0.2	0.3
e_{33}	$0.16\ C\ m^{-2}$	$0.23\ C\ m^{-2}$
$\tan \delta_m$	0.1	0.05
$\tan \delta_e$	0.25	0.15

The coupling factor k_{33} and the piezoelectric constant e_{33} of P(VDF-TrFE) are 50% higher than those of PVDF while the losses are reduced by a factor of two. As a result the transmission loss of P(VDF-TrFE) transducers is improved considerably (4). Very recently the application of this new material in linear arrays has been reported (5).

In conclusion, piezoelectric polymers and in particular the copolymers P(VDF-TrFE) can reach the performance of classical PZT transducers. Recommended for further reading is the excellent review article by Hunt et al (6).

REFERENCES

1. *Berlincourt DA, Curran DR, Jaffe H (1964) Piezoelectric and piezomagnetic materials and their function in transducers. In: Physical Acoustics (W.P. Mason, ed) Vol 1 Part A. Academic Press, New York: 169.*
2. *Defranould Ph, Souquet J (1979) Ultrasonic array design and performance. In: Echocardiology (C.T. Lancée, ed). Martinus Nijhoff, The Hague: 395.*
3. *Ohigashi N, Koga K (1982) Jap J Appl Phys 21(8): L455.*
4. *Ohigashi H, Koga K, Suzuki M, Nakanishi T, Kimura K, Hashimoto N. Piezoelectric and ferroelectric properties of P(VDF-TrFE) copolymers and their application to ultrasonic transducers. Ferroelectrics (to be published).*
5. *Takeda S, Hashimoto N, Miya T, Kimura K, Ohigashi H, Koge K, Asaki M, Kamatani S, Yoshizaki Y, Kobayashi M, Omoto R (1984) Development of electronic linear scanning ultrasound system equipped with piezoelectric polymer transducers. JSUM Proc (June 1984): 211.*
6. *Hunt WJ, Arditi M, Foster FS (1983) Ultrasound transducers for pulse echo medical imaging. IEEE Tran Biomed Engng BME 30 (8): 453.*

CHAPTER IV

DESIGN AND CONSTRUCTION OF AN ESOPHAGEAL PHASED ARRAY PROBE

C.T. Lancée, N. de Jong, N. Bom

Abstract

The clinical urge for echocardiographic data from patients with inadequate image quality at the precordial examination has initiated the development of transesophageal scanning techniques. The orientation of heart structures with respect to the transducer position in the esophagus, the absence of interfering structures in the soundbeam and the constraints imposed by the anatomy of the esophagus result in a different set of parameters for the optimization of the transducer and its assembly. In this article, the design and construction of a miniaturized 5 MHz phased array transducer optimized for transesophageal scanning is described. Relevant parameters and their influence on the design will be discussed, such as: bandwidth, sensitivity, resolution (in three dimensions), focal depth and the production method.

Submitted for publication.

INTRODUCTION

The first applications of transesophageal scanning have been reported by Hisanaga and Hisanaga (1) and were based on a rotating single element transducer in an oil-filled balloon. Inherent to this principle the size of the transducer was considerable. Recently electronic scanners mounted on the tip of standard gastroscopes were introduced, using the electronic phased array (2) and the linear array. The size of such a transducer can be kept within the gastroscope tube diameter. The phased array has the advantage of a small contact area combined with a large (90°) angle of view, resulting in an adequate coverage of heart structures through the esophagus. On the contrary, the rectangular scanning format of a linear array needs a considerable length to cover the same area, which will result in an endoscope with a long rigid tip. This will hinder the overall acoustic coupling.

During the last few years several phased array transducers have been developed at the Thoraxcenter in Rotterdam. The first transducer exhibited only 24 elements with a central frequency of 3 MHz and an aperture of 10 x 10 mm (3). The active acoustic plane of the transducer was mounted under a 20° angle, to ensure better acoustical coupling with the esophageal wall. Experiments in pigs revealed that it is not necessary to mount the scanning surface otherwise than in line with the gastroscope tube.

Our subsequent design was a 32-elements' transducer with the same aperture and frequency. This was interfaced to a modified Hewlett Packard (HP) sector-scanner. Image quality and resolution of the system were good and the probe proved to be of diagnostic value.

The follow-up of the 32-elements' was a 4.7 MHz probe with 52 elements. Our latest design is a 64-elements' probe with a center frequency of 5.6 MHz. These probes provide a very good image quality and the diagnostic and monitoring characteristics have proven to be excellent.

Design criteria

The performance of the transducer is determined by its axial, transversal and lateral resolution, assuming that the sensitivity is sufficient. For a total system (including the electronics), it is important to have prior knowledge of the area to be imaged, i.e. the acoustic impedance of the different structures, attenuation of the different tissues and the region of interest. As mentioned before, practical aspects limit the dimension of the transducer.

The sensitivity

The sensitivity has to be sufficient for imaging the desired region. To attain a sensitivity as high as possible one has to see to it that the conversion of electrical energy into acoustical energy is optimal. Under normal conditions element vibration in only one direction is required. Spurious modes in other directions may cause artifacts and energy loss. As will be shown, the mode of vibration is directly related to the element geometry of the ceramic.

For one-dimensional arrays, there are two important modes of vibration:

A. the plate mode: the width 'w' and the length 'L' of the transducer are much larger than the thickness 't'.
B. the thickness mode: the length 'L' of the element is much larger than the thickness 't' and the width 'w'. The width must be smaller than the thickness.

For elements where both the width and the length are much larger than the thickness, the mode of vibration is called lateral mode. However, this condition is not met in the case of arrays.

As indicated, only under special conditions of length, width, thickness ratios, it is valid to assume vibration of the ceramic in only one direction. When the ceramic does not satisfy the necessary relationship between length, width and thickness there are more than one vibration modes. These vibration modes are not all in the required direction, resulting in an energy loss. The effect of dimensional change of the element on the vibration modes has been simulated following the finite element method according to Souquet and Defranould (4). They also measured the variation in resonant frequency 'f_r'. In Fig. IV-1 the ratio of the width and thickness (w/t) is the parameter along the x-axis. The normalized resonant frequency 'f_r/f_a' is shown as a function of this ratio. Here 'f_a' is the antiresonant frequency, given by

$$f_a = \frac{V_3^D\,(\text{plate})}{2\,t}$$

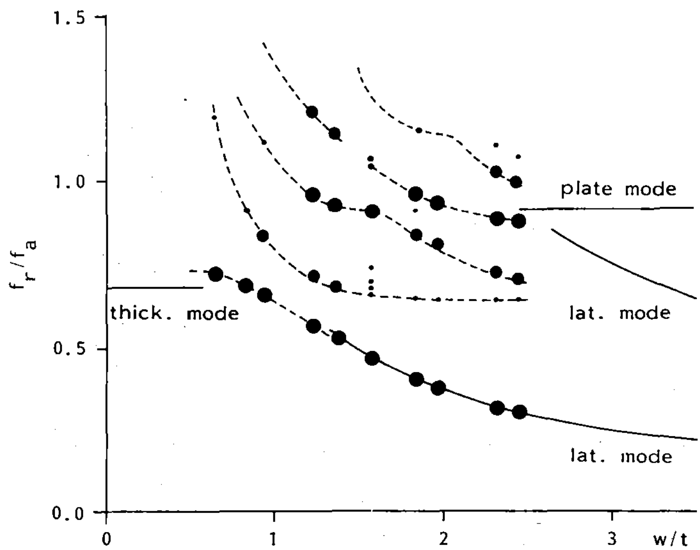

Figure IV-1. Normalized resonant frequency response for a rectangular transducer (air/PZT(P1-60)/air) as a function of the width to thickness ratio. The solid lines indicate the area where the one-dimensional vibration theory is valid. The dotted lines connect the measurement points. Strong coupling is indicated with a large dot and weak coupling with a small dot (Defranould et al; see Ref. 4).

The length 'L' remains constant and is at least an order of magnitude larger than width 'w'.

The measurements in Fig. IV-1 show that when $0.7 < w/t < 2.5$, it is not allowed to assume only one vibration mode. For a given w/t ratio in this region there are several frequencies at which the ceramic shows a specific activity. Those frequencies are hard to predict and the vibration cannot easily be described analytically.

The appearance of a frequency is marked from 'strong' (large dot) to 'weak' (small dot) in Fig. IV-1. Outside the abovementioned region for w/t the measured results approximate the theoretical value. For $w/t < 0.7$ the behaviour is called the thickness mode. For $w/t > 2.5$ the plate and the lateral modes are defined. So far the lateral mode has not been mentioned but this mode appears when in a plate there is a vibration in the width direction. Its harmonics are also present. The resonant frequency of this mode decreases when the w/t ratio is increased.

For the phased array transducer it is clear that for optimal conversion the individual elements have to act in the thickness mode. This requires a width to thickness ratio that is smaller than .7.

The resolution

The spatial resolution (the resolution cell) is determined by the axial, lateral and transverse response of the transducer. These three responses are more or less mutually independent and they will be discussed individually.

The axial resolution

In conventional transducers for medical application, the specific acoustic impedance of the ceramic and the load medium (the human body) differ. Hence the energy transmission factor is very low (order of magnitude 0.18) when the transducer is used without a matching layer directly on the human body. Most of the energy is reflected at this interface and lost in the backing when the transmission factor on the backing side of the transducer is close to 1. When this transmission factor on the backing side is close to zero, no energy is lost but it takes a long time before all the energy is transmitted into the human body. Therefore it is necessary to compromise between efficiency and impulse response. Transducer performance as to efficiency and impulse response can be improved by using a matching layer on the load side with an acoustic impedance matching the ceramic to the load.

Starting with the parameters of the ceramic itself it is necessary to design the matching layer(s) on the load side and on the backing side for an optimal impulse response and maximum efficiency. Belincourt (6) has described an electrical equivalent for the mechanical parameters of a transducer with backing and matching layer(s). The electrical equivalent circuit is one-dimensional. It can be used in a quantitative way when the transducer vibrates in one direction only. With this model (the so-called Mason model) the impulse response in the medium was simulated. This yields a plot of transmission loss versus frequency. The simulation has been carried out for two matching layer thickness conditions; correct thickness and 25% mismatch. The acoustical impedance of the matching layer has been chosen to be 4.5×10^6 kg m^{-2} s^{-1}.

Fig. IV-2 shows transmission loss versus frequency as results from the Mason equivalent circuit. In the figure the solid curve shows the transmission for perfect matching with a $1/4\ \lambda$ matching layer on the load side. A realistic backing impedance of 10^6 kg m^{-2} s^{-1} (foam) is used. This predicts a short pulse in the medium. The dashed line predicts the transmission for a matching layer which is 25% too thin. High frequencies have disappeared from the spectrum which leads to an elongated impulse response.

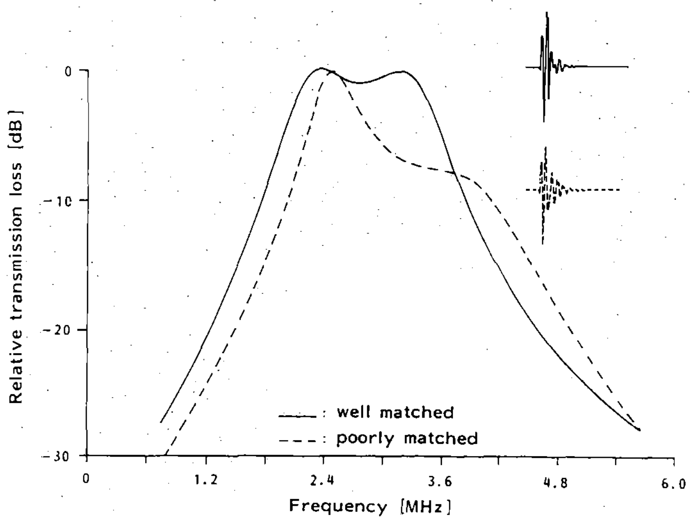

Figure IV-2. Simulations according to Mason equivalent circuit. The transmission loss is shown against frequency for an optimal matching layer and a matching layer which is 25% too thin. In the upper right-hand corner the resulting acoustic pulses are shown.

Optimal values of the density ρ and the velocity c of the quarter wavelength layer can be calculated. The acoustic impedance, $z_{l/4\lambda}$, has to be close to the optimal value:

$$z_{1/4\lambda} = (2z_1^2 z_2)^{1/3}$$

where z_1 is the acoustic impedance of the load medium (tissue), and z_2 that of the ceramic.

The optimal thickness and density of the 1/4 λ layer have to be determined experimentally because of the unpredictable change in velocity due to the necessary cutting of the material. With several combinations of density and thickness along an array, the values of these parameters yielding the shortest impulse response can be determined.

The transverse resolution (in the elevation plane)

Contrary to the beamwidth in the scanning plane, the transversal beamwidth cannot be controlled dynamically. The focussing in this plane is fixed and realized by a silicon rubber lens. The region of interest is between 2 and 12 cm of depth. In the majority of patients the most important structures (the valvular apparatus, left atrium and ventricle, the outflow tract and the large vessels) are within a dept of 4 to 8 cm.

For an optimal beam pattern in this region one has to determine two parameters: 1) the element dimension in transverse plane (L); 2) the geometrical focus (F). Computer simulations have been carried out to determine the influence of each parameter on the beamwidth and the focussing depth as function of the axial distance. For this purpose the following parameters were calculated:

BB_{min}/L : the minimal beamwidth normalized on the element length L, at the – 6 dB level;

D_{min}/L : the normalized position of the minimal beamwidth;

D_1/L : the aximal distance (normalized), where the beamwidth is twice the minimal beamwidth on the trajectory 0-D_{min};

D_2/L : the axial distance (normalized), where the beamwidth is twice the minimal beamwidth beyond D_{min}.

Fig. IV-3 shows an example for an aperture $L = 19\ \lambda_o$ (λ_o is the wavelength in water at the central frequency). In this figure the vertical axis is the axial distance, normalized on L, the horizontal axis the focussing distance also normalized on L.

Curve I shows D_1/L; curve II D_{min}/L; curve III D_2/L. The dots indicate the calculated values. The lines are curve fits. For $F/L > 3$, these curves can be described by the equation:

$$f(x) = \frac{Ax}{x + B} \quad \text{where } x = F/L \text{ and } f(x) = D/L. \qquad [1]$$

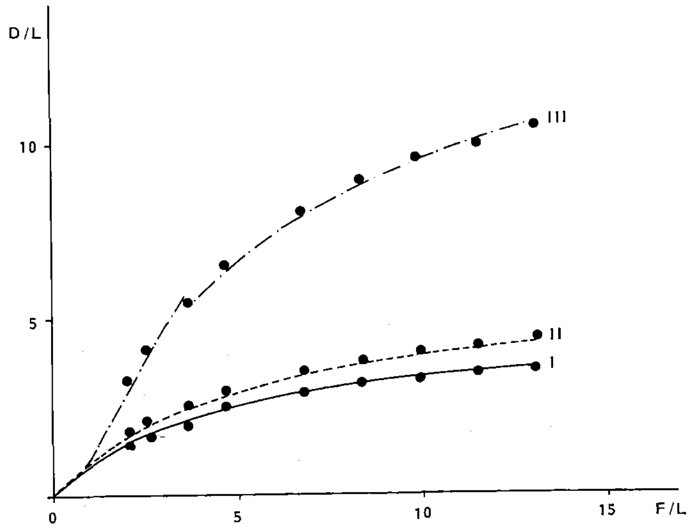

Figure IV-3. Normalized axial distance of D_1 (curve I); D_{min} (curve II) and D_2 (curve III) as function of the normalized focal distance.

By means of the least squares method parameters A and B can be calculated. Table IV-I shows the results.

With the two equations

$$D_1/L = \frac{A_1\, F/L}{F/L + B_1}$$

and

$$D_2/L = \frac{A_2\, F/L}{F/L + B_2}$$

one can solve the focus F and the aperture L. As mentioned before, the region of interest for transesophageal echocardiography is from 2 to 12 cm. So D_1 was set to 35 mm and D_2 to 100 mm. This resulted in an aperture L of 8 mm and a focus F of 70 mm.

Table IV-1. Parameters A and B of equation [1] for determination of D_1, D_2 and D_{min} at transmission or reflection.

f (x)	Transmission		Reflection	
	A	B	A	B
D_2L	L/λ_o	$.26L/\lambda_o$	$.87L/\lambda_o$	$.36L/\lambda_o$
D_1/L	$.20L/\lambda_o$	$.175L/\lambda_o$	$.26L/\lambda_o$	$.26L/\lambda_o$
D_{min}/L	$.40L/\lambda_o$	$.35L/\lambda_o$	$.33L/\lambda_o$	$.30L/\lambda_o$

The lateral resolution (in the azimuthal plane)

In order to avoid ambiguity, the main beam in transmission and reception should be narrow such as might be obtained with dynamic focussing techniques. Any sensitivity outside the main beam direction may result in image artifacts. Lobes appearing outside the main direction are called side-lobes. A special side-lobe is known as the grating lobe which finds its origin from the regular spacing of the transducer elements of the array.

The relationship between the angle of the grating lobe and the angle of the main lobe is given by the following equation:

$$\sin \phi = \frac{\lambda}{IN} - \sin \theta \qquad [2]$$

where ϕ = angle of the grating lobe
θ = angle of the main lobe
λ = wavelength (m)
IN = pitch (element to element distance in m)

The right-hand term of equation [2] will exhibit a range of λ/IN to $\lambda/IN - \sin(\theta_{max})$ when the beam is steered from $\theta = 0$ to θ_{max}. There will be no grating lobe when $\lambda/IN - \sin\theta$ remains greater than 1, i.e.:

$$\lambda/IN - \sin\theta > 1 \qquad [3]$$

For $\theta_{max} = 45°$, it follows from equation [3] that $\lambda/IN > 1.7$. The requirement for the absence of grating lobes will be

$$IN < .6\,\lambda \qquad [4]$$

When the array does not satisfay equation [4] for all occurring wavelengths there will be a grating lobe.

In general the directivity pattern in the lateral direction depends on the total available aperture, the number of elements and the bandwidth of the transducer. The total aperture determines the beamwidth, while the number of elements determines the occurrence of grating lobes. The bandwidth has a weak influence on the sidelobe level, but a strong influence on the grating lobe level.

Fig. IV-4 shows the theoretical beam pattern for four steering angles with the following parameters: pitch .16 mm, number of elements 64; bandwidth of each element 50%. In this figure the patterns are calculated in the focal point at 50 mm from the transducer. Tapering is applied in transmission. The 32 center elements have a factor 1, the 16 adjacent elements a factor .75 and the outer elements a factor .5. In the figure the beam patterns have been calculated for steering angles of 0, 13, 27 and 40 degrees. Only the last two steering angles have a grating lobe higher than –60 dB. The position and shape of the grating lobe change with the steering angle. The higher the steering angle, the smaller the angle of the grating lobe. In the grating lobe complex, the top moves to the left with an increase of the steering angle.

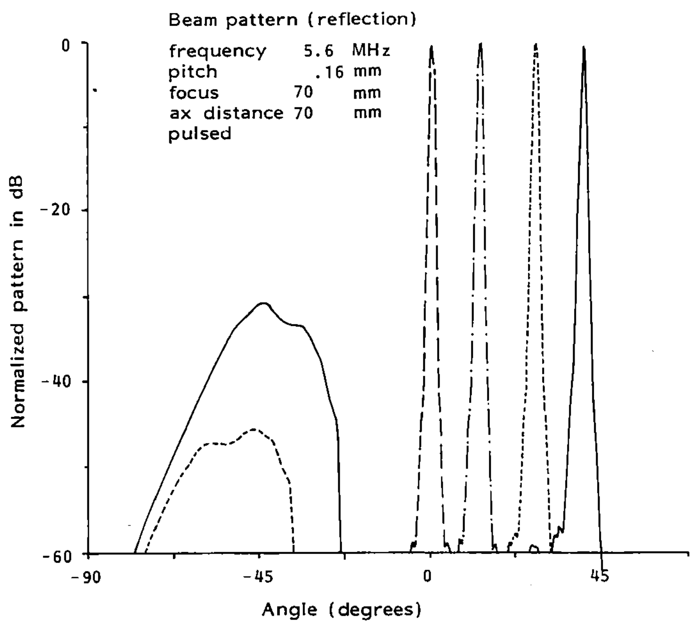

Figure IV-4. Calculated beam patterns for steering angles of 0, 13, 27 and 40 degrees respectively. For large steering angles the grating lobe appears.

Fig. IV-5 shows that there is no grating lobe at all at steering angles below 4°. At 4° the level is –90 dB and the position at –73°. The grating lobe level increases gradually to –28 dB at the highest steering angle with a position at –38°. Curve 1 (position of the top of the grating lobe) is not monotonously decreasing because of the change in shape of the grating lobe.

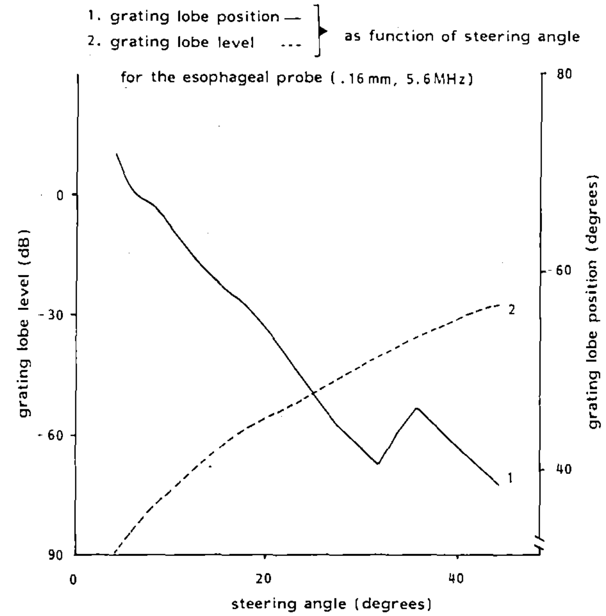

Figure IV-5. Grating lobe position and grating lobe level as function of the steering angle.

PRODUCTION METHODS

The transesophageal transducer is a phased array transducer, so it consists of a large number of individual elements. Starting from a slab of piezoelectric material there are several methods to dice this slab into small elements.

1. Wire-sawing
2. Cutting with a laser beam
3. Cutting with an ultrasonic drill
4. Cutting with an electronic beam
5. Sawing with a small diamond-coated disc
6. Etching

In general the following aspects have to be considered for the separation of the ceramic:

a. the produced heat;

b. the mechanical forces exercised;
c. the desired sawing depth;
d. the sawing speed;
e. the material to be sawed;
f. the flexibility (with regard to element pitch and shape);
g. the quality of the sawing groove;
h. production costs.

The multiwire saw exercises small forces and produces little heat. The sawing depth is not limited; the sawing speed is high because of the parallel sawing. The flexibility, however, is low and soft materials cannot be sawed with high precision.

The laser has a high flexibility. Not all materials can be sawed. The sawing speed is rather low because of the serial sawing and the small amount of heat permitted. Also the sawing depth is limited. For these reasons the laser is only used in specific cases, where the cost aspect is not the most important matter.

Cutting with an ultrasonic drill has two major disadvantages: the sawing groove is rather large and the fragile ceramic is exposed to large forces.

The electronic beam offers almost the same possibilities as the laser beam. Here also the production costs are high. This method is fit for other materials than those that can be sawed with the laser beam.

The diamond saw is frequently used. The sawing width can be kept small: 30 to 40 μm. The process is serial but the sawing speed can be improved by mounting several saws in parallel. The depth is limited (25 times the sawing width). Water cooling of the ceramic is applied to keep the temperature low. The mechanical forces are considerable. The production costs are rather low.

Etching of the electrode of the ceramic is only useful in the case of a low lateral coupling of the individual elements. For present-day ceramic transducers it is not acceptable.

Multiwire saws have traditionally been used for cutting semi-conductive materials. Nowadays this is done with a diamond-coated disc. Nevertheless, cutting piezoelectric material with a multiwire saw has advantages, such as

1) The parallel sawing and the consequent reduction in the costs of production.
2) The small forces exercised and the small amount of heat produced maintaining the optimal quality of the transducer.
3) The quality of the sawing groove is very good. The specific materials for backing and matching of the transducer can easily be sawed.
4) No limitation exists as to the depth of the groove so that elements with low mutual interaction can be produced.

A theoretical description of the sawing process has been given by Fujisawa (6). Baer described practical aspects of a wiresaw (communication Max-Planck-Institut, Stuttgart, FRG). The first wiresaw (7) developed at the Erasmus University dates as from 1975 and was constructed for the purpose of a special intracardiac scanner (8).

For high quality linear and phased array transducers a multiwire saw has been constructed (Fig. IV-6) which is described by De Jong (De Jong N, Den Ouden A, Brinkman JF, Niesing R, Lancée CT, Bom N: A multiwire saw for the production of ultrasound transducers. To be published in J Phys: E). This machine makes miniaturization of the present transesophageal probe possible.

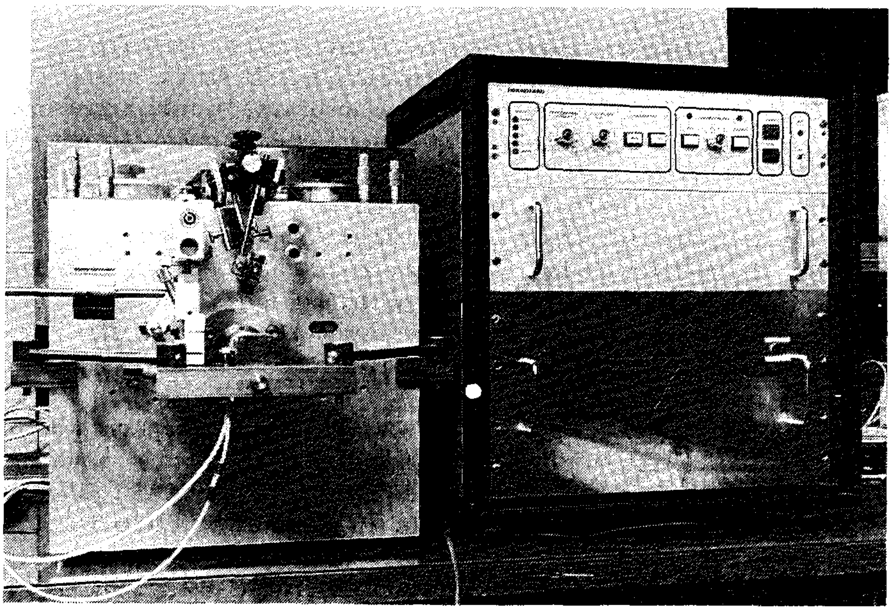

Figure IV-6. The multiwire saw developed at the Erasmus University Rotterdam.

RESULTS

For high performance good lateral resolution is important. Fig. IV-7 illustrates the measured and simulated beam profile of the esophageal probe at 40° steering angle. The simulation model and its applications are described in Chapters V and VI. Focussing was performed at 50 mm and measurements were made with digitally phased electronics. As can be observed the measured and simulated data correspond well. Given the measured data in the other resolution planes the total resolution cell at –6 dB level in the focal area showed to be within 1 x 1 x .3 mm^3 (Fig. IV-8).

The transesophageal probe is shown in Fig. IV-9. It turned out to exhibit excellent clinical performance. In patients in whom precordial investigation is inadequate, transesophageal scanning provides vital information. Based on a

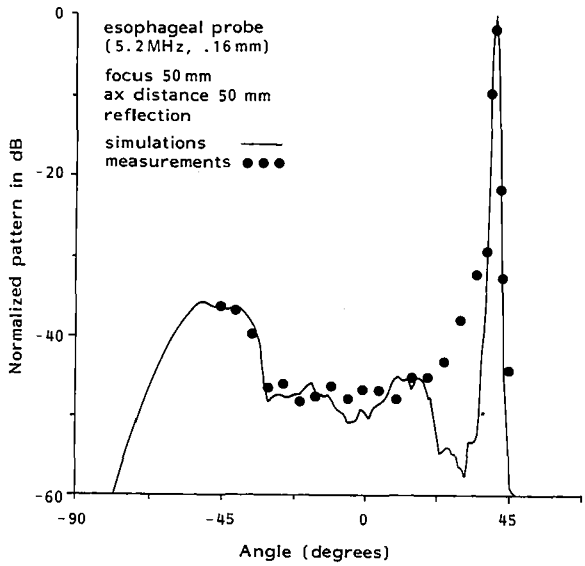

Figure IV-7. Simulated and measured beam profile of the esophageal probe at 40° steering angle.

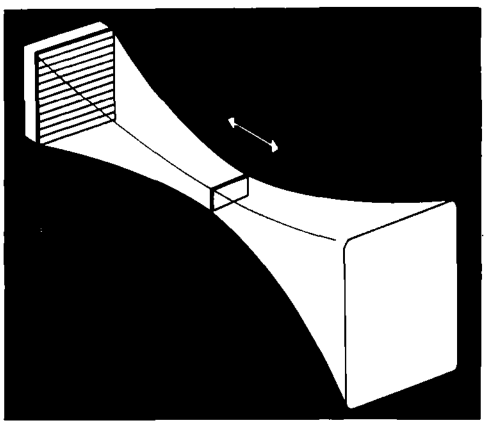

Axial resolution	(−20 dB)	5 periods
Lateral aperture angle	(−20 dB)	50°
Transversal aperture angle	(−20 dB)	1,5°
Resolution in focal area	(−6 dB)	1 × 1 ×.3 mm^3

Figure IV-8. The resolution of the esophageal probe.

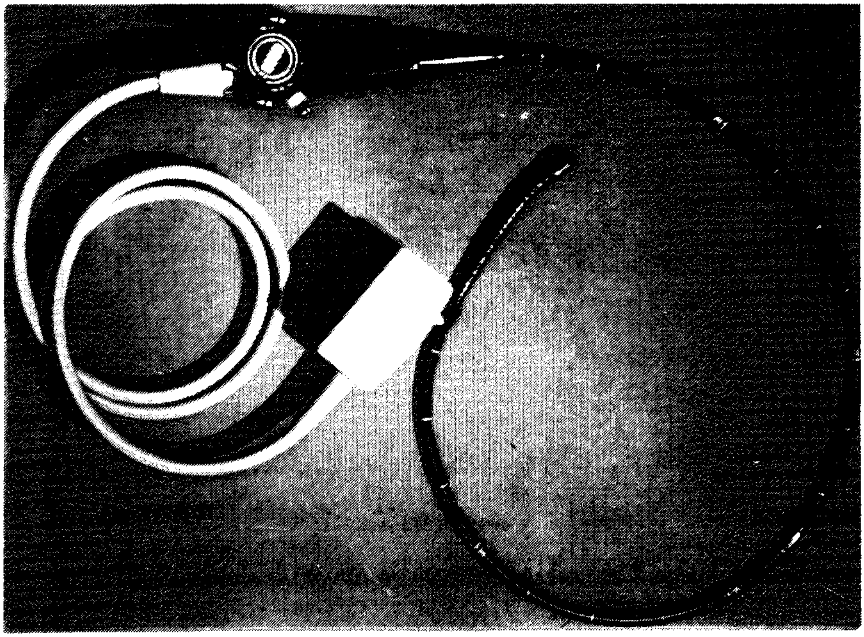

Figure IV-9. The esophageal probe as produced with the wiresaw.

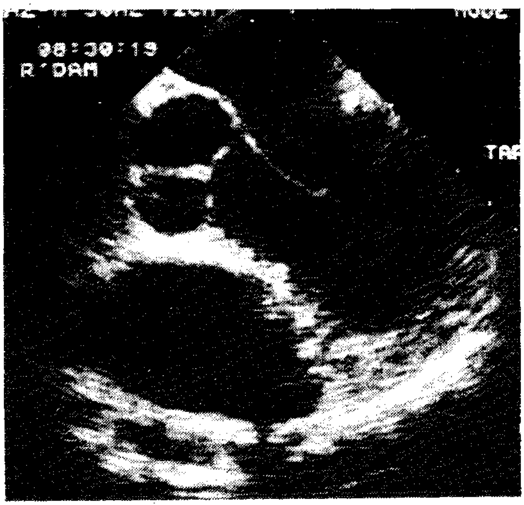

Figure IV-10. Cardiac cross-section obtained in diastole with the esophageal probe (the left atrium is at the top and the closed aortic valve cusps are seen in the middle of the image).

detailed study of the valve apparatus corrective surgery has in some cases been performed without angiocardiography. The investigation takes less than 5 minutes and is well-tolerated by the patients. The quality of the left ventricular cross-section images made during surgery is excellent and allows for quantitative analysis. An example of the resulting image is shown in Fig. IV-10.

REFERENCES

1. *Hisanaga K, Hisanaga A (1982) Transesophageal cross-sectional echocardiography with a mechanical scanning system. In: Hanrath P, Bleifeld W, Souquet J (eds) Cardiovascular Diagnosis by Ultrasound. Martinus Nijhoff Publishers, The Hague: 239-246.*
2. *Souquet J (1982) Phased array transducer technology for transesophageal imaging of the heart: current status and future aspects. In: Hanrath P, Bleifeld W, Souquet J (eds) Cardiovascular Diagnosis by Ultrasound. Martinus Nijhoff Publishers, The Hague: 251-259.*
3. *Lancée CT, Ligtvoet CM, De Jong N (1982) On the design and construction of a transesophageal scanner. In: Hanrath P, Bleifeld W, Souquet J (eds) Cardiovascular Diagnosis by Ultrasound. Martinus Nijhoff Publishers, The Hague: 260-269.*
4. *Defranould Ph, Souquet J (1979) Ultrasonic Array Design and Performance. In: Lancée CT (ed) Echocardiology. Martinus Nijhoff Publishers, The Hague: 395-412.*
5. *Berlincourt DA, Curran DR, Jaffe H (1964) Piezoelectric and piezomagnetic materials. In: Mason WP (ed) Physical Acoustics Vol. 1, Part A. Academic Press, New York/London: 170.*
6. *Fujisawa M et al (1983) Precision sawing with wire saw. Annals of the CIRP 32:1.*
7. *Niesing R (1976) Een draadzaag, konstruktie en resultaten. Mikroniek 16: 172-175.*
8. *Bom N, Lancée CT, Van Egmond FC (1972) An ultrasonic intracardiac scanner. Ultrasonics 10: 72-76.*

CHAPTER V

INFLUENCE OF AMPLITUDE ERRORS ON BEAM-STEERED PHASED ARRAYS

C.T. Lancée, J.M. Vissers, S. Mientki, C.M. Ligtvoet en N. Bom

Abstract

For the image quality of two-dimensional (2D) ultrasound systems, spatial resolution is one of the most important parameters. This resolution is determined by the directivity pattern. In practice, the directivity pattern of phased arrays will be distorted due to errors in critical components.

In this study two parameters describing the distribution of amplitude errors over the aperture, and the range of amplitude errors are dealt with. With these parameters qualitative predictions of the directivity pattern are possible. To keep the directivity pattern acceptable, error parameters must remain within certain limits. Practical guidelines to evaluate the beam distortion on the basis of a minimum number of simulations or measurements are given.

Published in Ultrasonics 25: 147-153, 1987.

INTRODUCTION

Ultrasonic imaging is nowadays established as an important tool in medical diagnosis. For real-time 2D-imaging three scanning methods are commonly used; mechanical sector scanning, lineair array scanning and phased array scanning. Each of these methods has its typical advantages and disadvantages. Phased arrays are preferred when a 2D image is required along with a high repetition rate M-mode and a small transducer size, in combination with a wide angle of view. These features make the phased array particularly suited to cardiology.

Fig. V-1 shows schematically the beam profile of an array. The resolution in both time and space are the primary parameters describing the quality of an ultrasonic image. For the phased array the temporal resolution (repetition rate)

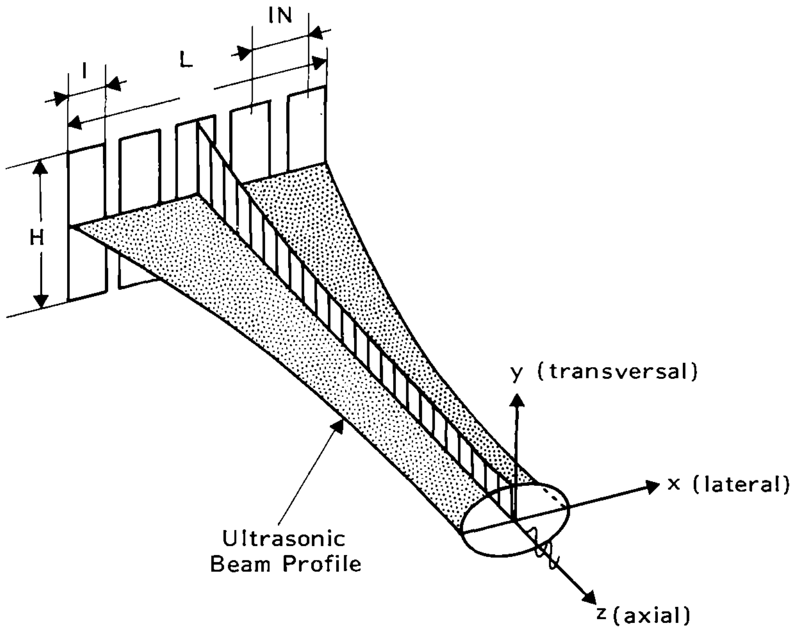

Figure V-1. Definitions of the array parameters and the ultrasonic beam profile. H = element height; IN = interelement spacing; I = element width; L = total active aperture.

depends on the maximum depth of interest and the number of scan lines (1). The axial resolution is determined by the length of the transmitted pulse. The capability to produce a short pulse is limited by the bandwidth of the total system. The elevation resolution depends on the height of the elements. For the region of interest, improvement of the elevation resolution can be obtained by means of a fixed acoustical lens.

The azimuthal (lateral)* resolution is the most complex parameter. The lateral resolution depends on the total aperture width, the number of elements, the uniformity of the individual channels and the accuracy of the phasing delays. In current phased array systems the lateral resolution is the major limiting factor in the image quality. In this Chapter the influence of amplitude errors on the lateral resolution is studied. In the following Chapter we will investigate the effects of phasing errors.

* Since in medical ultrasound the azimuthal resolution is mostly referred to as lateral resolution we will adopt the latter term furtheron in this Chapter.

PURPOSE OF THE STUDY

This study was initiated because the need was felt to be able to objectively judge the performance of a series of special transducers, apart from the subjective clinical tests. Those particular transducers are difficult to assemble, so in cases of inadequateness, early rejection would save money. The purpose was to obtain a criterion by which a transducer could be classified as being adequate or not as early as possible in the course of the manufacturing process.

DESCRIPTION OF THE SIMULATION MODEL

The impulse response of a piezoelectric transducer can be specified by its transfer function $H(\omega)$,

The transfer function can be calculated with a mathematical model or, for an existing transducer, measured in a water tank. Commonly used mathematical models for the derivation of $H(\omega)$ are the Mason (2) and KLM model (3).

In this paper the transfer function, $H(\omega)$, has been calculated with the Mason model.

In the transmitting mode (see Fig. V-2) the input of the piezoelectric transducer is an electrical signal. Output is the generated acoustic wave field. The generated acoustic wave field is described by the distribution over the aperture of the pressure and the normal component of the particle velocity (4). In the case of linear acoustics the velocity component can be expressed in terms of pressure and vice versa.

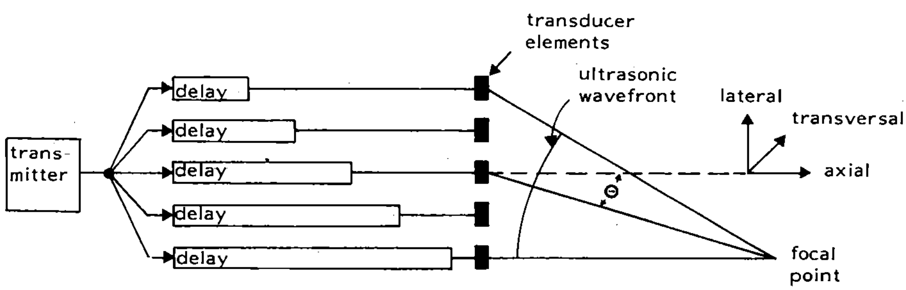

Figure V-2. Phased array principle (transmitting mode).

The simulation of an echo system involves the extrapolation of the generated wave field at the source surface to a measuring point A.

Denoting the propagation effects by $W(r,\omega)$ and the source field by $P_S(\omega)$, then the wavefield P_A can be computed by:

$$P_A(\omega) = \int_S W(r,\omega)\, P_S(\omega)\, dS \qquad [1]$$

where $P_A(\omega)$ – pressure in point A [Pascal]
$W(r,\omega)$ – operator for propagation effects [m^{-2}]
$P_S(\omega)$ – pressure distribution over the active surfaces of the transducer

The directivity pattern of a single array element will diverge from its theoretical sinc function because it is not behaving like a rigid piston in an infinite baffle. A reasonable approximation of its actual behaviour is found by multiplying the sinc function with a cosine (θ) weighting, where θ ranges from $-90°$ to $+90°$. This has also been found by Smith (5). Such a directivity is realized by a pressure-to-pressure simulation for which the Rayleigh-2 operator is used (4). Therefore both P_A and P_S in equation [1] are pressure components. The pressure in point A due to a number of emitting elements is expressed in the frequency domain as a summation of the individual contributions with respect to their individual phase and amplitude.

For round-trip measurements, as these are used later in this Chapter, the pressure in point A is used to define a point source emitting an omnidirectional pressure wavefield of the same amplitude. The round-trip angular sensitivity is then defined as the summation of the phased element responses as a function of the steering angle θ.

PULSED SIMULATIONS

Several methods exist for calculating the wide-band response of an array. In our model we calculated the contribution of every frequency component involved. Summation of these individual contributions produces the wide-band response. The resulting time series can be processed by a computer simulated idealized detection mechanism. In this case, peak detection on the pulse envelope, calculated with a Hilbert transform, is performed. As an illustration, Fig. V-3 shows the differences between the directivity patterns of pulsed and continuous wave (CW) simulations in the focal point of a 32-element array. According to Freedman (6), the peak side lobe sensitivity is reduced by –6 dB in the case of wide-band excitation, compared to the continuous wave situation.

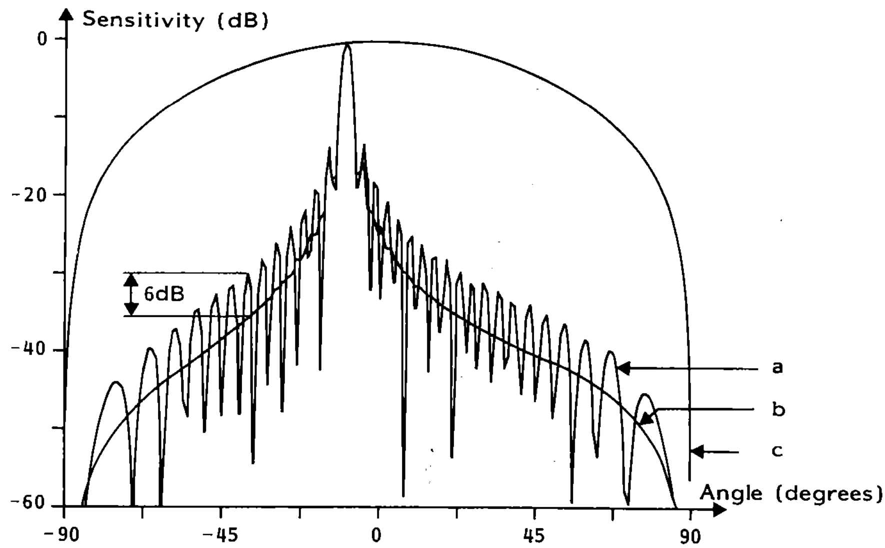

Figure V-3. Directivity pattern of a phased array in the far field for a steering angle of −10°. a) CW excitation; b) pulse excitation; c) directivity pattern of a single element of the phased array (element factor).

ARRAY CONFIGURATION

The simulations in this Chapter were carried out for a practical design of an esophageal phased array probe. A prototype of such an array has been described previously (7, 8). A clinically evaluated prototype is shown in Fig. V-4. The scan-head is mounted on a 9 mm diameter endoscope tube. The lens, which is used to define the scanning field in the elevation plane appears as a curved surface. Below the assembled scan-head the actual array is shown, together with a 15 mm diameter 10 cents coin. Because of constraints on the design due to its specific application the array dimensions are quite small. The relevant parameters, as explained in Fig. V-1 are listed in Table V-1.

One of the powerful applications of transesophageal scanning is the undisturbed investigation of the valvular apparatus, when external examination procedures failed to be conclusive.

CHARACTERISTICS OF THE DERECTIVITY PATTERN

The most commonly used quantities to characterize the directivity pattern (in the lateral direction) are the −6 dB beamwidth, the peak side-lobe level and the

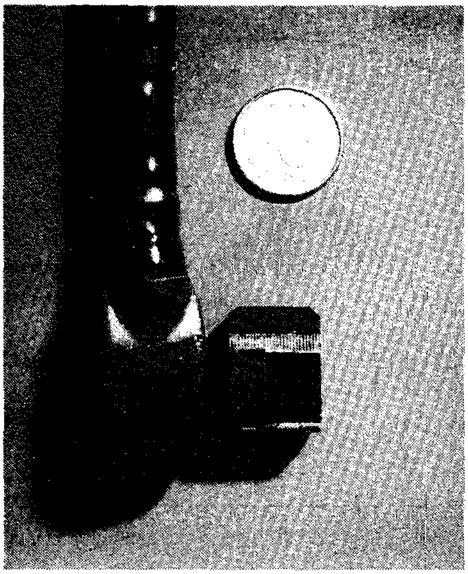

Figure V-4. Prototype next generation 52-element phased array mounted on an endoscope tube. For reference a coin with 15 mm diameter and the partly uncovered array are shown.

'far-off' mean side-lobe level. In ideal situations these quantities are sufficient to characterize the directivity pattern. In most practical systems for clinical diagnosis, however, the theoretical shape of the directivity pattern is distorted due to non-ideal components in the system. Therefore, the abovementioned quantities are insufficient to describe the directivity pattern of such systems completely.

Qualification of the round-trip beam pattern in this study involves the following parameters (see Fig. V-5):

Table V-I. Array parameters

N -	number of elements	=	32
H -	element height	=	10 mm
I -	element width	=	.2 mm
L -	total active aperture	=	7.5 mm
IN -	interelement spacing	=	.254 mm
f_o -	central frequency	=	3.1 MHz
BW -	−6 dB bandwidth	=	1.4 MHz
F -	focal distance	=	30 mm

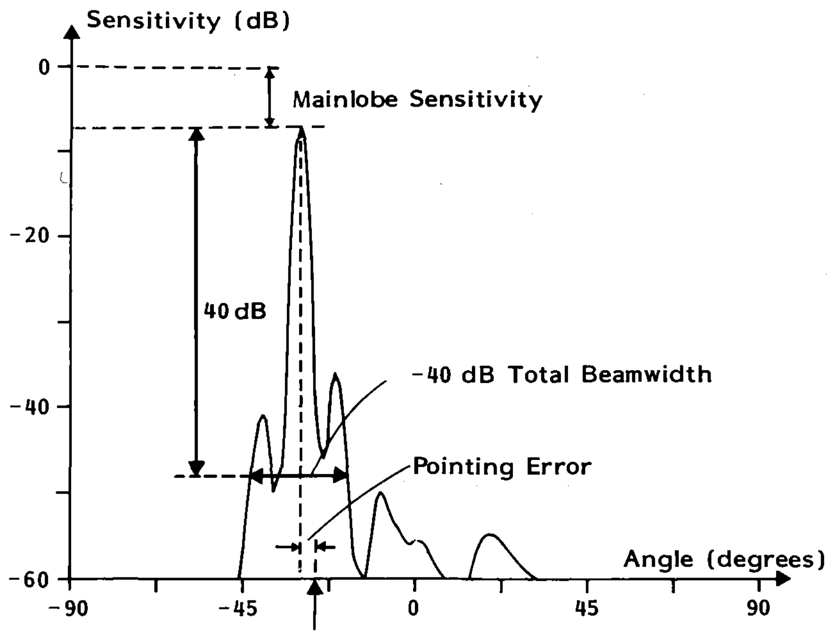

Figure V-5. Definition of the quantitative measures of the beam directivity pattern.

- the pointing error, here defined as the difference between the selected scan angle and the angle at which the maximum of the directivity pattern appears;
- the main-lobe sensitivity, here defined as the ratio between the actual level of the main-lobe and the level of the main-lobe of an ideal system without errors, and
- the –6, –10, –20, –30, –40 and –50 dB beamwidth; the beamwidth at a certain level being defined as the total width of the directivity pattern that exceeds that level.

The resolution and side-lobe structure can only be judged from the complete directivity pattern. However, it is impossible to present all the simulated directivity patterns. The beamwidth as defined above is a condensed method, which will give a fairly good impression of the resolution and side-lobe structure.

EFFECTS OF AMPLITUDE ERRORS ON THE DIRECTIVITY PATTERN

First, the sensitivity of the array elements will vary, because of size variations and inhomogeneities of the ferro-electric material. Second, there will be differences in the transmitted power of the elements due to variance in the electrical and acoustical matching. Finally, there will be variance in the gain of the channel (pre-)amplifiers. There may even be a variance of the impulse response of the elements. We did not include this in our simulations, because its effect should be of less importance, as we experimentally verified using a data set of an actual array. For the sake of simplicity we modelled all possible errors to be errors in sensitivity of the array elements connected to error-free electronics.

Steinberg (9) describes the effects of normally distributed amplitude errors on the far-field directivity pattern of a phased array with ideal omnidirectional elements excitated with a narrow-band signal. Although these limitations are hardly valid for practical phased arrays used for medical diagnosis, it is instructive to see how this theory can be applied to practical ultrasonic phased arrays.

From Steinberg, it follows that in the case of normally distributed amplitude errors compared to the error-free situation:

- the main-lobe of the directivity pattern is hardly affected, so pointing error and main-lobe sensitivity will remain almost unchanged;
- the side-lobe level will change considerably;
- the beamwidth measured at –6 dB will remain practically unchanged; and
- the beamwidth measured at low reference levels will be strongly influenced by side-lobes at those levels.

METHOD

First the array round-trip sensitivity was simulated exactly in the same way as Steinberg (9): the elements are considered point sources with continuous wave excitation at the centerfrequency of the array. The random amplitude over the array exhibited a standard deviation σ_a of 0.37 and a mean amplitude μ_a=1. This high value is chosen to represent a worst case situation. The result is shown in Fig. V-6. The dominant feature is a pronounced side-lobe level far away from the main-lobe. When the simulation is repeated with wide-band excitation, together with the introduction of the element factor, the resulting pattern is quite different, as is illustrated in Fig. V-7. The distribution of the errors has been kept identical. The differences can be explained by the combined effects of lowering of the side-lobe level due to the element factor and decrease of interference due to the wide-band excitation.

For different depths of scanning (20 - 60 mm) and scanning angles (–90° to 90°) we investigated the beam parameters as a function of the variance of the amplitude errors and as a function of the error distribution over the aperture. From the many simulations it is confirmed that, as might be expected, the main-lobe sensitivity depends only on the average sensitivity of the array. Also, the amplitude errors have no effect on the angle of maximum sensitivity, resulting in a negligible pointing error.

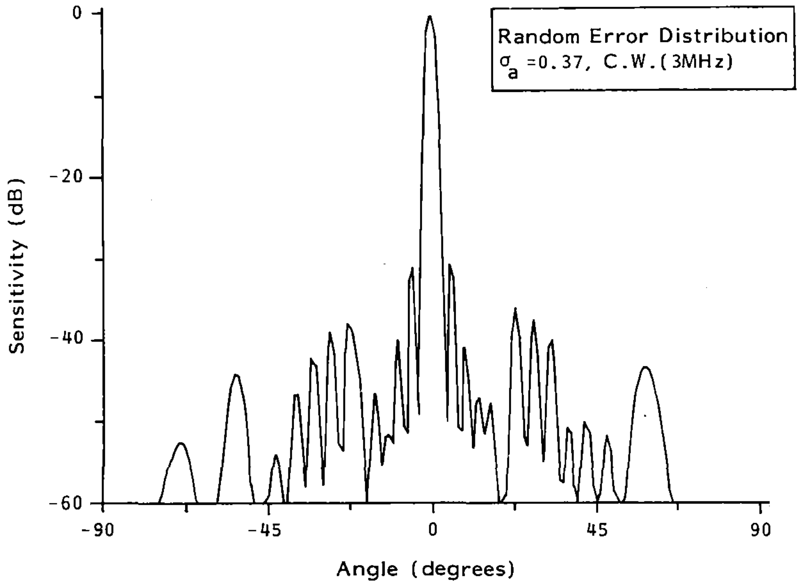

Figure V-6. Far field directivity pattern of a phased array with amplitude errors, CW excitation, element factor is unity (omni-directional elements) following Steinberg (9).

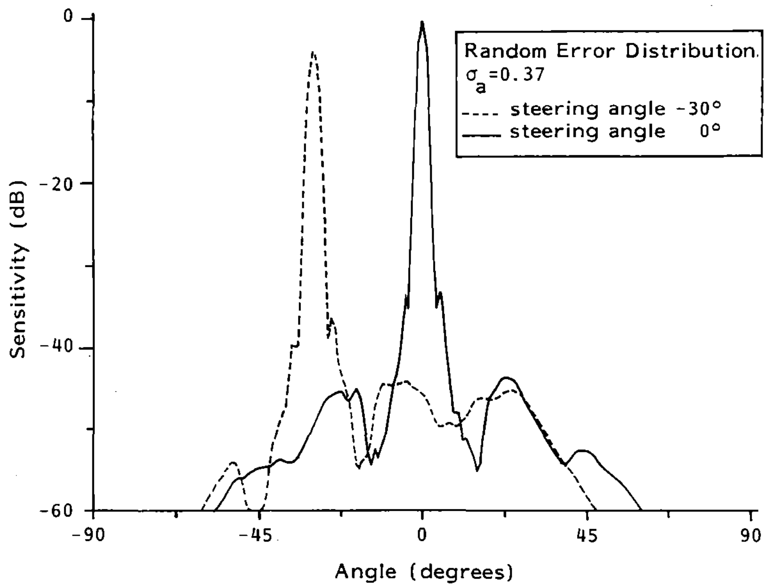

Figure V-7. Far field directivity pattern of a phased array with amplitude errors, pulse excitation and non omni-directional elements.

Calculations showed that with amplitude errors the beam parameters revealed the same dependance on scan angle and depth as without errors. The dashed curve in Fig. V-8 shows the angle dependance of the array with random amplitude error ($\sigma_a = 0.37$) at a steering angle of -30°. Due to the element factor, the sensitivity decreases as function of scan angle, while the beamwidth increases because of the change in effective aperture. At larger scan angles the pattern becomes more asymmetric. This process is almost identical to that of the error-free situation and yields no additional information about the tolerance level of amplitude errors.

From the experiments we concluded that to evaluate the effects of a given set of amplitude errors it is sufficient to compute the directivity pattern only at focal distance (30 mm) and steering angle zero. To reduce the number of simulations, two extreme spatial distributions of the amplitude errors are concerned: a distribution where the errors cause a greater sensitivity of the array at the centre (convex) and one yielding a greater sensitivity at the edges of the aperture (concave).

In order to characterize different sets of amplitude errors two parameters are used:

1. The variance of the amplitude over the array

$$\sigma_a^2 = \sum_{i=1}^{N} \frac{(a_i - \overline{a})^2}{N - 1}$$

where:
a_i = the individual element sensitivity relative to 1
σ_a = the standard deviation
$\overline{a}$ = the average sensitivity, set to be unity.

2. The second central moment of the array sensitivity distribution

$$\sigma_x^2 = \frac{\sum_{i=1}^{N} a_i (x_i - x_o)^2}{\sum_{i=1}^{N} a_i}$$

where:
x_i = the position of element i
x_o = the center of gravity of the array

$$x_o = \frac{\sum_{i=1}^{N} x_i \cdot a_i}{\sum_{i=1}^{N} a_i}$$

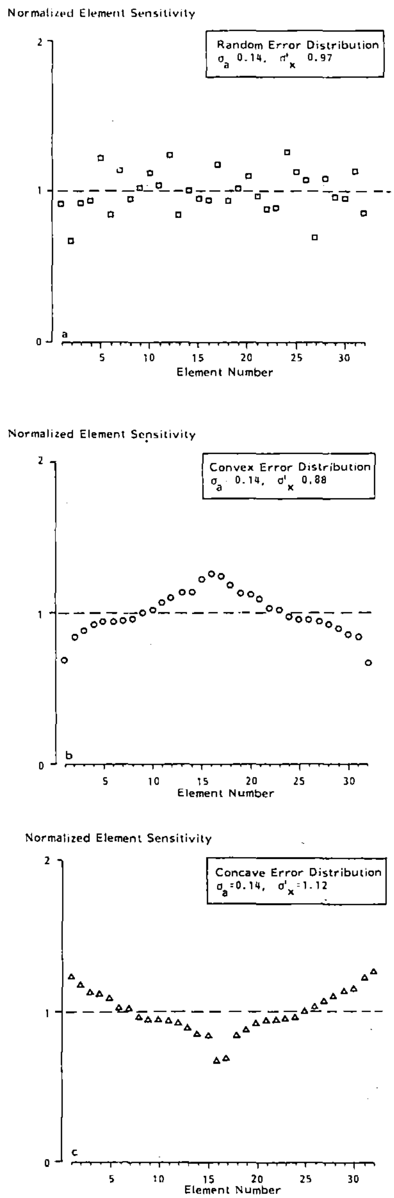

Figure V-8. The 3 selected different arrangements of the amplitude errors over the aperture. Error distribution, σ'_x = 0.14. (a) □, random distribution, σ'_x= 0.97; (b) ○, convex distribution, σ'_x = 0.88; (c) △, concave distribution. σ'_x= 1.12.

It is practical to define a normalized second central moment as:

$$\sigma_x' = \left(\frac{\sigma_x}{\sigma_x^N}\right)^2$$ where $(\sigma_x^N)^2$ is the second central moment of the uniform distribution, i.e. $a_i = 1$ for all i.

The distribution parameters σ_a and σ_x' will exhibit the following characteristics:
σ_a will be a measure of the variance of the element sensitivity.
σ_x' will be a measure of the dispersion of array sensitivity away from the center (9). A greater sensitivity at the center of the array yields $\sigma_x' < 1$. If the array is more sensitive at the edges, then $\sigma_x' > 1$. In the case of a random distribution of the errors, $\sigma_x' \approx 1$.

RESULTS

In Table V-2, a summary is given of the distribution parameters as used in our simulations.

For nine sets of element sensitivity distributions the wide-band round-trip response as a function of angle is calculated at focal distance while the steering angle is kept at 0°. At reference levels –6, –10, –20, –30, –40 and –50 dB a value of the angular resolution is then obtained. When these values are divided by those obtained with a uniform distribution (error-free) the result will be a normalized resolution.

Table V-2. Distribution parameters.

Distribution of element sensitivity	standard deviation σ_a	normalized 2nd central moment σ_x'
Uniform, error-free	0	1
Small variance - random	0.14	0.97
Small variance - convex	0.14	0.88
Small variance - concave	0.14	1.12
Medium variance - random	0.24	0.97
Medium variance - convex	0.24	0.81
Medium variance - concave	0.24	1.19
Large variance - random	0.37	0.93
Large variance - convex	0.37	0.66
Large variance - concave	0.37	1.34

A normalized resolution > 1 indicates that the associated beam is widef than the beam of the ideal array. A normalized resolution < 1 indicates that the associated beam is narrower than the beam of the ideal arrray.

First an array is simulated with small variations in sensitivity, σ_a=0.14. Three possible distributions of the sensitivity over the array are illustrated in Fig. V-8. The resulting beamdwidth at several reference levels normalized on the beam-width obtained with a uniform distribution is plotted in Fig. V-9. When the variations are randomly distributed, as illustrated in Fig. V-8a the differences with the uniform distribution are only marginal. When the sensitivity variations are arranged to produce a concentration around the centre of the array, a distribution is obtained which has been termed 'convex' (Fig. V-8b). This kind of tapering is generally known to broaden the main-lobe and decrease the side-lobe level. The side-lobe level will particularly influence the beamwidth when measured at low reference levels. As can be appreciated from Fig. V-9, the beamwidth at -40 and -50 dB is smaller than that with uniform distribution.

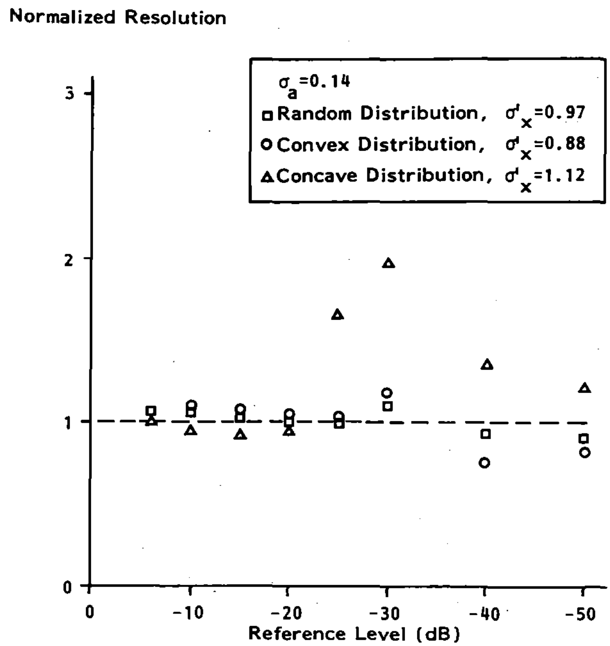

Figure V-9. Normalized lateral resolution in the case of a small range of amplitude errors for 3 different arrangements of the errors. Error distribution, σ_a = 0.14. □, random distribution, σ'_x = 0.99; ○, convex distribution, σ'_x = 0.88; △, concave distribution. σ'_x = 1.12.

An arrangement of the sensitivity distribution towards the edges of the array (Fig. V-8c) will yield the opposite. Now a decrease of the beamwidth at high reference levels is expected, at the cost of an increase in side-lobe level. Fig. V-9 shows that due to side-lobes the beamwidth at the –25 and –30 dB level is suddenly increased for the concave situations. At lower levels this effect is less pronounced.

Simulations performed with a medium variance in array element sensitivity ($\sigma_a = 0.24$) are summarized in Fig. V-10. The concave distribution yielding a σ'_x of 1.19, shows again a step in beamwidth due to increased side-lobe level at reference levels between –20 and –30 dB. The tapered 'convex' distribution, on the contrary, yields an acceptable beamwidth at reference levels above –40 dB. Below this level the beamwidth becomes smaller. The random distribution yields $\sigma'_x = 0.97$ and we may expect no large deviations. The effects of a large variance of the element sensitivity ($\sigma_a = 0.37$) is illustrated in Fig. V-11. The range of σ'_x is now 1 ± 0.35. For the random set, except the –50 dB level, there is still no large deviation, but both the convex and concave distributions show considerable beamwidth fluctuations.

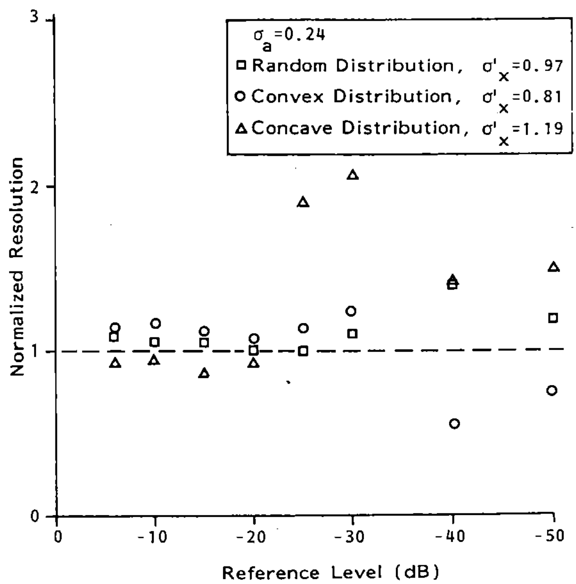

Figure V-10. Normalized lateral resolution in the case of a medium range of amplitude errors for 3 different arrangements of the errors. Error distribution, $\sigma_a = 0.24$. □, random distribution, $\sigma'_x = 0.97$; ○, convex distribution, $\sigma'_x = 0.81$; △, concave distribution. $\sigma'_x = 1.19$.

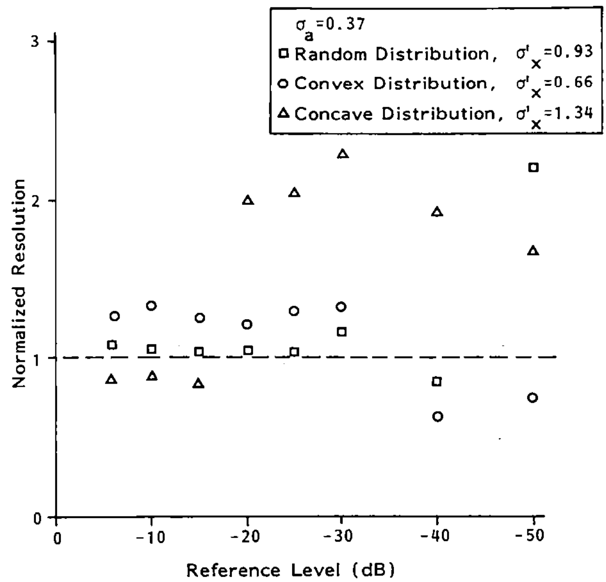

Figure V-11. Normalized lateral resolution in the case of a large range of amplitude errors for 3 different arrangements of the errors. Error distribution, $\sigma_a = 0.37$. □, random distribution, $\sigma'_x = 0.93$; ○, convex distribution, $\sigma'_x = 0.66$; △, concave distribution. $\sigma'_x = 1.34$.

The normalized second central moment σ'_x appears to be a sensitive indicator of the beamwidth at different levels, relative to the uniform distribution. When $\sigma'_x \approx 1$ the beamwidth will not differ much. When σ'_x is > 1.1, the side-lobe level will be responsible for a sudden increase in beamwidth at a level of –20 to –30 dB. If, however, σ'_x is < 0.8 the beam will broaden only slightly at high reference levels, while at lower levels the beamwidth will be superior to the uniform distribution.

The model was applied to a prototype array which exhibited an element sensitivity pattern described by $\sigma_a = 0.21$ and $\sigma'_x = 1.03$. With respect to the abovementioned simulation results, we considered this array to be an acceptable and desirable product.

CONCLUSIONS

To evaluate the effect of a given set of amplitude errors it is sufficient to evaluate the beam parameters obtained at zero degrees steering angle in the focal area. Amplitude errors will have only marginal effects on phased array performance when they are randomly distributed and the variance is not too large ($\sigma_a < 0.3$). A measure of the distribution of the errors is given by the second central moment, normalized on the error-free situation; σ_x'. For a prototype array the element sensitivities can be regarded as a sample taken at random from a normally distributed set, with mean 1.00 and variance σ_a^2.

When the value of σ_x' is > 1.2, or < 0.7 serious doubts on the performance of the phased array may be justified.

It may be shown (see Appendix) that for normally distributed errors rearranged as continuously increasing towards the centre (extreme convex), the analytical relation between σ_x' and σ_a becomes:

$$\sigma_x' = 1 - \frac{3\,\sigma_a}{2\sqrt{\pi}}$$

For the extreme concave distribution the analytical relation between σ_x' and σ_a becomes:

$$\sigma_x' = 1 + \frac{3\,\sigma_a}{2\sqrt{\pi}}$$

Therefore, we may expect a value for σ_x' in the range

$$1 - \frac{3\,\sigma_a}{2\sqrt{\pi}} \leqslant \sigma_x' \leqslant 1 + \frac{3\,\sigma_a}{2\sqrt{\pi}}$$

There are two criteria to estimate the quality of the array performance:

1. σ_a is small, yielding a possible extreme of σ_x' close to the optimal value of 1. Performance will be adequate; and
2. σ_a is large, then the actual value of σ_x' will be conclusive whether or not the array performance will be adequate.

For a certain array much can be gained if the associated electronics are designed in such a way that overall transfer characteristics can be tuned to obtain a more acceptable distribution. However, instruments with different plug-in transducers will depend on properly designed transducers meeting the requirements mentioned above.

ACKNOWLEDGEMENT

We would like to thank Dr. W.J. Gussenhoven, who clinically evaluated the described transesophageal scanning system.

REFERENCES

1. *Von Ramm OT et al (1983) Beam Steering with Linear Arrays. IEEE Transactions on Biomedical Engineering. Vol. BME-30, No. 8: 438-452.*
2. *Berlincourt NA, Curran DR, Jaffe H (1964) Piezo-electric and piezomagnetic materials. In: Physical Acoustics (W.P. Mason, ed) Vol I-A. Academic Press, New York: 170.*
3. *Krimholtz R, Leedom DA, Matthaei GL (1970) New equivalent circuits for elementary piezo-electric transducers. Electronic Letters 6(13): 63.*
4. *Berkhout AJ (1980) Seismic Migration, Elsevier, Amsterdam.*
5. *Smith SW, Von Ramm OT, Haran ME, Thurstone FL (1979) Angular Response of piezoelectric elements in phased array ultrasound scanners. IEEE Trans Sonics Ultrasonics SU-26(3): 185.*
6. *Freedman A (1971) Far Field of Pulsed Rectangular Acoustic Radiator. J Acoust Soc Am 49: 738.*
7. *Lancée CT, Ligtvoet CM, De Jong N (1982) On the design and construction of a transesophageal scanner. In: Cardiovascular Diagnosis by Ultrasound (P. Hanrath, W. Bleifeld and J. Souquet, eds). Martinus Nijhoff Publishers, The Hague/Boston/London: 208-215.*
8. *De Jong N, Lancée CT, Gussenhoven WJ, Bom N, Ligvoet CM (1985) Transesophageal Echocardiography. Proc XIV Int Conf Med Biol Engng and VII Int Conf Med Phys, Espoo, Finland (J Int Med & Biol Engng 23 (Suppl 1): 204-205.*
9. *Steinberg BD (1967) Principles of Aperture and Arrays System Design. Wiley, New York.*

CHAPTER VI

INFLUENCE OF PHASE ERRORS ON BEAM-STEERED PHASAED ARRAYS

C.T. Lancée, J.M. Vissers, S. Mientki, C.M. Ligtvoet and N. Bom

Abstract

For the image quality of two-dimensional ultrasound systems spatial resolution is one of the most important parameters. This resolution is determined by the directivity pattern. In practice the directivity pattern of phased arrays will be distorted due to errors in critical components. In a previous study, the influence of amplitude errors has been dealt with. In this second study, the parameters describing the range and the nature of phase errors are derived. With these parameters a qualitative prediction of the directivity pattern seems to be possible. Within the design limits of a given phased array, means are indicated to minimize the beam distortion due to occurring phase errors.

Published in Ultrasonics 25: 154-159, 1987.

INTRODUCTION

In this Chapter the effect of phase errors on the beam profile of phased arrays is discussed. The transducer used as an input model for this study has been described previously (1) and the relevant data are summarized in Table VI-1. The phase errors in the combined system of transducer and mainframe are assumed to result from the mainframe electronics alone. The first part of this Chapter will discuss the validity of previously used approximations such as continuous wave (CW) field, and the stochastic nature of phase errors (3-5). In the second part we will discuss the relation between phase truncation and beam steering, together with focussing.

To facilitate comparison of the results to previous theories, the element factor is set to unity. This is done by means of calculating with the Rayleigh 1 operator (2) and infinitely small elements. In practical systems a different phasing can be

Table VI-1. Array parameters used in input model.

Number of elements, N	32
Element height, H (mm)	10
Element width, I (mm)	0.2
Total active aperture, L (mm)	7.5
Interelement spacing, IN (mm)	0.254
Central frequency, f_o (MHz)	3.1
-6 dB bandwidth, BW (MHz)	1.4
Focal distance, F (mm)	30
Time discretization, ϕ step (ns)	$1/4f_o = 80$

applied in the emission and reception mode. In this study the effects of phase-errors are analysed in the emission mode only. Furthermore, phasing means a different time correction for every frequency component and, therefore, the necessary corrections are treated in terms of travel times of a broad-band signal.

THEORY

To control the beam steering and focussing of a phased array the signals of the individual elements must be phase corrected. Errors in this phasing are caused by the inaccuracy of the transmitter and receiving electronics and the delays used for phasing. In most clinical phased array systems the phase correction is achieved by tapped delay lines.

The phase errors introduced by the discretisation of the delays are usually greater than those introduced by other parts in the electronic circuitry. In this Chapter only the effect of phase quantization is investigated. Zeger (3) has studied the effects of quantization of the time delays by means of continuous wave (CW) simulations. In that study the effects on beamwidth, side-lobe level, pointing error and main-lobe sensitivity are analysed. An assumption commonly made in studies on the effect of phase errors, is that the phase errors can be described by a stochastic process. The phase errors are then assumed to have a certain probability distribution, for instance a uniform or a normal distribution. For all distributions of the phase errors, the characteristic function, Φ, can be defined as:

$$\Phi = E\{e^{-j\delta\phi}\} = \int_a^b p(\delta\phi)\, e^{-j\delta\phi}\, d(\delta\phi) \qquad [1]$$

where:

a, b = boundaries of the phase error
Φ = characteristic function
E{} = expectation
$p(\delta\phi)$ = probability distribution of the phase error
$\delta\phi$ = the phase error

Compared to the situation without errors, phase errors reduce the main-lobe sensitivity. For an array with N independent elements this reduction can be seen as the reduction of the mean element sensitivity. The mean element sensitivity is given by $|\Phi|^2$, the main-lobe sensitivity is reduced by a factor of

$$1 - |\Phi|^2 \qquad [2]$$

The side-lobe level will follow an increase proportional to:

$$\frac{1 - |\Phi|^2}{2} \cdot \frac{1}{N} \qquad [3]$$

Zeger (3) has studied the effects of phase errors for the case of a uniform distribution over plus or minus half the quantization step. Steinberg (4) has considered the normally distributed phase errors.

The major objection against the abovementioned stochastic approach is, that for an existing array configuration and a given quantization step of the time delays, the phase error of each element can be calculated exactly. It is, therefore, incorrect to assume that these errors are independent of each other. This has also been noted by Bates (6) and 't Hoen (7).

For the far-field situation without beam steering we calculated the phase errors of each element. The use of time quantization in discrete steps causes the errors to remain within plus or minus half this step size. As a measure of the severity of the phase errors we calculated the standard deviation, σ, of the phase errors, defined as:

$$\sigma = \left(\frac{\sum_{i=1}^{N} (\delta\phi_i - \mu_{\delta\phi})^2}{N - 1} \right)^{1/2} \qquad [4]$$

where

$\delta\phi_i$ = phase error of element i
$\mu_{\delta\phi}$ = mean phase error
N = number of elements

A mean value of the phase errors has no effect on the directivity pattern because it only yields a time shift of the scanline concerned.

For a steering angle of zero degrees, we simulated two extreme error distributions, for which one half of the array exhibits an error of plus half a step and the other half of minus half a step. σ reaches its maximum value under these circumstances (i.e. $\sigma_{max} = [(0.5)^2 x\,(32/31)]^{1/2} = 9.508$ step).

The first extreme distribution occurs when the errors are concentrated in two opposite parts of the array, as illustrated in Fig. VI-1. The corresponding beam

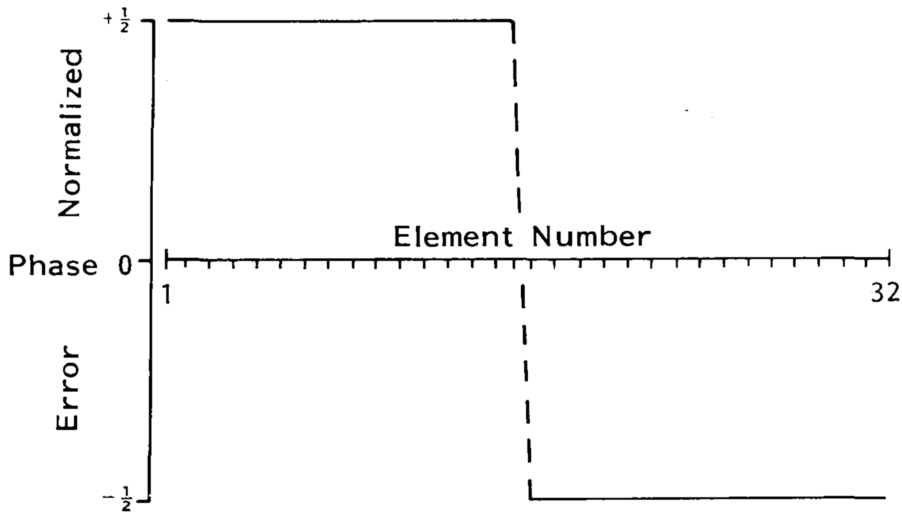

Figure VI-1. Normalized phase error over the array for the maximum value of the standard deviation (σ).

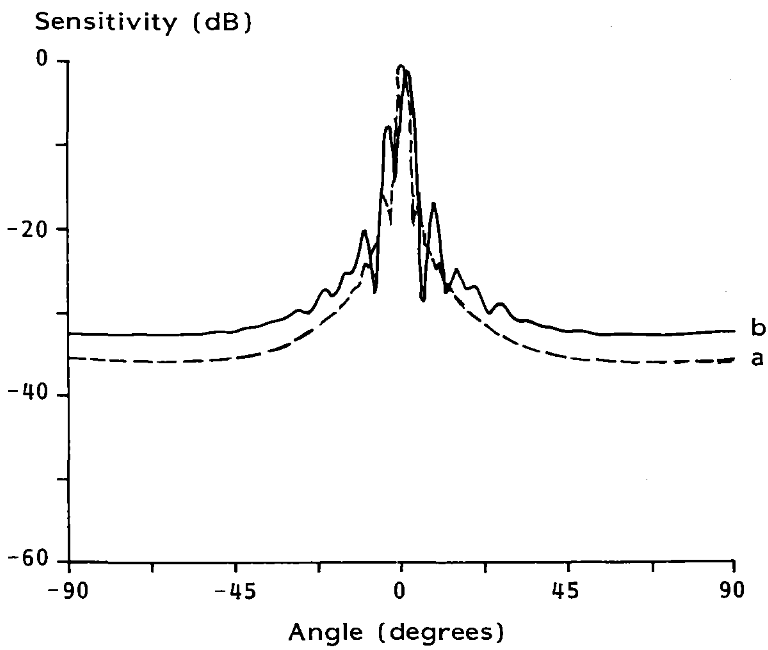

Figure IV-2. a, optimal far-field pattern for the configuration used in this Chapter; b, Far-field pattern when the phase errors from Fig. VI-I are applied.

pattern is shown in Fig. VI-2. The pattern shows a large pointing error and increased beamwidth. The 'far-off' side-lobe level is acceptable. At exactly zero degrees the main-lobe is 3 dB down. Since the stepsize has been chosen to be one quarter the period of the central frequency, consuquently $1 - |\Phi|^2$ amounts to -3 dB.

The second extreme distribution occurs when the errors are distributed so that the delay between neighbouring elements equals the time quantization step, as illustrated in Fig. VI-3. The corresponding beam pattern is shown in Fig. VI-4. One curve is the normally generated broadband simulation, the other is the center frequency CW simulation to emphasize the appearance of grating lobes. The patterns again show a 3 dB reduction of the main-lobe at zero degrees, with no pointing errors or increased beamwidths. The increased far-off side-lobe level is caused by grating lobes generated as a result of the doubled effective interelement spacing, yielding a grating lobe at 70°. The array can be thought to be composed of two separate arrays, each with a doubled interelement spacing and time shifted relative to each other by one quantization step (one quarter period of the central frequency).

Although for these two spatial distributions of the phase errors the characteristic function, Φ, is the same, Figs. VI-2 and VI-4 differ substantially. The general prediction of the side-lobe level increase as given by Equation [3] is not applicable here. From these figures it is also concluded that the analysis of the effects of phase errors on the directivity pattern with the aid of one parameter σ, describing the range of errors, irrespective of their spatial distribution, will in general not provide a predictive value.

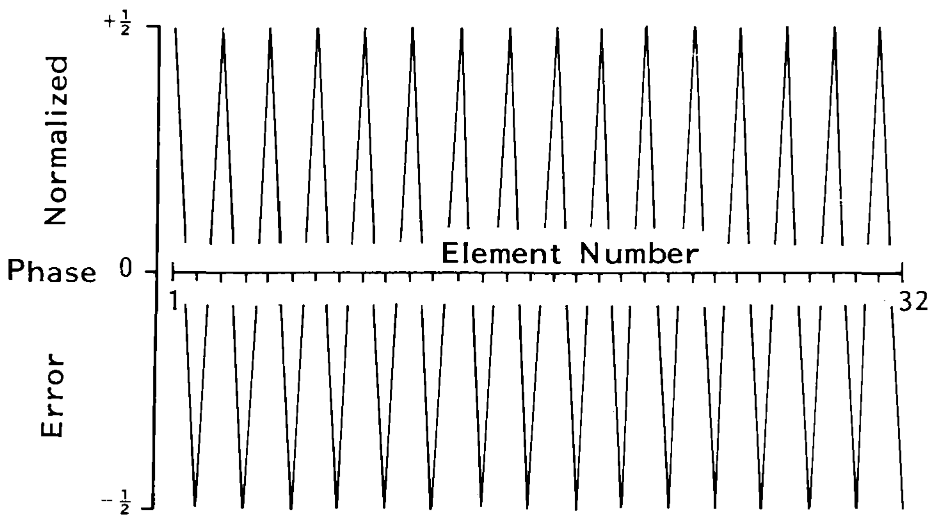

Figure VI-3. Normalized phase error over the array for the maximum value of σ. The phase of adjacent elements differs by one quantization step.

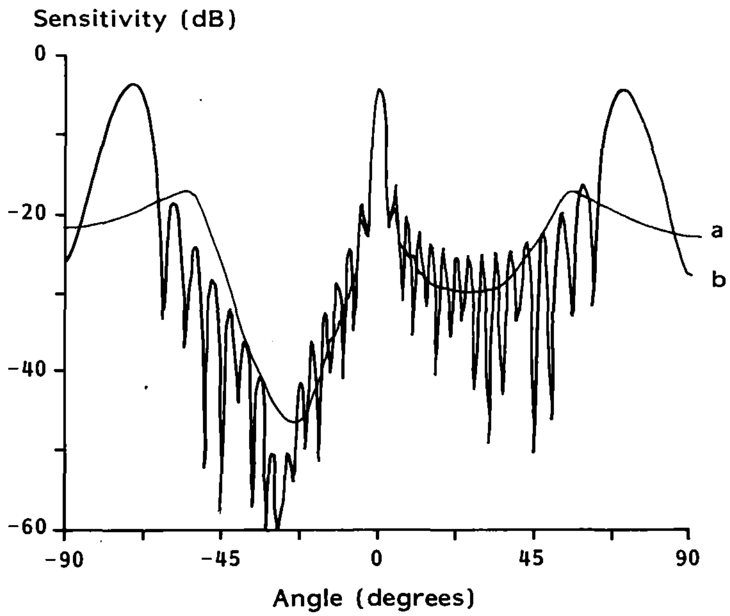

Figure VI-4. Far-field pattern with phase errors corresponding to Fig. VI-3. a, pulsed simulation; b, CW-simulation.

Effects of phase errors on beamsteering

To ensure that all beam deformations are caused by phase errors, amplitude errors are excluded from the calculations. To understand the effects of time discretization it is convenient to first consider a continuous aperture with a corresponding travel time correction at steering angle θ_o:

$$\phi_c(x) = \frac{-x \sin \theta_0}{c} + \phi_0 \qquad [5]$$

where:

$\phi_c(x)$ = correction time for a continuous aperture
x = coordinate over the aperture
θ_o = steering angle
c = sound velocity
ϕ_o = constant time offset.

In practical systems the constant offset, ϕ_o, is added to ensure only positive time delays.

For discrete elements the position of the elements along the axis is given by

$$x_n = (n + \Delta) \cdot IN \qquad [6]$$

where:
x_n = position of element n
n = element number (+ or –)
IN = interelement spacing
Δ = offset: an odd number of elements yields $\Delta = 0$,
and an even number $\Delta = 1/2$.

Let the time quantization step be ϕ_{st}, then, with discrete elements and a quantization of the delays, the discrete phase is given by:

$$\phi_n(x_n) = \phi_{st} \cdot \mathrm{Int}\left\{\frac{-x_n \cdot \sin\theta_0}{c \cdot \phi_{st}} + \frac{\phi_0}{\phi_{st}}\right\} \qquad [7]$$

where Int {...} denotes truncation to the nearest integer value. The phase error function is now a discrete function given by the difference between ϕ_c and ϕ_n at position x_n.

$$\phi_c(x_n) - \phi_n(x_n) = \frac{-x_n \sin\theta_0}{c} + \phi_0 - \phi_{st} \cdot \mathrm{Int}\left\{\frac{-x_n \cdot \sin\theta_0}{c \cdot \phi_{st}} + \frac{\phi_0}{\phi_{st}}\right\} \qquad [8]$$

This discrete error function may be normalized to ϕ_{st}, and division by ϕ_{st} yields:

$$\frac{\phi_c(x_n) - \phi_n(x_n)}{\phi_{st}} = \frac{-x_n \sin\theta_0}{c\phi_{st}} + \frac{\phi_0}{\phi_{st}} - \mathrm{Int}\left\{\frac{-x_n \cdot \sin\theta_0}{c \cdot \phi_{st}} + \frac{\phi_0}{\phi_{st}}\right\} \qquad [9]$$

The function of Equation [9] will vary within the range of + 1/2 to –1/2. Extreme examples of Equation [9] are given in Figs. VI-1 and VI-3.

A first indication of the severity of the phase errors of Equation [9] is obtained by the value of σ/σ_{max} from Equation [4], although it is not always conclusive, as we showed earlier. For a given array with steering angle θ_o all parameters of Equation [9] are known except for the time offset ϕ_o. Variation of ϕ_o will directly influence the truncation term in combination with element position x_n. Consequently for each particular value of ϕ_o a unique error distribution over the array will result exhibiting a unique value of σ. In the next section we will show that an optimal value of ϕ_o for each steering angle ϕ_o will minimize the value of σ and, consequently, improve the resulting beam pattern.

For our configuration the maximum and minimum value of σ are numerically calculated for steering angles between 0° and –40°. For each steering angle a minimum value of ϕ_o is established providing positive delays for all elements. The resulting truncated delays yield a unique error distribution over the array for which σ is calculated. Then ϕ_o is incremented with a fraction of the quantization step. Again, σ of the resulting error distribution is calculated. This process is repeated until the maximum value of ϕ_o is reached, i.e. $\phi_{[start]}+\phi_{step}$. The minimum and maximum value of σ are plotted in Fig. VI-5 together with σ for the starting value of ϕ_o. The next steering angle is selected and the procedure is repeated.

The results are shown in Fig. VI-5. The dashed line indicated by 'b' shows the typical normalized σ associated with a fixed value of the time offset, ϕ_o, as a function of steering angle. The curve 'a' shows the angle dependance of the minimized σ while curve 'c' shows the maximized σ. Notice the large value of the maximum σ for steering angles close to 0° and –28°. For these angles, the phase error distribution over the aperture is similar to the one shown in Fig. VI-1. The corresponding beam pattern is shown in Fig. VI-6 for a scan angle of –28°. Both continuous wave (curve b) and braodband (curve a) simulations are shown.

The extreme values of σ occur when the sound travel time at angle θ_o results in a phase between adjacent elements of precisely ϕ_{st}. If this condition is met, with a time off-set $\phi_o = 0$, one side of the array has a normalized phase error of $+ 1/2$ and the other side of $-1/2$. This is identical to the situation described earlier (Fig. VI-1), $\sigma = \sigma_{max}$ or $\sigma/\sigma_{max} = 1$. In this case the minimum value of σ is obtained by taking a time offset $\phi_o = 1/2\ \phi_{st}$. The phase errors are now zero for all the elements. The artifacts in the generated beam pattern have disappeared as shown in Fig. VI-7.

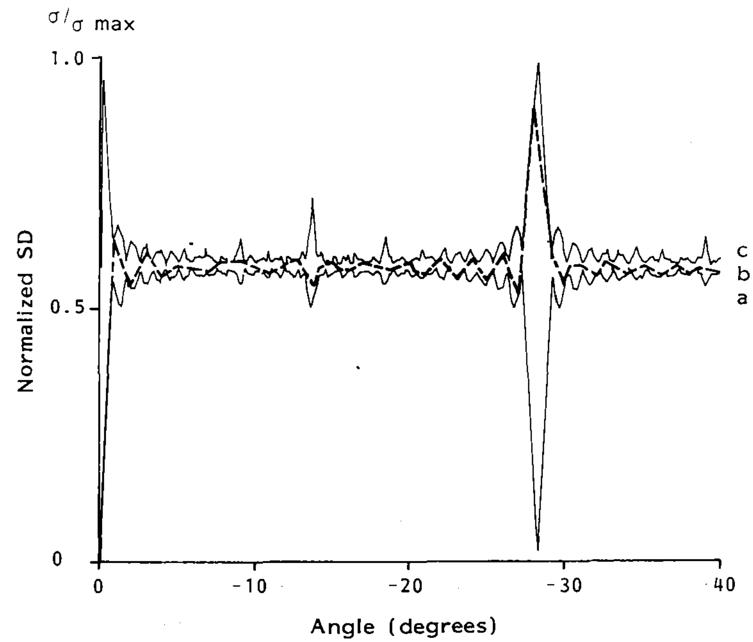

Figure VI-5. Normalized values of σ of the phase errors, as a function of steering angle, without focussing. a, Numerically minimized values of σ by varying the time offset; b, σ with constant time offset, typical value; c, numerically maximized values of σ.

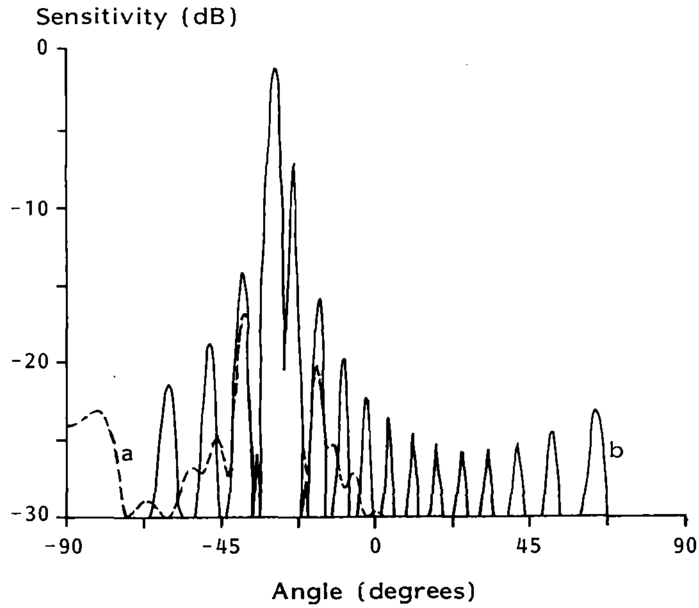

Figure VI-6. Far-field pattern with phase errors corresponding to the maximum value of σ with steering angle of −28°. a, Pulsed simulation; b, CW-simulation.

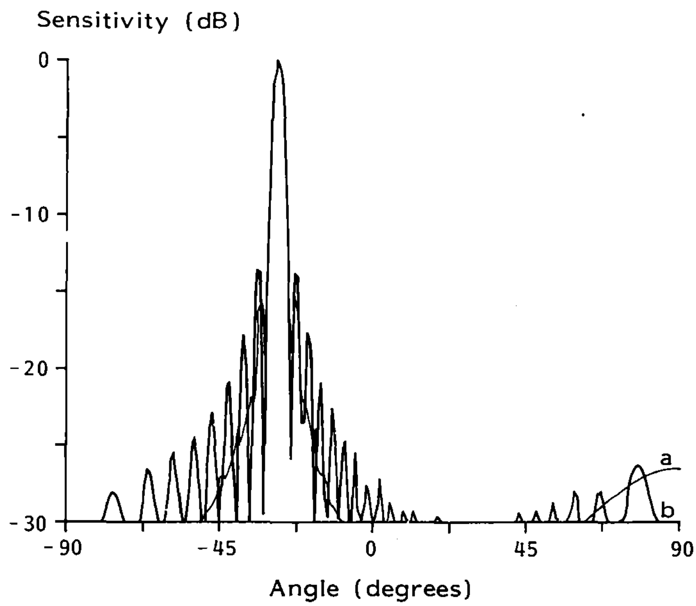

Figure VI-7. Far-field pattern with phase errors corresponding to the minimum value of σ (i.e. zero) with steering angle of −28°. a, Pulsed simulation; b, CW simulation.

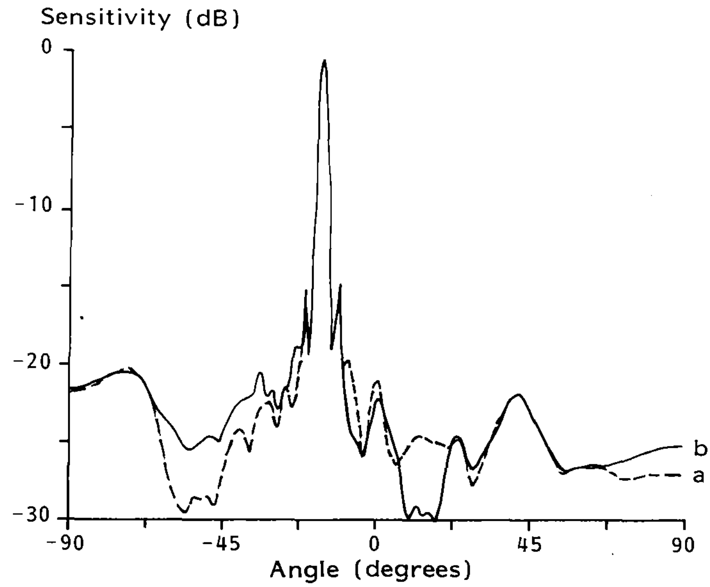

Figure VI-8. Far-field pattern for a steering angle of −16°. a, Normalized phase errors corresponding to minimized value of σ; b, Normalized phase errors corresponding to maximized value of σ.

The difference between the minimum and maximum σ, i.e. the difference between curves a and c in Fig. VI-5, is small for other steering angles. As an example, the situation for a steering angle of 16° is shown in Fig. VI-8.

Effects of phase errors on beamsteering and near field focussing

In the previous section we discussed the effects of phase errors on beam steering alone. This paragraph will deal with the effects of phase errors on the beam profile of a beam-steered and focussed array. The focussing of this particular array will be calculated for a focal distance of 30 mm yielding an F-number of F = 4. As in the case of beamsteering alone, the σ of the phase errors is used as an indication of the severity of the phase errors. Again, numerically minimizing and maximizing σ by means of varying the time offset is performed (Fig. VI-9) for a focus at 30 mm and a steering angle of 0 to −40°. The obtained values of the normalized results are shown in Fig. VI-9. As may be expected, less pronounced extreme values of σ are found. The largest difference between the maximum and minimum value is found to be 0.19 σ_{max} at steering angles of −4° and −28°.

For a steering angle of −4° a relative large difference is found. The corresponding beam patterns are shown in Figs. VI-10 (minimum σ) and VI-11 (maximum σ). For a steering angle of 16° the difference between the extreme values of σ is small (0.05 σ_{max}). The influence on the beam pattern is only marginal (Figs. VI-12 and

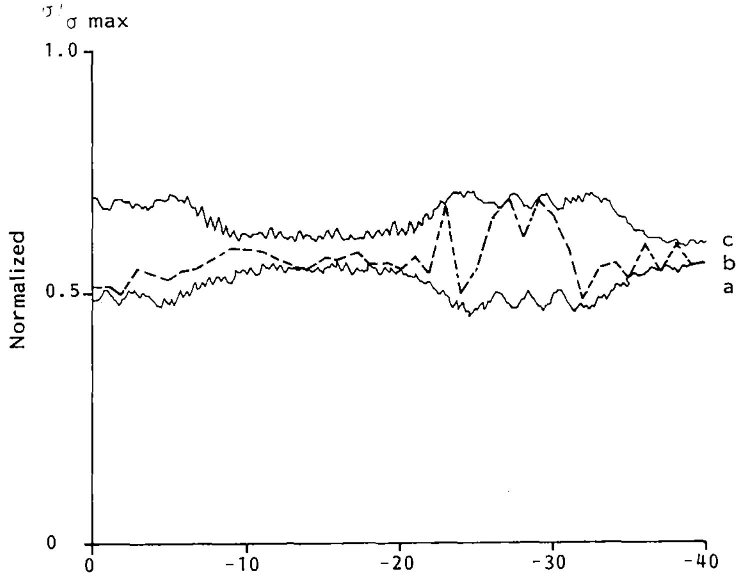

Figure VI-9. Normalized values of σ of the phase errors as a function of steering angle, while focussing at 30 mm. a, minimized values of σ; b, calculated with fixed time-offset; c, maximized values of σ.

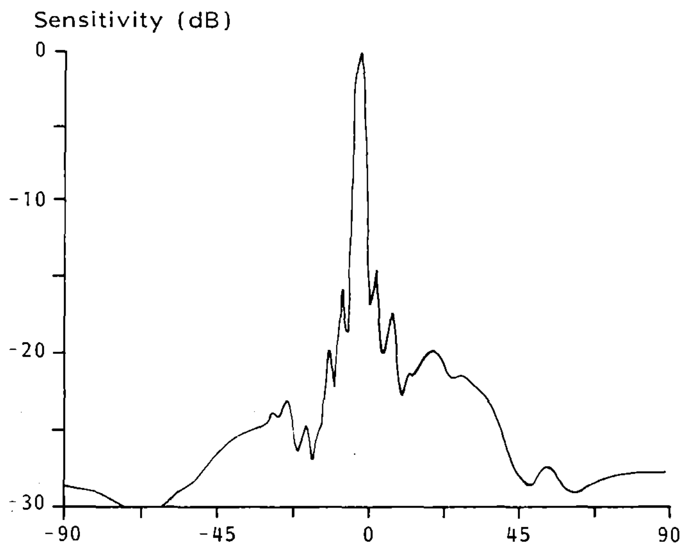

Figure VI-10. Directivity pattern in the focal plane, with minimized value of σ (0.49 σ_{max}), for a steering angle of −4° and focus at 30 mm.

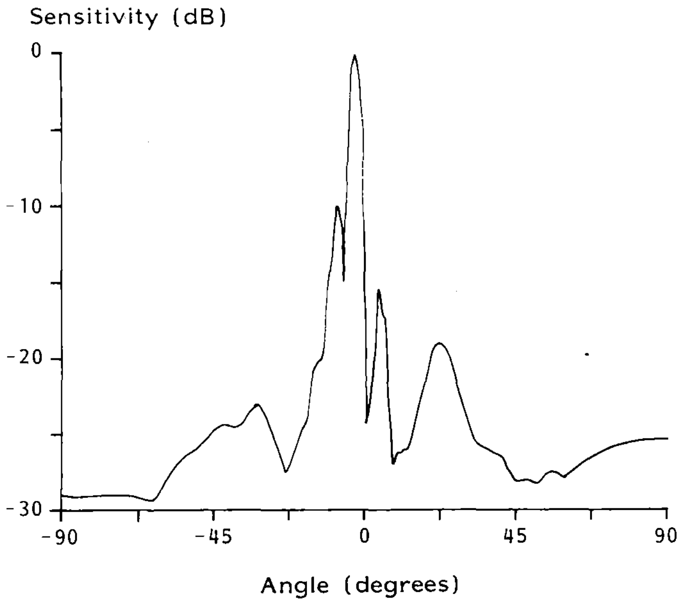

Figure VI-11. Directivity pattern in the focal plane, with maximized value of σ (0.67 σ_{max}) for a steering angle of –4° and focus at 30 mm.

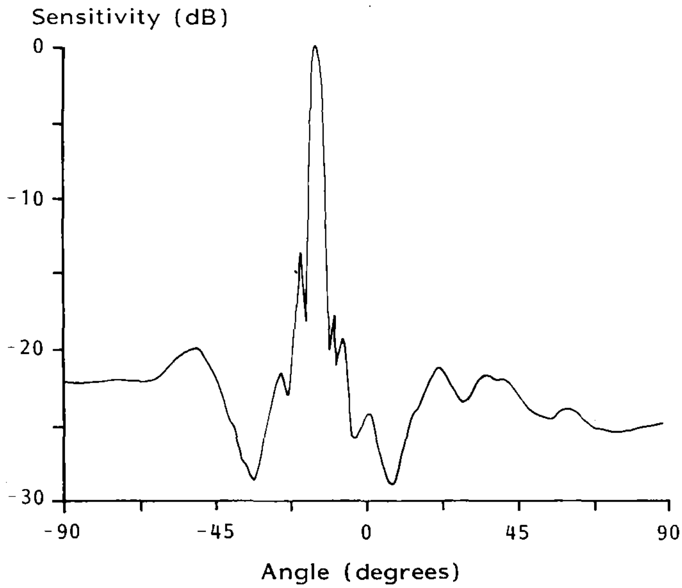

Figure VI-12. Directivity pattern in the focal plane, with minimized value of σ (0.56 σ_{max}) for a steering angle of –16° and focus at 30 mm.

VI-13). For a steering angle of −28° the difference is relatively large again (i.e. 0.19 σ_{max}). The corresponding beam patterns (Figs VI-14 and VI-15) show a large difference in side-lobe level. When the focus is moved away from the array, the variance of the phase errors increases and tends towards the far-field situation. This effect is illustrated in Fig. VI-16 for the curves with foci at 20 and 50 mm (F-numbers 2.7 and 6.7, respectively).

CONCLUSIONS

It is shown that the effects of phase quantization cannot be described as a stochastic process. A parameter proportional to only the range of the phase errors, instead of including dependence on their spatial distribution, will not be sufficient to predict the effects of these errors on the directivity pattern. Minimizing the range of the phase errors will reduce the possible distortions of the beam pattern. The effects of the set of phase errors actually obtained can then be evaluated with the aid of the simulated directivity pattern. A parameter applicable to specify the severity of possible distortions of the beam pattern due to phase errors, is the minimized standard deviation, σ, of those errors. For an array with discrete elements and the use of tapped delay lines the value of σ varies with focussing

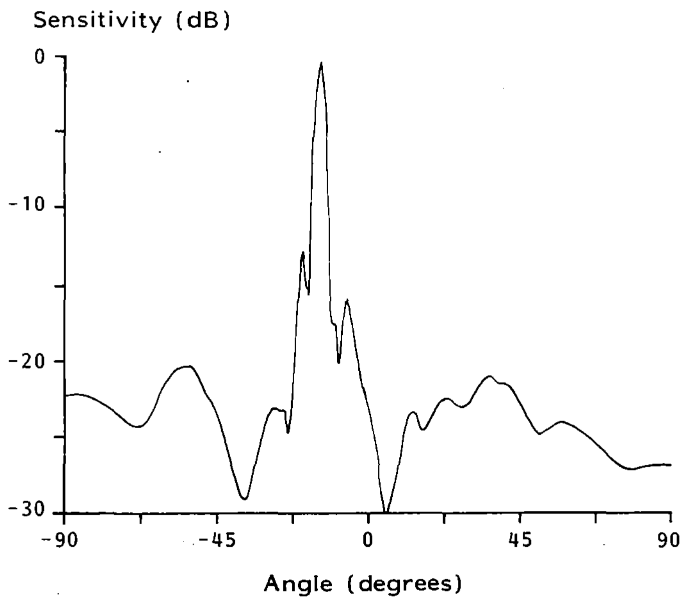

Figure VI-13. Directivity pattern in the focal plane, with maximized value of σ (0.61 σ_{max}) for a steering angle of −16° and focus at 30 mm.

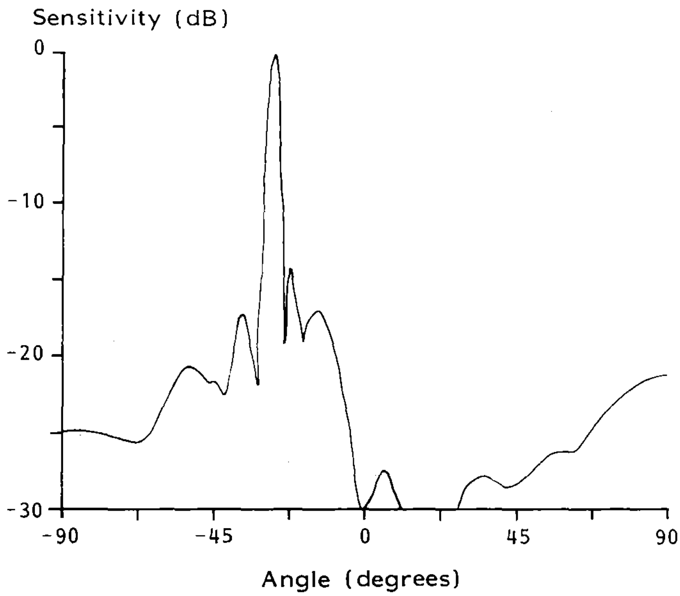

Figure VI-14. Directivity pattern in the focal plane; with minimized σ (0.48 σ_{max}) for a steering angle of −28° and focus at 30 mm.

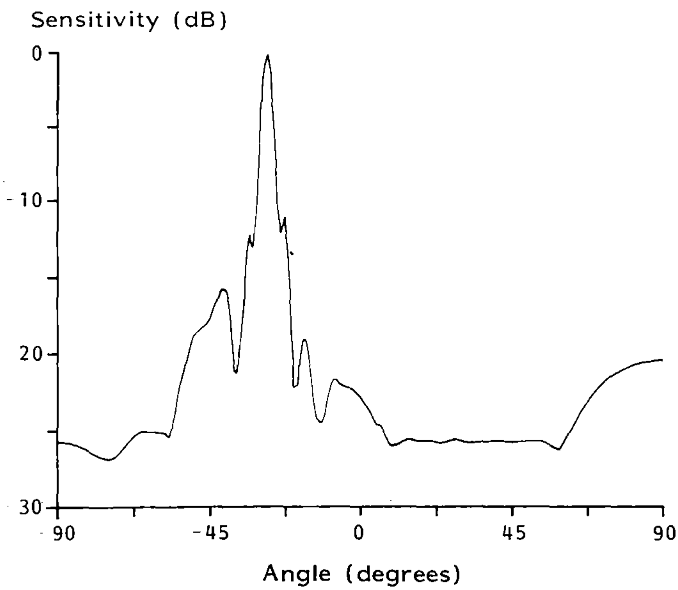

Figure VI-15. Directivity pattern in the focal plane; with maximized σ (0.68 σ_{max}) for a steering angle of −28° and focus at 30 mm.

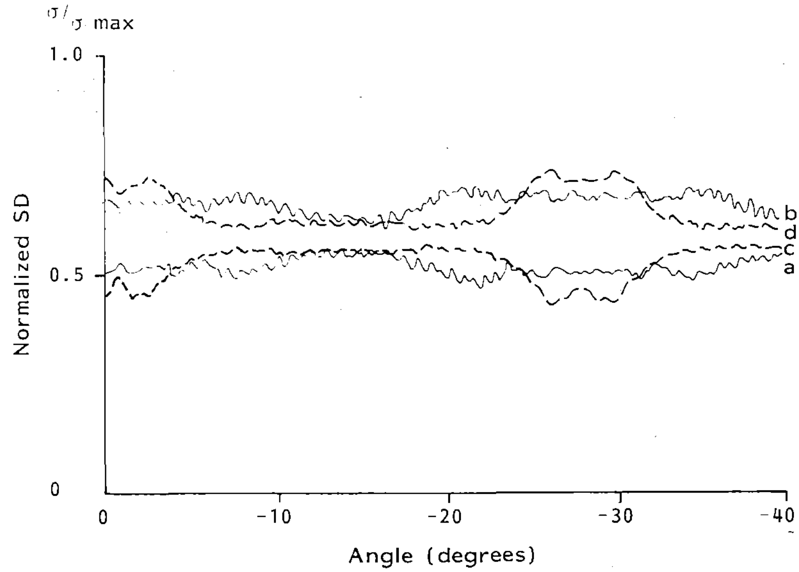

Figure VI-16. Normalized σ of the phase errors as a function of steering angle for different foci. a, Minimized σ for focussing at 20 mm; b, Maximized σ for focussing at 20 mm; c, Minimized σ for focussing at 50 mm; d, Maximized σ for focussing at 50 mm.

depth and steering angle. The criterion used to truncate the optimal time delays can be selected in such way that a minimum value of σ occurs. This is achieved by applying a time shift to the scan-line concerned, before the truncation is executed. Minimizing the phase errors is reduced to minimizing the value of σ. If the directivity pattern for the worst case of this minimum value is still unacceptable, according to the designer's specifications, only a smaller time quantization stap can improve the pattern. We found that for all quantization steps the value of the worst case minimized σ : $\sigma_{min} \approx 0.5\ \sigma_{max}$.

Future developments of phased arrays in medical ultrasound will be in the digital processing of transducer signals. Consequently, not only will the signals be discretizised in time, but in amplitude as well. Further investigation is required to evaluate the combined effect of errors both in time and in amplitude. The amplitude errors due to discretization will be negligible in most practical situations when compared to those arising from the variance in element and channel sensitivities.

REFERENCES

1. *Lancée CT, Vissers JM, Mientki S, Ligtvoet CM, Bom N. (1987) Influence of amplitude errors on beam-steered phased arrays. Ultrasonics 25: 147-153.*
2. *Berkhout AJ (1980) Seismic Migration. Elsevier, Amsterdam.*
3. *Zeger AE (1972) Antenna Array Tolerance Theory, unpublished course notes, University of Pennsylvania, July 1972.*
4. *Steinberg BD (1967) Principles of Aperture and Arrays System Design. New York, Wiley.*
5. *Beaver WL (1977) Phase Error Effects in Phased Array Beam Steering, Ultrasonics Symposium Proceedings, Phoenix, IEEE Cat#77CH1264-ISU: 264-267.*

5\. *Bates KN (1980) Tolerance Analysis for Phased Arrays. Acoustical Imaging 9 (Visualisation and Characterization, Proceedings 9th International Symposium, Houston, Texas, 3-6 Dec. 1979) New York, Plenum Press: 239-262.*

7\. *'t Hoen PJ (1983) Influence of component errors in the directivity function of pulsed, ultrasonographic linear arrays. Ultrasonics 21: 275-279.*

CHAPTER VII

MONITORING ASPECTS OF AN ULTRASONIC ESOPHAGEAL TRANSDUCER

C.T. Lancée, H. Rijsterborgh, N. Bom

Abstract

A method of semi-automatic contour detection is described using a commercial (Kontron) image analysis instrument. Input data consists of high-quality transesophageal echocardiograms of short-axis left ventricular cross-sections. The purpose of the study is to evaluate the feasibility of such a method for the quantitative monitoring of the dynamic behaviour of the left ventricle during high risk surgery.

It is concluded that, although qualitative results may be useful, the derived dynamic contour depends too much on circumstantial parameters which renders impredictable variation in the quantitated function descriptors.

Submitted for publication.

INTRODUCTION

Since the introduction of M-mode echocardiography, the possible application of ultrasound for monitoring purposes has intrigued many investigator. Practical limitations such as probe fixation, and manipulation have blocked the way to successful clinical application of such a method using the classical precordial approach. Also for two-dimensional echocardiography no practical solution has been reached to obtain a consistent cross-sectional image of the heart during the whole monitoring episode.

With the introduction of the endoscope-mounted electronic sector scanner monitoring came within reach. Now a probe became available that remained stationary at a selected position inside the patient.

Monitoring during surgery using this technique yields the following operational advantages:

- the thoracic area is not occupied with interfering instrumentation;
- patients with substandard precordial image quality may still be studied;

- interference with the anaesthetist's equipment is minimal;
- image quality will be optimal during the whole procedure with minimal adjustments;
- there is no need for the transducer assembly to be sterile.

Several institutes reported on the use of such an instrument in a great many surgical cases (1-2).

PROBE POSITIONING

If one is concerned about the function of the heart during a longer period of time it is of course of great help to have a continuous cross-sectional image. In our experience the transesophageal scanner provides cross-sections of high quality at the level of the great arteries, the atria and foreshortened long-axis images of the left ventricle. The view that is considered the most illustrative for the function of the cardiac muscle is the short axis cross-section of the left ventricle at the level of the papillary muscles. At that particular level the anatomical relation between esophagus and left ventricle is unfortunately ill defined. In many cases interfering structures appear between the esophagus and the left ventricular posterior wall degrading image quality in particular at higher frequencies (5.4 MHz). In such cases the transducer is manoeuvred further down into the stomac and angled upwards to obtain the short-axis cross-section through the left upper lobe of the liver and the diaphragm. Using either position we were able to obtain adequate short-axis images in the vast majority of our patients. This requires an angulation range of up to 80° for the flexible tip of the endoscope.

MONITORING IN A QUALITATIVE WAY

A real-time display of the selected cardiac image will be provided during the whole of the monitoring period. A qualitative validation of the cardiac function or even regional wall motion will be based on visual inspection of the images. Of particular interest is the early detection of ischaemic episodes or the occurrence of gas bubbles (3). The latter will be detected with high precision, when the plane of scanning is positioned at the level of the atria.

The occurrence of ischaemic episodes will be reflected in a change in (local) cardiac muscle contraction. This will be much harder to detect. Without a solid reference the memory of a trained observer has to act like one. An M-mode through the suspected area may then provide evidence on the contractile behaviour of the muscle. State of the art technology enables the use of solid state memory instead of human brains to capture a complete sequence of videoframes of one heart cycle. Subsequent replay in a closed cine loop will then serve as dynamic reference. Using a split screen representation one can observe the actual image together with its reference on the same screen (4). One of the requirements for the detection of changes in cardiac function is the availability of a reference. It is our experience that during the monitoring period the transducer is not completely stationary, and therefore needs to be repositioned occasionally. When this results in a slightly altered scanning plane, reference with the previously obtained images may be lost. Despite the inherent limitations the visual and qualitative monitoring is still considered to be extremely important and when more transducers become commercially available an increase of monitoring applications is to be expected.

QUANTITATIVE MONITORING — A FEASIBILITY STUDY

The purpose of this study is to investigate the feasibility of automatic feature extraction from real-time image sequences as obtained with an esophageal probe. The study is aimed at the detection of the dynamic contour in the short-axis cross-section of the left ventricle. If such a contour is generated in real time a continuous registration of cardiac function becomes available. Parameters useful for monitoring are:

- contour area; the difference between end diastolic and end systolic area can be used as an estimator of the ejection fraction;
- local contour displacement, being indicative for possible wall excursion disturbances;
- rate of area change; this parameter may be related to the contractility.

Automatic contour detection

In a short-axis cross-section the contour we wish to construct is that of the epicard-blood interface. The ultrasound image of that interface is unfortunately not without artifacts.

At some positions the ultrasound beam will hit the interface almost perpendicular, which theoretically will produce a maximal echo-amplitude when the interface acts as a specular reflector. However, when the interface is irregular (because of trabeculae) the echo-amplitude may be reduced as a result of unpredictable interference phenomena. In general we may expect a variable interface echo-amplitude as a function of orientation and as a function of cardiac phase.

The endocardium will produce scattering of the incident ultrasound energy. The backscattered part of this energy will produce an image of the muscles that is less dependent on the orientation of the ultrasound beam when compared with the specular reflection of the blood-muscle interface. However, the orientation of the muscle fibers relative to the angle of incidence of the ultrasound beam is an additional factor influencing the echo-amplitude. We may therefore expect that different parts of the cardiac muscle will be imaged with varying echo-amplitudes. Superimposed on the scattering signal is a speckle pattern due to the transducer itself, resulting in a separate source of echo-amplitude variance. Another source of (local) echo-amplitude variation is shadowing due to strong reflectors in the propagation path of the ultrasonic beam.

Although the blood within the left ventricular cavity will normally produce very low amplitude scattering, the image of the cavity will contain echoes from beam artifacts such as sidelobes and/or grating lobes and this results in noise over the total image.

All the previously mentioned processes will degrade the sharpness of the imaged endocardial interface and thus affect the success rate of any automatic contour detection algorithm.

In order to obtain a fair estimate of the contour the images need to be of reasonable quality while still a large amount of preprocessing is required. This is illustrated with a typical example.

The automatic contour detection as described in the following section has been performed on a Kontron image analysis instrument using a dedicated echo module, based on the initial work of Grube et al (5).

In Fig. VII-1 an end-systolic frame is shown from a typical short-axis cross-section of the left ventricle at the level of the papillary muscles. This image is the start of a sequence of images recorded in real time in the mass memory of the instrument, with a capacity of over 100 video frames.

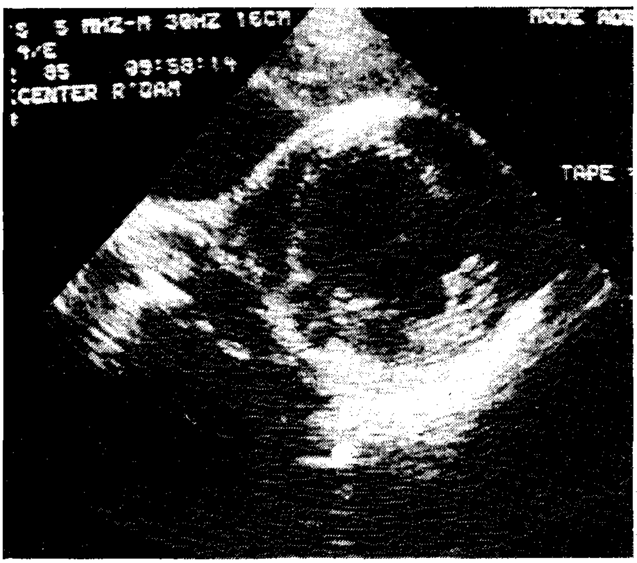

Figure VII-1. Original end-systolic video frame of left ventricular short-axis cross-section at the level of the papillary muscles.

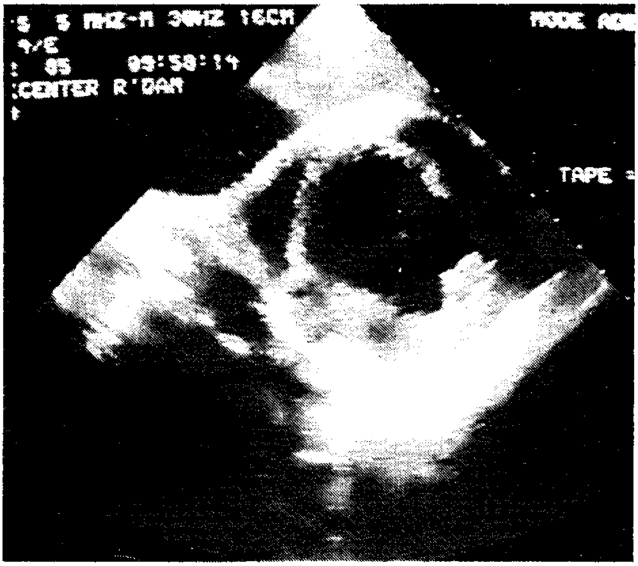

Figure VII-2. Contrast enhanced and filtered image of Fig. VII-1.

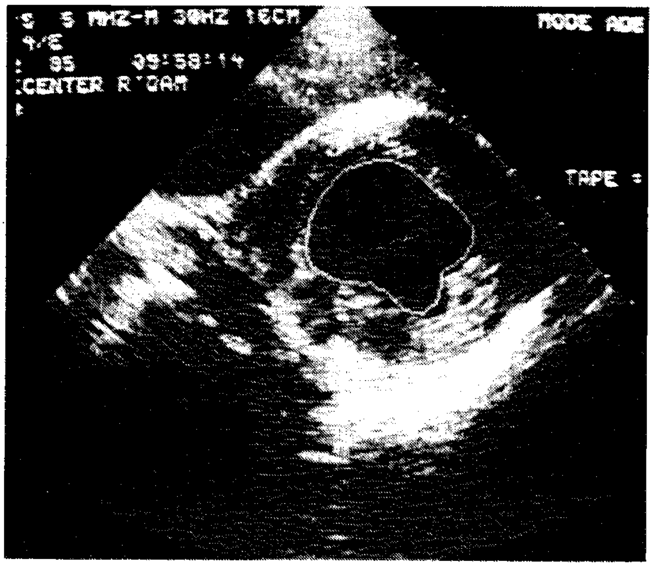

Figure VII-3. Automatically detected contour superimposed on Fig. VII-1.

After the selection of a closed loop of video frames representing one cardiac cycle, the images are optimized for maximum contrast in the area of interest. In order to prepare the image sequence for automatic contour detecion, a noise reduction filter is applied to all images (Fig. VII-2). The contour may now be detected as the significant change in grey-scale level of echoes from the blood -muscle interface. A time series of raw contours will be generated. The final sequence of contours is obtained after a combination of both temporal and spatial filtering, resulting in a closed loop of smoothed contours.

The contours can be superimposed on the original images thus providing a qualitative judgement about the accuracy of the procedure and, if necessary, changes can be made in the parameters used at each step (Fig. VII-3). In Figs. VII-4, VII-5 and VII-6 the processing sequence is illustrated for an end-diastolic frame.

Quantitative analysis of contour data

The complete set of left ventricular contours during one heart cycle allows for the derivation of the quantitative parameters. A typical example is given in Fig. VII-7, where the area A, enclosed by the contour, is plotted as a function of time. The relative change in area may be used as a quantitative estimation of the ejection

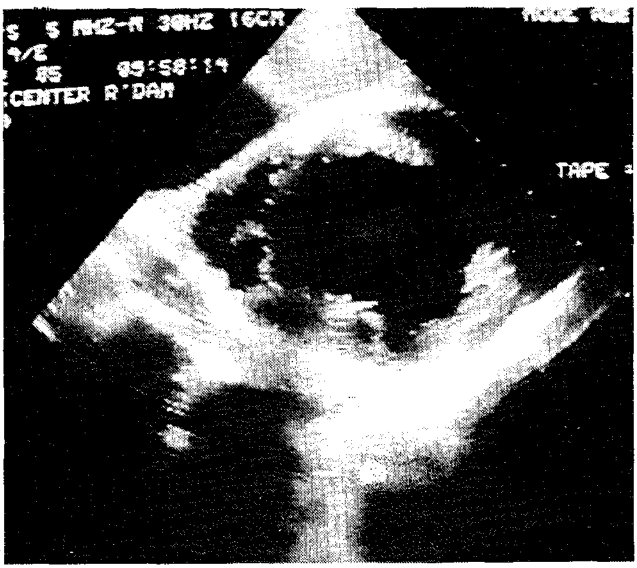

Figure VII-4. Original end-diastolic video frame of same cross-section as in Fig. VII-1.

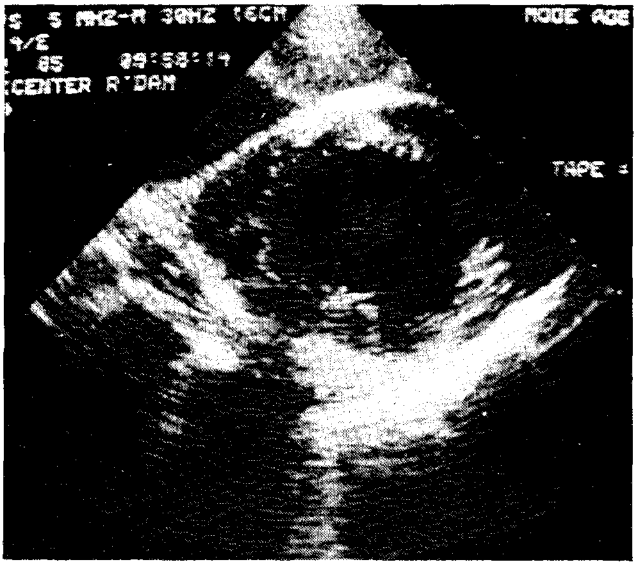

Figure VII-5. Contrast enhanced and filtered image of Fig. VII-4.

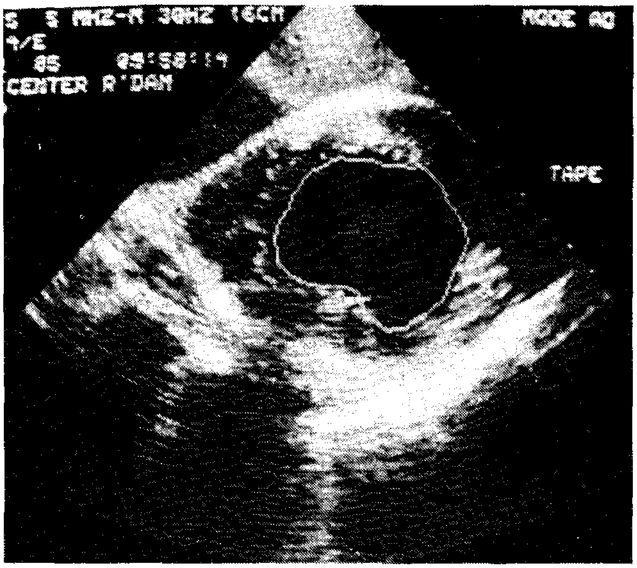

Figure VII-6. Automatically detected contour superimposed on Fig. VII-4.

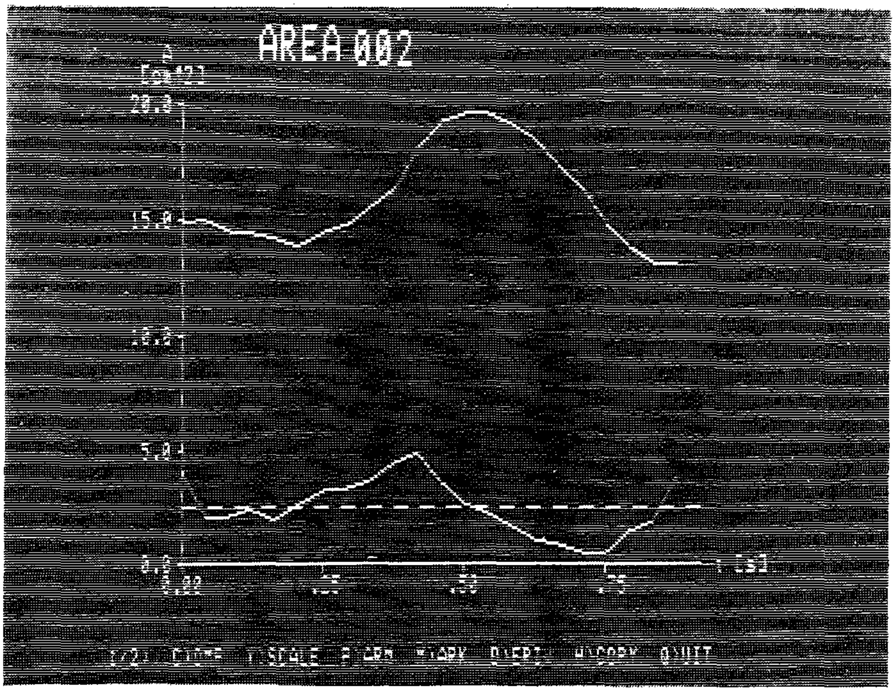

Figure VII-7. Area enclosed by the contour as a function of time (upper curve). The lower curve illustrates the time derivative with dotted zero line. The range is $\pm\, 50\ cm^2\ s^{-1}$.

fraction. Even if the absolute value of this estimation is not an accurate representation of the (unknown) true EF, monitoring of its value over longer periods of time will allow for the detection of trends.

The first time derivative of the area curve dA/dt provides a quantitative evaluation of the rate of change, which may be used as an indicator for the overall contractile behaviour in the observed cross-section. Here again, the absolute values do not need to be very accurate estimations of true cardiac parameters, but they will reflect progressive changes in ventricular function when monitored.

Another parameter accessible from the dynamic contour is segmental wall motion relative to the common midpoint. This parameter will allow for the detection of abnormalities in local wall motion and may be used as an early indicator for (transient) ischaemic episodes.

Discussion of quantitative contour analysis

The parameters discussed in the previous paragraph are susceptible of errors induced by the method itself as well as operational conditions. One of the dominant sources of error is of course the fidelity of the generated contour. The geometry of the contour is determined primarily by the edge detection algorithm. Although images of good quality are used in the examples of Figs. VII-1 to 6, it may be appreciated that in particular the posterior wall at times is hard to detect. This causes the detected contour to show a tendency to bulge, thereby overestimating the true cross-sectional area.

On the contrary erroneous echoes situated proximal to the wall will result in an underestimated radial distance of that part of the contour.

Furthermore the fidelity of the contour is affected by the smoothing operations. Since the spatial smoothing acts as a low pass filter sharp edges in the original contour will be rounded.

Finally the temporal smoothing also acts as a low pass filter. Consequently the dynamic contours will show a phase lag relative to the original raw contour proportional to the effective time constant of the filter. Because of this phase lag the temporal relation between the final contour and the original image will be disturbed. Temporal smoothing will also influence the facilities, for instance real-time 2D Fast Fourier Transform. Till then quantitative image analysis will be restricted to off-line use on time limited sequences of cardiac cross-sections in an interactive way. As for the probe position, the esophageal application during surgery seems to hold promise for the future.

REFERENCES

1. *Topol EJ, Weiss JL, Guzman PA, Dorsey-Lima S, Blanck TJJ, Humphry LS, Baumgartner WA, Flaherty JT, Reitz BA (1984) Immediate improvement of dysfunctional myocardial segments after coronary revascularization: detection by intraoperative transesophageal echocardiography. J Am Coll Cardiol 4:1123-1134.*
2. *Smith JS, Cahalan MK, Benefiel DJ, Byrd BF, Lurz FW, Shapiro WA, Roizen MF, Bouchard A, Schiller NB (1985) Intraoperative detection of myocardial ischemia in high risk patients: electrocardiography versus two-dimensional transesophageal echocardiography. Circulation 72:1015-1021.*
3. *Topol EJ, Humphry LS, Borkon AM, Baumgartner WA, Dorsey DL, Teitz BA, Weiss JL (1985) Value of intraoperative left ventricular microbubbles detected by transesophageal two-dimensional echocardiography in predicting neurologic outcome after cardiac operations. Am J Cardiol 56:773-775.*
4. *Feigenbaum H (1985) Echocardiography - 1985. WFUMB '85 Proceedings, Gill RW and Dadd MJ, eds. Pergamon Press, Sydney: pp 11-12.*
5. *Grube E, Becher H, Backs B, Schmidt D (1985) Automatische Konturerkennung im zweidimensionalen Echokardiogram. In: Erbel R, Meyer J, Brennecke B (eds) Fortschritte der Echokardiographie. Springer, Berlin: pp 16-29.*

CHAPTER VIII

CLINICAL APPLICATIONS OF TRANSESOPHAGEAL ECHOCARDIOGRAPHY

C.T. Lancée, J.R.T.C. Roelandt

INTRODUCTION

In this chapter we describe the extension of diagnostic possibilities of echocardiology by the introduction of the transesophageal approach. Not only are chest wall problems avoided but the versatility of orientation of the interrogating ultrasonic beam allows structures to be imaged that were 'invisible' with the precordial approach. The unique advantages of transesophageal echocardiography for solving clinical problems concerning morphology and hemodynamics, in the echocardiography laboratory, intensive care and during surgery will be discussed and illustrated by case studies.

In Table VIII-1 the use of transesophageal echocardiography is schematically indicated.

Table VIII-1. Use of transesophageal echocardiography.

Clinical site:	Outpatient clinic	Hospital ICU/CCU	During surgery
Primary targets:			
Morphology of			
– Left and right atrium	*	*	
– Cardiac valves	*	*	
– Great vessels, aorta, superior caval vein	*	*	
– Left coronary arteries	*	*	
Evaluation of valve prosthesis	*	*	
Decision-making in the critically ill patient		*	
Monitoring of			
– LV function			*
– Occurrence of ischaemia			*

DETAILED MORPHOLOGY ASSESSED BY TRANSESOPHAGEAL ECHOCARDIOGRAPHY

Structures of the heart that are rarely imaged by the precordial scanning, even in patients with excellent image quality, are: the left atrial appendage, the great vessels and the coronary arteries. Transesophageal echocardiography excels in image quality when these areas are concerned (1). Its clinical use is listed in Table VIII-I and will be discussed in the following:

- The left atrial appendage is an important structure to image, because it is a common site of early thrombus formation when the flow patterns in the left atrium are disturbed as a result of dilatation and/or mitral valve stenosis. An example of the nature of such a disease will be treated in case example 1 (Chapter IX).

- Pathology of the great vessels, and more particularly of the aorta, is difficult to demonstrate during routine precordial echocardiographic examination. The orientation of a transducer situated within the esophagus favours the continuous scanning of the left ventricular outflow tract, the aortic valve, the aortic root, the aorta ascendens, the aortic arch as well as a large part of the thoracic aorta. In addition, the pulmonary veins and the vena cava superior can also be studied transesophageally. Aneurysmata and dissections have been diagnosed by use of this technique. Figure VIII.1 shows a typical example of an extended aneurysm of the descending aorta, scanned from three positions.

- The visualization of the coronary arteries, in particular the left main coronary artery, its bifurcation and the two branches left anterior descending and left circumflex artery has challenged the echocardiographers for years (2-4).

Precordial imaging, however, is not always clinically useful because of its low successrate and poor image quality. Mainly because of the high resolution associated with the high ultrasound frequency and the shorter distance of the transesophageal transducer to the target we have shown in a retrospective study (5) that the proximal left coronary arteries can be studied in great detail with a high successrate. It should be noted that the patients involved were referred for transesophageal echocardiography because of their poor precordial image quality, and that no specific search for the coronaries had been performed. In Figure VIII-2 a typical image of the coronary bifurcation is shown. The scanning plane is through the base of the left atrium and the auricle.

We anticipate that the diagnosis of obstruction of the left main coronary artery is possible by transesophageal echocardiography when the precordial approach fails to provide clinical evidence.

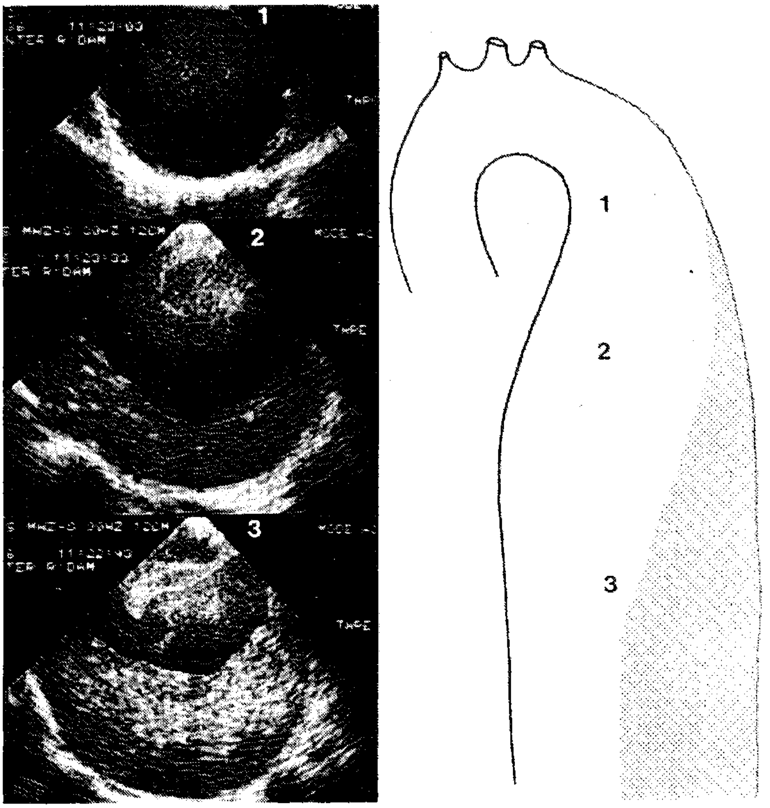

Figure VIII-1. To the right a large aneurysm in the descending aorta is schematically drawn. The numbers refer to three different scanning positions corresponding to the three cross-sectional images shown in the left panel.

HEMODYNAMIC STUDIES FOR THE EVALUATION OF (PROSTHETIC) VALVES

Blood flow studies in the heart by the Doppler technique have evolved over the last decade from continuous wave peak velocity measurement to colour Doppler flow imaging (6). The combined effect of theoretical advance in signal processing and the steady improvement in instrument- and transducer technology allowing the non-invasive detection of cardiac blood flow abnormalities, has been responsible for the progress. Since the ultrasound signals reflected from the red blood cells are extremely weak, the Doppler applications suffer from poor signal/noise rate and diagnostic information is not always obtained, especially in those patients

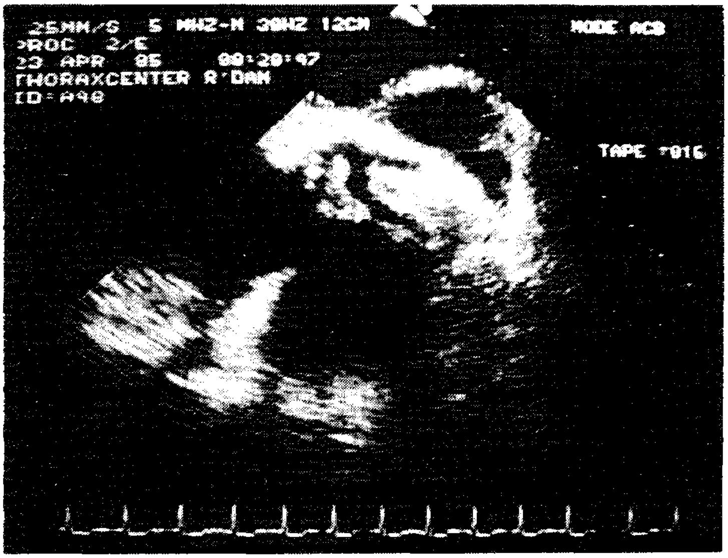

Figure VIII-2. A typical cross-sectional image of the bifurcation of the left main coronary artery. The circumflex extends anteriorly while the descendens is more posteriorly oriented. Manipulating the transducer allows for the complete coverage of the coronary lumen between the aortic root and the bifurcation. (The structure in the left atrium is part of the auricle).

where ultrasound attenuation in the thoracic wall lowers the signal strength outside the instrument's dynamic range. Furthermore the distance between transducer and areas of interest is often long, yielding too much signal attenuation as well as ambiguity due to the necessarily reduced sampling frequency. Because of the inherent physical limitations of the precordial approach, transesophageal echocardiography will undoubtedly expand the diagnostic Doppler capabilities.

With colour Doppler flow imaging central or paraprosthetic mitral valve insufficiency is visualized with high sensitivity. In Figure VIII-3 a colour Doppler flow image is shown triggered at systole. A paravalvular leakage of the prosthetic mitral valve results in a turbulent jet projected into the left atrium.

Both defects exhibit jets in the left atrium that are difficult to visualize from the precordial transducer position because the ultrasound energy does not pass the prosthetic material and information from behind the prosthesis cannot be obtained. The transesophageal echocardiographic approach yields an unobstructed sampling for abnormal flow anywhere in the left atrium and hence superior sensitivity for detecting regurgitant flow jets.

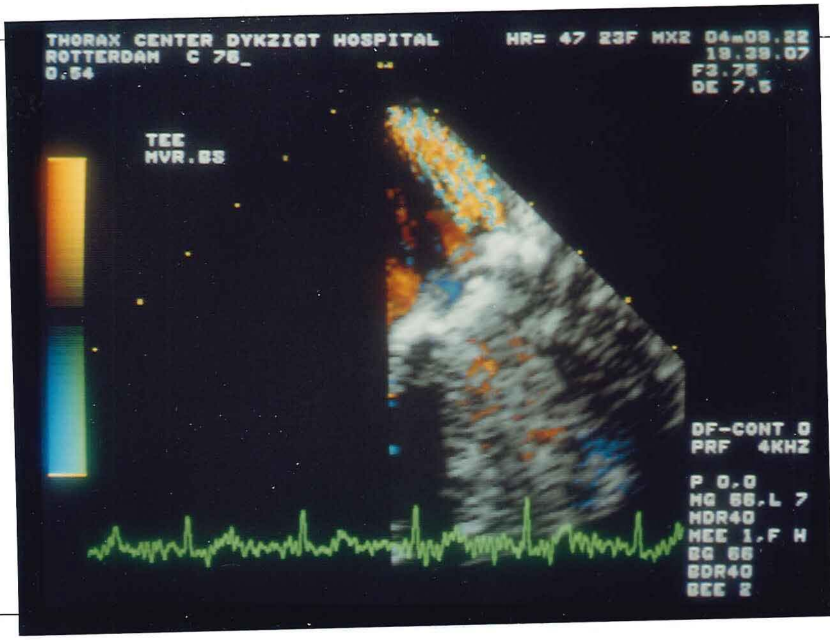

Figure VIII-3. A triggered colour Doppler flow image at systole. A narrow turbulent jet originating in the circumference of the prosthetic mitral valve can be appreciated, projecting itself towards the transducer in the left atrium.

INCREASED DIAGNOSTIC VALUE IN CRITICALLY ILL PATIENTS

Mobility of the echocardiographic equipment and hence the possibility of bedside echo study of critically ill patients makes echo a unique diagnostic technique. In ventilated patients, however, it is virtually impossible to obtain echocardiographic images from the precordium because the standard acoustic windows are obstructed by lung tissue and the patient is in an unfavourable (supine) position. The transesophageal approach allows for a detailed study of the cardiac morphological and/or hemodynamic disturbances. This is illustrated by case example 2 (Chapter IX).

CONCLUSION

In conclusion we may summarize the clinical applications of transesophageal echocardiography (TEE) in the following characteristics.

Indications for TEE are:
- Clinical suspicion of serious cardiac pathology combined with inadequate precordial study.
- Additional and/or detailed information in patients with serious cardiac pathology.
- Suspected mitral prosthesis dysfunction.
- Pathology of the aorta or the aortic root.
- Suspicion of left main coronary artery obstruction.
- Monitoring of left ventricular dynamics during high-risk surgery.

Contra-indications for TEE are:
- Swallowing problems and/or extreme fear.
- History of esophageal disease.
- After radiation therapy.
- During barium roentgenogram or endoscopic examination.

Typical clinical advantages of TEE are:
- No obstruction to ultrasound by chestwall structures, lung tissue or intracardiac prosthesis. Ribs and calcified intercostal spaces exhibit a high reflection coefficient combined with an increased absorbtion. Lung tissue exhibits an extremely large attenuation due to its air content. Common materials for cardiac prostheses are plastics and stainless steel. These materials will degrade the image with strong reflections, reverberations and attenuation, thereby inhibiting the visualization of posteriorly located structures.
- Higher ultrasound frequencies provide better resolution and more detailed imaging. The lack of intervening structures with a high frequency dependent attenuation coefficient allows for a high ultrasound frequency. Consequently a higher axial and lateral resolution can be obtained, combined with an increased sensitivity.
- Reduced target range for pulsed Doppler (colour) allows a higher pulse repetition frequency to be used. Since the maximum Doppler shift to be detected unambiguously is directly related to the pulse repetition frequency, a larger range of velocities can be displayed without aliasing artifacts.
- Different imaging planes allow for visualization of structures not seen from the precordium.
- Atrial flow components due to valvular malfunction (in particular in the presence of stenotic or prosthetic valves) can be measured without interference of the valve apparatus itself.

REFERENCES

1. *Gussenhoven EJ, Taams MA, Roelandt JRTC, Ligtvoet CM, McGhie J, Van Herwerden LA, Cahalan MK (1986) Transesophageal two-dimensional echocardiography: its role in solving clinical problems. J Am Coll Cardiol 8:975-979.*
2. *Chandraratna PAN, Aronow SW (1980) Left main coronary arterial patency assessed with cross-sectional echocardiography. Am J Cardiol 46:91-94.*
3. *Reeder GS, Seward JB, Tajik AJ (1982) The role of two-dimensional echocardiography in coronary artery disease: a critical appraisal. Mayo Clin Proc 57:247-258.*
4. *Block PJ, Popp RL (1985) Detecting and excluding significant left main coronary artery narrowing by echocardiography. Am J Cardiol 55:937-940.*
5. *Cornel JH, Gussenhoven EJ, Roelandt JRTC, Taams MA, Ligtvoet CM. Improved visualization of the left coronary artery by transesophageal echocardiography. Submitted to Eur Heart J.*
6. *Roelant JRTC (1986) Clinical experience with the Toshiba SSH-65A color Doppler flow imaging apparatus. Toshiba Medical Review 17:15-25.*

CHAPTER IX - CASE EXAMPLES

LEFT ATRIAL VASCULARIZED THROMBUS DIAGNOSED BY TRANSESOPHAGEAL TWO-DIMENSIONAL ECHOCARDIOPGRAPHY

Meindert A. Taams, Elma J. Gussenhoven, Charles T. Lancée

(Case example 1)

Abstract

This report describes a patient with a Björk-Shiley mitral valve prosthesis in whom transoesophageal two-dimensional echocardiography revealed a large vascularized mass lesion within the left atrial appendage while a 'smoke-like' opacification of blood flow in the left atrium was seen. These findings are discussed in relation to precordial two-dimensional echocardiography and Doppler investigation, cardiac catheterization, angiography and the surgical findings.

Accepted for publication in Br Heart J

INTRODUCTION

Left atrial thrombi are common in patients with low cardiac output and are predominantly localized in the left atrial appendage (1). Precordial two-dimensional echocardiography is the technique of choice for the identification of intracardiac mass lesions. However, the left atrial appendage is difficult to visualize and morphologic details are rarely obtained (2). Transoesophageal echocardiography offers the potential to visualize this cardiac area in detail (3, 4).

This report describes the role of transoesophageal two-dimensioinal echocardiography for detailed analysis of a left atrial vascularized thrombus.

CASE HISTORY

A 66-year-old woman was admitted with congestive cardiac failure and central cyanosis. In 1976 she underwent mitral valve replacement with a spherical 25 Björk-Shiley prosthetic valve for severe mitral valve stenosis and moderate regurgitation due to rheumatic fever. For many years she had been known to have atrial fibrillation. Five months before admission a VVI pacemaker was implanted for symptomatic sick sinus syndrome. Three weeks prior to admission she had noticed increasing fatigue and general malaise. On admission she was in functional class IV according to NYHA criteria and medication consisted of digitalis, diuretics and oral anticoagulants.

On physical examination she had orthopnea and was afebrile. The bloodpressure was 170/60 mmHg and the pulse rate 90 beats/min. The jugular venous pressure was elevated. A strong right ventricular lift was palpated at the left sternal border. A loud pulmonic closure sound was heard. Crisp metallic opening and closing clicks of the prosthesis were present. Mitral incompetence was absent, but there was a grade III/VI tricuspid incompetence murmur.

The liver was 5 cm enlarged. There was no peripheral edema. Neither were physical signs present of endocarditis nor of peripheral embolization. The electrocardiogram showed atrial fibrillation and right ventricular hypertrophy. The cardiothoracic ratio on the chest X-ray was 66% with signs of pulmonary congestion. Arterial bloodgas analysis with oxygen support displayed severe hypercapnea, hypoxemia and low saturations. Routine laboratory investigations were within normal limits. There were no signs of hemolysis. Emergency right heart catheterization established MIRU class III, with pulmonary hypertension, elevated pulmonary capillary wedge pressure and right atrial pressure.

Precordial two-dimensional echocardiography with a 3.5 MHz transducer demonstrated left atrial dilatation with a left atrial dimension of 100 mm, while the left ventricle was of normal size with good contractility. Continuous wave Doppler investigation suggested normal prosthetic valve function.

She improved dramatically with intravenous vasodilators, diuretics and oxygen. After 2 weeks repeat catheterization showed that right and left cardiac pressures had dropped to normal. The cardiac index was 1.8 $l/min/m^2$. There was no mitral valve incompetence. No gradient was found over the mitral prosthesis. The disc motion seemed unimpaired at screening. There was a grade 2 aortic incompetence. The coronary arteries appeared normal. Cinefilm analysis revealed that the atrial branch of the left coronary artery supplied a mass lesion within the left atrium (Fig. IX-1). From these angiograms, however, specific details about the mass lesion could not be obtained.

Since precordial echocardiography provided unsatisfactory image quality, it was decided to use transoesophageal echocardiography in order to obtain more details about the nature, extent and location of the mass lesion. A 5.6 MHz

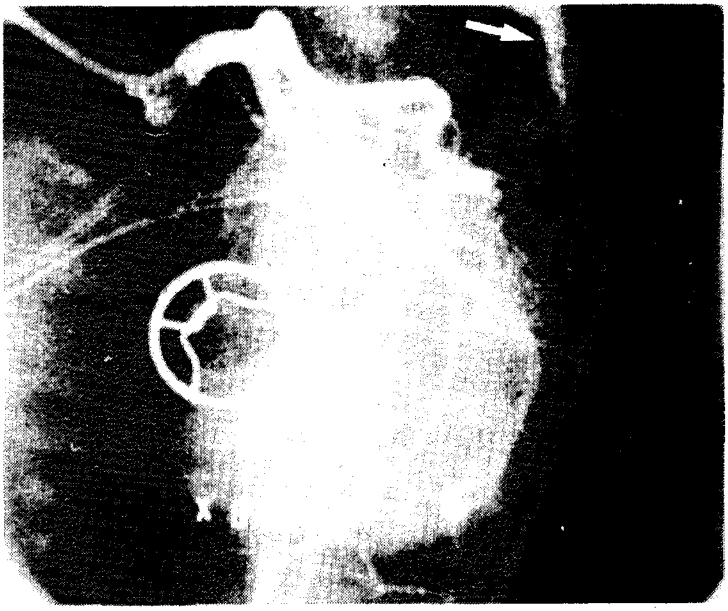

Figure IX-1. Left coronary artery angiogram demonstrating the presence of a vascularized structure in the left atrium (arrow).

64-elements transducer was used that was mounted on an Olympic gastroscope interfaced with a commercially available ultrasonograph (4). The active area of this transducer is comparable with the active area of precordial 5 MHz phased array transducers. The enclosure obviously is much smaller. The Björk-Shiley prosthesis and disc showed no apparent abnormalities and its motion was undisturbed. The extremely enlarged left atrial cavity was completely filled with echoes swirling in phase with the inflow of blood from the pulmonary veins (Fig. IX-2). From the dilated left atrial appendage a mass lesion emerged into the left atrial cavity along the lateral wall, reaching the orifices of the left pulmonary veins. Its cross-section measured approximately 20 by 80 mm. Within this lesion several echo-free spaces were identified presumably representing its vascularization also noted with angiographic studies (Fig. IX-2). The image of the mass suggested a thrombus. These findings were highly suggestive for intermittent valve obstruction due to dislodgements of thrombus material. Therefore it was decided to perform cardiac surgery. At surgery a large organized thrombotic mass was found to be attached to the atrial lateral wall partially obstructing the entrance of the left pulmonary veins. The patient's postoperative course was uneventful.

Microscopy showed typical thrombus material with fibrin layers and scar tissue.

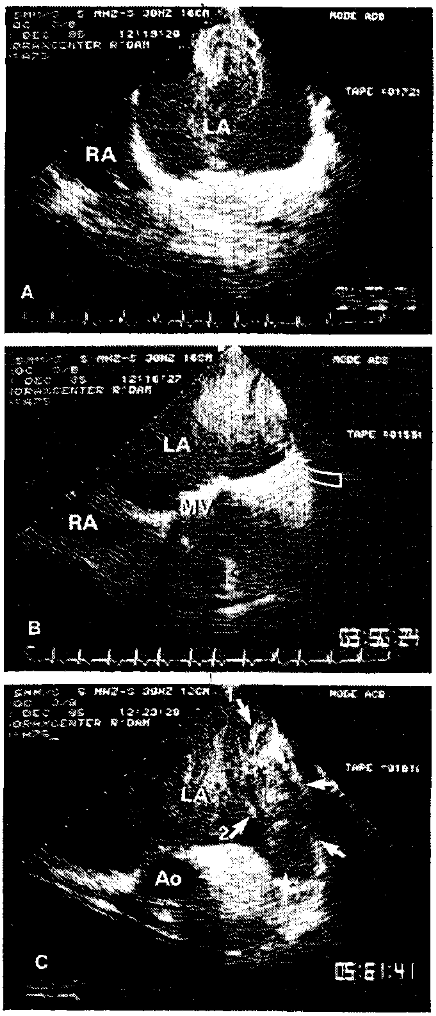

Figure IX-2. *Transesophageal two-dimensional echocardiograms taken at the level of the left atrium (LA) showing the dilated left atrium opacified with numerous micro-echoes (A). The bloodflow coming from the pulmonary veins had immediate effect on the microbubble movement. A slight tilt of the transducer revealed a mass lesion attached to the left atrial lateral wall (B; open arrow) which emerged into the left atrial appendage (C; arrows). Within this mass lesion oblong echo-free spaces were visible (arrow 1; 2). Ao = aorta; RA = right atrium; MV = mitral valve prosthesis.*

Small and medium-sized vessels were present. The left atrial endocardium consisted of elastic fibers mixed with scar tissue. The myocardium was collagenous with scattered elastic tissue.

DISCUSSION

Echocardiographic imaging of circulating blood in the left atrium has been described in relation to obstructive mitral valve disease (5, 6). It has been reported that low shear rates associated with low blood flow conditions would favour the rouleaux formation of red cells (7, 8). Its presence may include a warning for thrombus formation (7). The patient we described in this paper exhibits both criteria: scattering echoes from the atrial blood pool and the presence of a mass lesion in the left atrium. Doppler, cardiac catheterization studies and surgical inspection revealed no evidence of mitral valve obstruction. We assume that the cause of the echogenicity of the atrial blood is two-fold. First the low blood flow conditions established by the aneurysmatic left atrial dilatation due to the long-standing mitral valve disease before valve replacement. Secondly it may be the result of low cardiac output. The causative underlying pathology might be the partial loss of atrial muscular fibers confirmed at postoperative microscopic investigation. This resulted in progressive left atrial enlargement and impaired atrial function. A similar condition of the right atrium has been described by Baily in 1955 (9).

The use of transoesophageal echocardiography enables the choice of a high frequency transducer since the attenuation along the ultrasound propagation path is drastically reduced. The practical consequence of a high frequency for the diagnostic quality of the images is not only improved resolution, but also an increase in sensitivity for backscattering. In particular small particles will produce a backscattered signal intensity (I) which exhibits a strong non-linear relationship with frequency f, where $I : f^4$ (10). Thus, the sensitivity for back-scattering objects will increase with frequency.

The source of echoes generated by the blood itself may be explained by increased backscattering at diagnostic frequencies (2-5 MHz). The only possible explanation for this phenomenon is an increase, with respect to normal conditions, in blood particle size/wavelength ratio. The mechanism for the increment in size must be an aggregation of blood cells associated with low blood flow conditions. A high frequency transoesophageal transducer will therefore detect stagnant blood flow sooner than precordial examinations at lower frequencies do (11).

The reason why precordial echocardiography failed to image the mass lesion may be two-fold. In the first place the unique position of the oesophageal transducer results in a much better signal to noise ration compared to the precordial position. This can be the reason why the mass lesion was not recorded precordially. On the other hand the thrombus position relative to the available precordial acoustic window may have hampered adequate imaging. The high resolution images also revealed oblong echo-lucent areas within the mass lesion which indicate the vascularization of this lesion also noted with angiographic studies.

Thus, where other investigations were not specific about the nature, extent and location of a serious intracardiac problem, transoesophageal echocardiography revealed detailed information on left atrial morphology and pathology. On the basis of this information, surgical intervention was performed.

ACKNOWLEDGEMENT

The authors gratefully acknowledge the contributions to this case study of Max Haalebos, who performed cardiac surgery, Nienke Essed who conducted the pathologic-anatomic tests and of Kees Ligtvoet who gave technical advice.

This work has been supported in part by grants of Oldelft Industries and Pie Medical, the Netherlands.

DISSECTING ANEURYSM OF THE BASE OF THE AORTA DIAGNOSED BY TRANSESOPHAGEAL TWO-DIMENSIONAL ECHOCARDIOGRAPHY

C.T. Lancée, J.R.T.C. Roelandt

(Case example 2)

Abstract

In this case report a patient is described in whom transesophageal two-dimensional echocardiography revealed acute aortic root disorder (possibly a ruptured aortic valve). On the basis of this finding the patient was immediately scheduled for surgery.

INTRODUCTION

Critically ill patients with instable hemodynamic conditions in an intensive care department, who require ventilation are very difficult to investigate precordially. When it is felt necessary to obtain an echocardiographic diagnosis despite the fact that precordial procedures failed to produce conclusive evidence, the transesophageal approach is the method of choice. In this case report the detection of a serious morphologic problem in the aortic valve area is described.

CASE HISTORY

A 33-year-old man, known to have trivial aortic regurgitation, experienced a crushing thoracic pain during a training. He progressively became dyspneic and was admitted with pulmonary edema a few hours later. The instabile hemodynamic condition required intubation and PEEP ventilation. His hemodynamic state did not improve. Precordial echocardiography was inadequate and on transesophageal echocardiography a redundant aortic valve with possible rupture was found. During systole there appeared to be no complete closure of the valve.

Surgery was subsequently performed and a dissecting aneurysm of the base of the aorta with an intima flap interfering with the normal aortic valves was found. Surgery was done on the basis of the esophageal echocardiographic findings.

DISCUSSION

The position of the transesophageal transducer relative to the heart and the large vessels allows for the screening of a large part of the aorta. Cross-sections of the ascending aorta, aortic arch and descending aorta can be obtained at close intervals down to the diaphragm.

In this case example the area of interest, the aortic root, was visualized through the left atrium. In Figure IX-3 the abnormal anatomy of the aortic valve area is shown. From the real-time images it was hard to discriminate between a severely damaged aortic valve or a dissecting aneurysm at the base of the aorta. Because of the rareness of dissections of the intima of the aortic root we were not accustomed to its morphologic representation on the echocardiogram. In this figure, the arrows point at the loose flaps of the intima. In real time these flaps were seen moving freely in the same pattern as may be seen with an abnormal aortic valve. The dissection may be explained as a consequence of the Ehlers-Danlos syndrome.

This example proves the value of transesophageal echocardiography as a decision-making tool under extreme conditions such as intensive care instrumentation, intubation and PEEP ventilation.

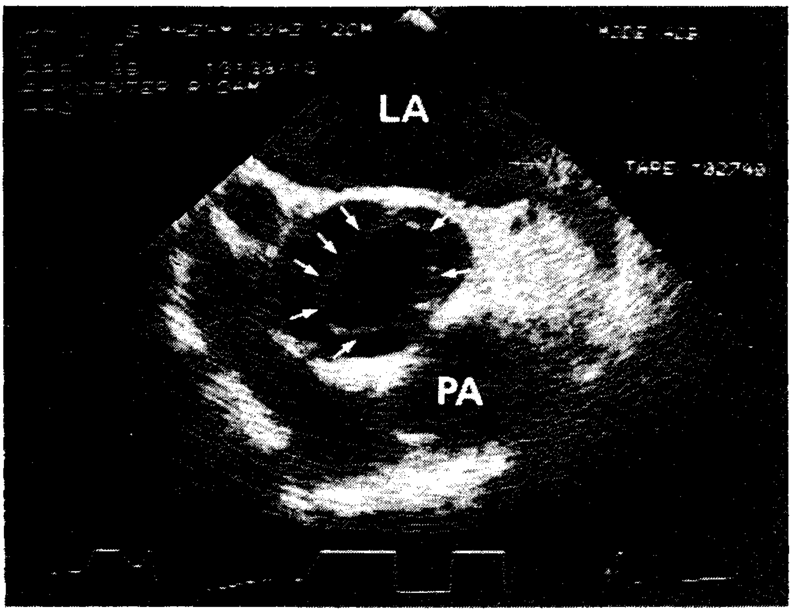

Figure IX-3. *Cross-sectional image through the base of the aorta. The arrows point at the dissected intima flaps of the aortic root. LA = left atrium; PA = pulmonary artery.*

REFERENCES

1. *Wallach JB, Borgatta EF (1962) Rheumatic Heart Disease. Springfield, Illinois, Charles C. Thomas.*
2. *Herzog CA, Bass D, Kane M, Asinger R (1984) Two-dimensional echocardiographic imaging of left atrial appendage thrombi. J Am Coll Cardiol 3:1340-1344.*
3. *Aschenberg W, Schlüter M, Kremer P, Schröder E, Siglow V, Bleifeld W (1986) Transesophageal two-dimensional echocardiography for the detection of left atrial appendage thrombus. J Am Coll Cardiol 7:163-166.*
4. *Gussenhoven EJ, Taams MA, Roelandt J et al (1986) Transesophageal two-dimensional echocardiography: its role in solving clinical problems. J Am Coll Cardiol 8:975-979.*
5. *Garcia-Fernandez MA, Moreno M, Banuelos F (1985) Two-dimensional echocardiographic identification of blood stasis in the left atrium. Am Heart J 109:600-601.*
6. *Beppu S, Nimura Y, Sakakibara H, Nagata S, Park YD, Izumi S (1985) Smokelike echo in the left atrial cavity in mitral valve disease: its features and significance. J Am Coll Cardiol 6:744-749.*
7. *Mikell FL, Asinger RW, Elsperger S, Anderson WR, Hodges M (1982) Regional stasis of blood in the dysfunctional left ventricle: echocardiographic detection and differentiation from early thrombosis. Circulation 66:755.*
8. *Sigel B, Coelho UCV, Spigos DG et al (1981) Ultrasonography of blood during stasis and coagulation. Invest Radiol 16:71.*
9. *Baily CP (1955) Surgery of the heart. Philadelphia, Lea and Febiger: 413.*
10. *Morse PM, Ingard KU (1968) Theoretical Acoustics. New York, Saint Louis, San Francisco, Toronto, London, Sydney, McGraw Hill Book Company:400-466.*
11. *Iliceto S, Papa A, Antonelli G, Sorino M, Amico A (1985) Spontaneous contrast echocardiography. Echocardiography 2:455-465.*

SUMMARY

In this thesis the development of a miniaturized phased array ultrasound transducer is described. The application of this transducer in the field of echocardiology is devoted to transesophageal cross-sectional scanning of the heart and its great vessels. The enormous increase in diagnostic applications of ultrasound over the last three decades is particularly due to the non-invasive character of this technique. Consequently the developments of transcutaneous scanning techniques have outnumbered all other possibilities, but researchers have continuously been investigating the alternatives of scanning organs from within the human body. In those patients in whom inhibiting factors preclude adequate diagnostic information to be obtained transcutaneously, alternative scanning techniques still may provide vital information.

For cardiac imaging two possibilities exist to enter the human body, invasively by means of a catheter or 'non-invasively' by means of an endoscope. In Chapter I, the introduction, our early experiences with a catheter-mounted scanning system are described. The limited possibilities of such a system combined with the inherent technological complications, as well as the invasive character of such a technique favoured the search for a different approach. The idea to advance in the catheter direction was never left but first the experience gained has been applied to transesophageal scanning with an endoscope-mounted transducer as described in this thesis.

In Chapter II the various methods of ultrasound scanning are reviewed. In order to obtain cross-sectional imaging the investigating ultrasonic beam has to be steered over the area of interest. For echocardiology in particular the beating of the heart requires a high scanning rate. This may be obtained by either electronic means or by means of a mechanical driving mechanism. Comparison of all existing techniques yields the conclusion that the scanning mechanism best suited for transesophageal imaging is the electronic phased array system.

A comparative model study of two basic ultrasonic transducer materials is described in Chapter III. PZT ceramic is compared to PVDF polymer (PZT is lead zirconate-titanate; PVDF is polyvinylidene fluoride). The family of PZT materials is large, each member exhibiting specific material constants optimized for different applications such as non-destructive testing, power ultrasonics, medical

transducers, etc. The PVDF polymer material is relatively new in the field of ultrasonics, therefore experience with practical applications is limited.

In a one-dimensional model supplied with typical material constants, the two materials are compared with respect to impuls response, sensitivity, electric and acoustic impedance. PVDF has certain advantages over the well established PZT (superior impuls response, reduced parasitic vibration modes, low price). The major obstacle for the application of PVDF in a phased array is the high impedance of the small elements, requiring a multitude of electrical power matching circuits. It is concluded that PZT remains the material of choice for the esophageal phased array transducer.

In Chapter IV the actual design and the construction of a transducer mounted on a standard gastroscope is described. The most important array parameters to be determined are: aperture, number of elements, element geometry, central frequency, bandwidth, focal length. The clinical performance of the array has to comply with standards in terms of resolution, sidelobe level, sensitivity and area of interest. The case in which the transducer is used in the daily practice of a clinical environment sets the limits for probe dimensions and profile. Furthermore the materials used for the probe assembly will have to meet electrical safety standards as well as clinical safety requirements, i.e. easy to clean and non-toxic.

In Chapters V and VI respectively, a theoretical study is performed on the influence of amplitude- and phase errors of a phased array on the quality of the ultrasonic beam profile. In a practical situation, the combination of a transducer and its driving electronics will be susceptible to component variability, which yields beam profiles differing from the theoretical ones. While the amplitude errors will be mainly introduced by the variance in the element sensitivity of the transducer itself, the prime source of phase errors is the time-delay section in the transducer supporting electronics.

In Chapter V the influence of amplitude variations over the array is treated. The non-uniform sensitivity distribution over the elements may constitute the source of such variations. From previous reports in the literature it is generally known that an increase in amplitude error variance results in an increasing average sidelobe level. In our study we introduce the spatial distribution of the errors as an extra parameter. It is shown that by combining the variance of the amplitude errors with the central second moment of their distribution over the array, a more specific criterion can be stated for the quality of the resulting beam profile.

In Chapter VI the influence of phase errors on the beam profile is dealt with. In previous reports in the literature the effects of stochastic phase errors are described. However, the nature of phase errors in ultrasound phased arrays is far from stochastic, being primarily the result of discretization of a continuous time-delay function. When the discretization stepsize is given, a worst case variance of the phase errors can be formulated. Beamsteering and focussing produce for each steering angle and focal distance a typical variance value. However, it is shown that by manipulating the common time offset the variance value can be minimized, thereby optimizing the beam profile.

Present and apparent near future cardiological applications of the transesophageal phased array transducer can be subdivided into two categories: 1) monitoring during high risk surgery and 2) diagnostic imaging of the heart and its great vessels.

In Chapter VII a feasibility study is described of the quantitative monitoring possibilities given by the transesophageal image quality. In this study video recordings are analyzed by making use of a Kontron image processing system. The technical purpose of this image processing is to obtain an automatic tracking of the inner contour of a short axis left ventricular cross-section. If the contour is reliably detected over the heart cycle a number of quantitative parameters, for instance cross-sectional area, area rate of change, segmental wall motion, can be generated at regular intervals. The usefulness of the quantitative data depends strongly on the accuracy of the detected contour. It is concluded that this is the limiting factor.

The contour detection itself depends on a variety of parameter settings, each of them being interactively optimized by the human operator, which is a time-consuming process. Furthermore a change in the image plane orientation often requires readjustment of said parameters, jeopardizing the reproducibility of the results. More powerful processing algorithms need to be developed to let truly automatic image analysis allow for on-line quantitative patient monitoring. Nevertheless, with the image quality now available through transesophageal echocardiography, automatic contour analysis may become important in future.

In Chapter VIII the clinical applications of transesophageal echocardiography as an additional diagnostic technique are described. When the probe is connected to a state-of the art electronic mainframe its applications include both two-dimensional imaging and Doppler flow registration. This allows for the assessment of morphologic as well as hemodynamic information. Typical problems to be solved by transesophageal echocardiography after an unsuccessful precordial examination are: pathology of the atria, the aorta, mitral and aortic valve and, sometimes, main coronary arteries. Hemodynamic studies can be performed in great detail of the left atrium and the left ventricular outflow tract, which is particularly useful for the evaluation of prosthetic valve function.

The diagnostic value of transesophageal echocardiography is furthermore illustrated by two case examples in Chapter IX.

The first case history reveals the diagnostic power of the transesophageal approach in a patient with an atrial thrombus in whom precordial images were of poor quality. The second case history describes the contribution of transesophageal echocardiography, under 'battle field' conditions, to the decision making process. In this case severe disorder of the aortic valve area could be positively identified.

SAMENVATTING

In dit proefschrift wordt de ontwikkeling van een miniatuur phased array ultrageluidstransducent beschreven. De specifieke toepassing van deze transducent is het vanuit de slokdarm opnemen van echocardiografische dwarsdoorsneden van het hart en de grote vaten. De enorme toename van diagnostische toepassingen van ultrageluid in de afgelopen dertig jaar is voornamelijk te danken aan het niet-invasieve karakter van deze techniek. De nadruk van de ontwikkelingen in dit vakgebied heeft dan ook steeds op transcutane scanning technieken gelegen. Een gering aantal onderzoekers heeft echter voortdurend gezocht naar mogelijkheden om organen vanuit het inwendige van het menselijk lichaam in beeld te brengen. Bij die patiënten bij wie bepaalde factoren het onmogelijk maken bruikbare informatie voor het stellen van een diagnose transcutaan te verkrijgen, kunnen alternatieve scanmethoden toch belangrijke informatie verschaffen.

Er bestaan twee methoden voor het in beeld brengen van het hart vanuit het menselijk lichaam; invasief met behulp van een catheter of 'niet-invasief' met behulp van een endoscoop. In Hoofdstuk I, de inleiding, zijn onze eerste ervaringen met een op de tip van een catheter gemonteerd scan systeem beschreven. De beperkte mogelijkheden van een dergelijk systeem in combinatie met de technologische complicaties en ook het invasieve karakter ervan werkten het zoeken naar een andere aanpak in de hand. Het idee om met de catheter verder te gaan is nooit helemaal losgelaten, maar eerst is de daarmee opgedane ervaring gebruikt voor het maken van opnamen vanuit de slokdarm met een op een endoscoop gemonteerde transducent zoals beschreven in dit proefschrift.

In Hoofdstuk II is een overzicht gegeven van de diverse scan methoden met behulp van ultrageluid. Voor het verkrijgen van doorsnedebeelden moet de uitgezonden ultrageluidsbundel worden gestuurd over het te onderzoeken oppervlak. Het kloppen van het hart maakt in de echocardiologie een hoge scan snelheid noodzakelijk. Deze kan zowel electronisch als door mechanische aandrijving worden verkregen. Vergelijking van alle beschikbare technieken levert de conclusie op dat voor het in beeld brengen van het hart vanuit de slokdarm het electronisch phased array systeem het meest geschikt is.

Een vergelijkende modelstudie van twee basismaterialen voor ultrageluidstransducenten is beschreven in Hoofdstuk III. Het keramisch materiaal PZT wordt vergeleken met het polymeer PVDF. De groep PZT materialen is groot en elke vertegenwoordiger ervan heeft zijn specifieke materiaalconstanten met optimale waarden voor verschillende toepassingen zoals niet destructief testen, opwekken van hoog vermogen ultrageluid of toepassing in transducenten voor medisch gebruik, enz. Het polymeer PVDF is een betrekkelijk nieuwe verschijning op het gebied van ultrageluid. Daarom is er nog slechts een beperkte ervaring met praktische toepassing ervan in de medische wereld.

In een één-dimensionaal model met typische materiaalconstanten zijn de twee materialen vergeleken ten aanzien van pulsresponsie, gevoeligheid, electrische en akoestische impedantie. PVDF heeft bepaalde voordelen boven het welbekende PZT (betere pulsresponsie, geringe gevoeligheid voor parasitaire trillingen, lage prijs). Het grootste bezwaar dat aan de toepassing van PVDF in een phased array kleeft, is de hoge impedantie van de kleine elementen, wat een veelheid van electrische aanpassingsnetwerken noodzakelijk maakt. De conclusie is, dat PZT de voorkeur verdient voor de oesophagale phased array transducent.

In Hoofdstuk IV worden het huidige ontwerp en de constructie van een transducent voor montage op een standaard gastroscoop beschreven. De belangrijkste parameters van het array die bepaald moeten worden zijn: apertuur, aantal elementen, vorm van de elementen, centrumfrequentie, bandbreedte, focusafstand. De prestaties van het array bij klinisch gebruik moeten voldoen aan de eisen gesteld met betrekking tot resolutie, zijlob niveau, gevoeligheid en penetratie diepte. Het doel waarvoor de transducent in de dagelijkse praktijk in de kliniek wordt gebruikt, bepaalt de grenzen van de afmetingen van de probe en de vorm. Verder dienen de bij de samenstelling van de probe gebruikte materialen niet alleen te voldoen aan electrische veiligheidseisen, maar ook aan klinische, d.w.z. gemakkelijk schoon te maken en niet giftig zijn.

De Hoofdstukken V en VI behandelen verrichte studies naar de invloed van respectievelijk amplitude- en fasefouten op de kwaliteit van de ultrageluidsbundel. In een praktische situatie zal de combinatie van een transducent met de daarbij behorende electronica onderhevig zijn aan variatie in de samenstellende delen, wat bundels oplevert die afwijken van de theoretische. Worden de amplitudefouten voornamelijk veroorzaakt door de variatie in gevoeligheid van de elementen van de transducent zelf, de voornaamste oorzaak van fasefouten is gelegen in het vertragingsgedeelte van de bij de transducent behorende electronica.

In Hoofdstuk V wordt de invloed van de variaties in amplitude over het array behandeld. De ongelijke verdeling van gevoeligheid over de elementen kan de bron zijn van deze variaties. Uit eerder verschenen literatuur is algemeen bekend dat een toename van de amplitudefouten variatie resulteert in een toename van het gemiddeld zijlob niveau. In onze studie introduceren wij de ruimtelijke verdeling van deze fouten als een extra parameter. Aangetoond is dat door de variatie van de amplitudefouten in verband te brengen met het centrale tweede moment van hun verdeling over het array, een meer specifiek criterium kan worden vastgesteld voor de kwaliteit van de gevormde bundel.

In Hoofdstuk VI wordt de invloed van fasefouten op de geluidsbundel behandeld. Eerder verschenen literatuur maakt melding van de effecten van stochastische fasefouten. Echter, de aard van fasefouten in ultrasonische phased arrays is verre van stochastisch, daar ze in de eerste plaats het gevolg zijn van discretisatie van een continue vertragingsfunctie. Als de grootte van de discretisatiestap is gegeven, kan een meest ongunstige spreiding van de fasefouten worden geformuleerd. Sturing en focussering van de bundel leveren voor iedere stuurhoek en focus afstand een typische waarde voor de spreiding. Echter, wanneer de gemeenschappelijke begintijd van elk vertragingskanaal variabel wordt gemaakt, kan deze variantie steeds tot een minimale waarde worden teruggebracht, hetgeen resulteert in een optimale bundel.

Huidige en in de nabije toekomst waarschijnlijke toepassingen in de cardiologie van de transoesofagale phased array transducent kunnen in twee categorieën worden gesplitst: 1) monitoring gedurende operaties met hoog risico en 2) in beeld brengen van het hart en de grote vaten voor diagnostische doeleinden.

In Hoofdstuk VII wordt een haalbaarheidsstudie beschreven ten aanzien van de mogelijkheden van kwantitatieve monitoring geschapen door de kwaliteit van de transoesofagale beelden. Voor deze studie werden video-opnamen geanalyseerd met gebruikmaking van een Kontron beeldverwerkingssysteem. Het uiteindelijk doel van deze beeldverwerking is het automatisch trekken van de inwendige contour van een korte as doorsnede van de linker ventrikel. Als gedurende een hartcyclus een betrouwbare contour gevonden is, kunnen een aantal kwantitatieve parameters, bij voorbeeld oppervlakte van de doorsnede, dynamische oppervlakte-veranderingen, beweging van wandsegmenten, met regelmatige tussenpozen verkregen worden. De bruikbaarheid van de kwantitatieve gegevens hangt sterk af van de betrouwbaarheid van de verkregen contour. Geconcludeerd wordt dat deze de beperkende factor vormt.

De contourdetectie zelf hangt af van een groot aantal parameters voor de beeldverwerkingsalgorithmen, welke ieder voor zich interactief worden geoptimaliseerd door de bediener van het apparaat. Dit is een tijdrovende bezigheid. Voorts vraagt een verandering van het scanvlak vaak aanpassing van deze parameters, wat een nadelig effect heeft op de reproduceerbaarheid van de resultaten. Er dienen krachtiger verwerkingsalgorithmen te worden ontwikkeld om on-line monitoring van patiënten mogelijk te maken met werkelijk automatische beeldanalyse. Niettemin kan de huidige beeldkwaliteit van transoesofagale echocardiografie automatische contouranalyse in de toekomst binnen bereik brengen.

In Hoofdstuk VIII wordt de klinische toepassing van transoesofagale echocardiografie als een aanvullende diagnostische techniek beschreven. De probe, indien aangesloten op een daartoe geschikt electronisch mainframe, kan zowel tweedimensionale echobeelden als een Doppler registratie van de bloedstroom leveren. Dit maakt het mogelijk zowel morfologische als haemodynamische informatie te verkrijgen. Typische problemen die opgelost kunnen worden door transoesofagale echocardiografie na een precordiaal onderzoek zonder succes zijn: pathologie van de atria, de aorta, de mitralis- of aortakleppen, of zelfs aandoeningen van de coronaire hoofdstam. Gedetailleerd haemodynamisch onderzoek kan worden verricht met betrekking tot het linker atrium en het linker ventrikel uitstroom traject, wat bij voorbeeld van groot nut is voor de beoordeling van het functioneren van een kunstklep.

De diagnostische waarde van transoesofagale echocardiografie wordt voorts geïllustreerd aan de hand van een tweetal klinische voorbeelden in Hoofdstuk IX. In het eerste voorbeeld wordt de diagnostische waarde van de transoesofagale onderzoekstechniek naar voren gebracht bij een patiënt met een atriale thrombus. De verkregen beelden leverden een gedetailleerde diagnose, terwijl de precordiale beelden van slechte kwaliteit waren. In het tweede voorbeeld wordt de waarde van transoesofagale echocardiografie voor het te voeren beleid in een kritieke situatie aangetoond. In dit geval kon een ernstige afwijking van de aortakleppen worden vastgesteld, terwijl de patiënt volledig geïnstrumenteerd op de intensive care afdeling lag.

APPENDIX

In Chapter V it is stated that the extreme values for the normalized second central moment of an array with distributed element sensitivities are given by

$$\sigma'_{x\,(min)} = 1 - \frac{3\sigma_a}{2\sqrt{\pi}} \text{ and } \sigma'_{x\,(max)} = 1 + \frac{3\sigma_a}{2\sqrt{\pi}} \qquad [A1]$$

The only assumption needed to obtain this analytical expression, is a monotonous increase or decrease of the sensitivities with respect to the center of the array.

In this Appendix the relation between the standard deviation σ_a of the array sensitivity and the extremes of the normalized second central moment σ'_x of the sensitivity distribution over the array is derived.

The problem here is to relate a particular value of the sensitivity on the array to its coordinate when only the statistical distribution of all sensitivities is given.

In order to obtain an analytical solution it is assumed that, instead of an array of discrete elements, the array is continuous with a tapering of the sensitivity. This assumption enables a definition of the problem in an integral form.

Let the sensitivity (a) be normally distributed with mean $\mu_a = 1$ and variance $\sigma_a{}^2$. Then the probability that a sensitivity X is lower than (a) is defined as

$$\Pr\{X \leqslant a\} = \frac{1}{\sigma_a\sqrt{2\pi}} \int_{-\infty}^{a} e^{-\frac{(t-1)^2}{2\sigma_a{}^2}}\, dt \qquad [A2]$$

Although a negative value for the sensitivity has no physical meaning, it has to be introduced here in order to obtain a general expression.

The second central moment is defined as

$$\sigma_x^2 = \frac{\int_{-1/2\,L}^{1/2\,L} l^2 \cdot a(l)\, dl}{\int_{-1/2\,L}^{1/2\,L} a(l)\, dl} \qquad [A3]$$

where the array is considered to be of length L centered around the origin.

For the uniform distrubition with a = 1 we obtain

$$(\sigma_x^N)^2 = \frac{\int_{-1/2L}^{1/2L} l^2\, dl}{\int_{-1/2L}^{1/2L} dl} = \frac{L^2}{12} \qquad [A4]$$

We have previously defined the normalized second central moment $\sigma_x' = (\sigma_x / \sigma_x^N)^2$, which in combination with [A-3] and [A-4] yields

$$\sigma_x' = \frac{12}{L^3} \int_{-1/2L}^{1/2L} l^2 a\,(l)\, dl \qquad [A5]$$

using

$$\int_{-1/2L}^{1/2L} a\,(l)\, dl = \mu_a \cdot L = L$$

Extreme values for (σ_x') are obtained:

- when $a(l)$ is symmetrical around $L = 0$, i.e. $a(l) = a(-l)$,
- and $a(l)$ is a monotonous function of l for each half of the array.

σ_x' will be maximal when $a(l)$ reaches its maximum value at $l = \pm 1/2\,L$ while $a(l)$ is minimal at $l = 0$ (i.e. dispersion away from the center)
σ_x' will be minimal when $a(l)$ reaches its minimal value at $l = \pm 1/2\,L$ while $a(l)$ is maximal at $l = 0$ (i.e. dispersion towards the center).

As a consequence of this condition $a(l) = a(-l)$ we can redefine expression [A-5]:

$$\sigma_x' = 2 \cdot \frac{12}{L^3} \int_0^{1/2L} l^2 \cdot a\,(l)\, dl \qquad [A6]$$

By defining a normalized sensitivity $s = \frac{a - 1}{\sigma_a \sqrt{2}}$, then $\mu_s = 0$ and variance $\sigma_s^2 = 1/2$, while

$$\Pr\{X \leqslant s\} = \frac{1}{\sqrt{\pi}} \int_{-\infty}^{s} e^{-t^2}\, dt \qquad [A7]$$

In order to write σ_x' as a function of s we have to subsitute $a = 1 + \sqrt{2}, \sigma_a \cdot s$ in [A-6]:

$$\sigma_x' = \frac{24}{L^3} \int_0^{1/2L} l^2 (1 + \sqrt{2} \cdot \sigma_a\, s\,(l) \cdot dl$$

or

$$\sigma_x' = 1 + \frac{24}{L^3} \sqrt{2} \cdot \sigma_a \int_0^{1/2L} l^2\, s\,(l)\, dl \qquad [A8]$$

Here s represents the distribution of $s(l)$ as described by [A-7] and $s(l)$ is a yet unknown function of l for $0 \leqslant l \leqslant 1/2$ L. $s(l)$ is either a monotonously increasing function (associated with σ_x' (max)) or a monotonously decreasing function (associated with σ_x' (min)).

Let α be a variable along the array such that $l = \alpha . 1/2$ L, with $0 \leqslant \alpha \leqslant 1$, then [A8] can be written as

$$\sigma_x' = 1 + 3\sqrt{2}\,\sigma_a \int_0^1 \alpha^2 s(\alpha)\, d\alpha \qquad [A9]$$

Because of its normal distribution s has a probability density function or frequency function

$$f(s) = \frac{1}{\sqrt{\pi}} e^{-s^2} \qquad (A10]$$

which may be associated with the relative area of the array exhibiting the sensitivity s.

We can now formulate the relation between the relative area and the corresponding range of sensitivities

$$\int_0^\alpha dx = c_l \int_{-\infty}^{s(\alpha)} \frac{1}{\sqrt{\pi}} e^{-t^2} dt \qquad [A11]$$

for σ_x' (max)

and

$$\int_0^\alpha dx = c_2 \int_{\infty}^{s(\alpha)} \frac{1}{\sqrt{\pi}} e^{-t^2} dt \qquad [A12]$$

for σ_x' (min)

c_l and c_2 are definted by the boundary conditions $\alpha = 1$, $s(l) = \infty$ respectively $\alpha =$, $s(l) = -\infty$

Expressions [A11] and [A12] result in $c_l = 1$ and $c_2 = -1$.

We obtain a general expression in the form

$$\alpha = \pm \int_{\infty}^{s(\alpha)} \frac{1}{\sqrt{\pi}} e^{-t^2} dt \qquad [A13]$$

or, with

$$\operatorname{erf}(s) = \int_0^s \frac{2}{\sqrt{\pi}} e^{-t^2} dt \qquad [A14]$$

$$\alpha = \pm \frac{1 + \mathrm{erf}(s)}{2} \qquad [A15]$$

and

$$d\alpha = \pm 1/2 \frac{\delta\, \mathrm{erf}(s)}{\delta s} \cdot ds \qquad [A16]$$

Since $\frac{\delta\, \mathrm{erf}(s)}{\delta s} = 2 \cdot \frac{1}{\sqrt{\pi}} e^{-s^2}$

we find that $d\alpha = \pm \frac{1}{\sqrt{\pi}} \cdot e^{-s^2} ds$ [A17]

With the relations [A15] and [A17], the expression for σ_x' in [A9] can be written as a function of s:

$$\sigma_x' = 1 \pm 3\sqrt{2} \cdot \sigma_a \int_{-\infty}^{\infty} \left(\frac{1 + \mathrm{erf}(s)}{2} \right)^2 \cdot s \cdot \frac{1}{\sqrt{\pi}} \cdot e^{-s^2} \cdot ds \qquad [A18]$$

since erf (— s) = — erf (s) [A18] reduces to

$$\sigma_x' = 1 \pm 3\sqrt{2} \cdot \sigma_a \int_{-\infty}^{\infty} 1/4 \cdot 2\, \mathrm{erf}(s) \cdot s \cdot \frac{1}{\sqrt{\pi}} \cdot e^{-s^2} \cdot ds$$

or

$$\sigma_x' = 1 \pm 3\sqrt{2} \cdot \sigma_a \cdot 2 \int_{0}^{\infty} 1/2\, \mathrm{erf}(s) \cdot s \cdot \frac{1}{\sqrt{\pi}} \cdot e^{-s^2} \cdot ds \qquad [A19]$$

Introducing the variable $t = s^2$, [A19] can be written as

$$\sigma_x' = 1 \pm \frac{3}{2} \cdot \frac{\sqrt{2}}{\sqrt{\pi}} \cdot \sigma_a \int_0^{\infty} \mathrm{erf}(\sqrt{t})\, e^{-t} dt \qquad [A20]$$

According to the Handbook of Mathematical Functions (1) 7.4.19:

$$\int_0^{\infty} \mathrm{erf}(\sqrt{t})\, e^{-t} \cdot dt = \frac{1}{\sqrt{2}}$$

We therefore obtain the relation between the extremes of σ_x' and σ_a as

$$\sigma_{x'(max)} = 1 + \frac{3}{2} \cdot \frac{\sigma_a}{\sqrt{\pi}} \qquad [A21A]$$

and

$$\sigma_{x'(min)} = 1 - \frac{3}{2} \cdot \frac{\sigma_a}{\sqrt{\pi}} \qquad [A21B]$$

For a given σ_a the possible range of σ_x' can be expressed as

$$1 - \frac{3}{2}\frac{\sigma_a}{\sqrt{\pi}} \leqslant \sigma_x' \leqslant 1 + \frac{3}{2}\frac{\sigma_a}{\sqrt{\pi}} \qquad \text{[A22]}$$

The extreme values of σ_x' as given in Table V-2 are in good agreement with the range given by [A22].

REFERENCE

1. *Handbook of Mathematical Functions (Abramowitz M and Stegun IA, eds) National Bureau of Standards Applied Mathematic Series No. 55, NBS, Washington DC, 1967.*

CURRICULUM VITAE

Charles Theodoor Lancée is geboren te Haarlem op 19 oktober 1944. Hij volgde het lager onderwijs van 1950 tot 1956 in achtereenvolgens: Tandjung, Balikpapan, Tarakan, Utrecht, Sanga-sanga, Balikpapan en Badjubang. Voor het volgen van middelbaar onderwijs keerde hij terug naar Nederland, alwaar hij in Utrecht de HBS-B opleiding volgde op eerst de Gemeentelijke HBS en later de Rijks HBS. In 1961 volgde het eindexamenjaar op het Rembrandt Lyceum te Leiden. Na gedurende een jaar onderwijs te hebben gevolgd aan de HTS te Haarlem, afdeling Elektrotechniek, volgde in 1963 de definitieve keuze voor een opleiding aan de TH in Delft. Hier werd in 1965 de propaedeuse afgerond en tevens het student-assistentschap aanvaard bij de afdeling Meettechniek. In 1967, na het behalen van het kandidaatsexamen, koos hij voor de toen nieuwe afstudeerrichting Medische Elektrotechniek op het Laboratorium voor Meettechniek.

In 1968 werden contacten gelegd met de Medische Faculteit in oprichting van de Erasmus Universiteit Rotterdam, welke resulteerden in een afstudeeropdracht voor Professor Nauta: een implanteerbare en flexibele electromagnetische bloedstroommeter. In 1969 werd het student-assistentschap in Delft omgeruild voor eenzelfde aanstelling bij de Erasmus Universiteit om de afdeling Experimentele Echocardiografie van het Thoraxcentrum te helpen oprichten.

In 1970 werd het ingenieursdiploma behaald en volgde een definitieve aanstelling aan de Erasmus Universiteit, op de eerdergenoemde afdeling Experimentele Echocardiografie.

In 1973 wordt hij tevens voor enkele jaren aangesteld als leraar van de avond-HTS in Den Haag, voor de cursus Meet- en Regeltechniek.

Vanaf 1975 tot heden is hij redacteur van het wetenschappelijke tijdschrift "Ultrasonoor Bulletin" van de Nederlandse Vereniging voor Ultrageluid in de Geneeskunde en de Biologie. Vanaf 1984 is hij voorzitter van laatstgenoemde vereniging.

PUBLICATIONS OF THE AUTHOR

N. Bom, C.T. Lancée, G. van Zwieten (1971) Calibration of an Ultrasound Sensor, Ultrasonics 71 Conference Papers: 73.

N. Bom, C.T. Lancée, J. Honkoop, P.G. Hugenholtz (1971) Ultrasonic viewer for cross-sectional analysis of moving cardiac structures, Bio-Medical Engineering 6 (11): 500-508.

N. Bom, C.T. Lancée, F.C. van Egmond (1972) An ultrasonic intracardiac scanner, Ultrasonics 10: 72-76.

N. Bom and C.T. Lancée (1972) Algemene Inleiding tot de Echografie. Het Ingenieursblad 3: 3-6.

N. Bom and C.T. Lancée (1972) A Non-Invasive System for Two-dimensional instantaneous Observation of moving cardiac Structures, The Third International Conference on Medical Physics, including Medical Engineering, Chalmers University of Technology, Goteborg, Sweden: 35.5.

J. Roelandt, F. Kloster, F.J. ten Kate, N. Bom, C.T. Lancée, P.G. Hugenholtz (1973) Multiscan Echocardiography, Description of the System and Initial Results in 100 patients, Hart Bulletin 4: 51-56.

N. Bom, C.T. Lancée, G. van Zwieten, F.E. Kloster, J. Roelandt (1973) Multiscan Echocardiopgraphy Part 1: Technical Description, Circulation XLVIII: 1066-1074.

N. Bom, C.T. Lancée, J. Roelandt, F.C. van Egmond (1973) Two Multi-Element Systems for Real Time Cross-sectional Analysis of the Heart, Ultrasonics Symposium Proceedings IEEE Cat//73 CHO 807-8SU.

C.T. Lancée, N. Bom (1974) On the Design of a Multi-Element Acoustic Transducer, Nederlands Akoestisch Genootschap Publ 26.

N. Bom, J. Roelandt, C.T. Lancée (1974) Analysis of the Heart with Ultrasound, Nederlands Akoestisch Genootschap Publ 26.

N. Bom, J. Roelandt, F.E. Kloster, C.T. Lancée, P.G. Hugenholtz (1974) Multi-Element System and its Application to Cardiology, Proceedings of the Second World Congress on Ultrasonics in Medicine (June 1973) Excerpta Medica I.C.S. 309 Amsterdam.

N. Bom, C. Ligtvoet, C.T. Lancée, J. Roelandt (1974) Echocardiographic Information Recording and Display of Real-Time Cross-Sectional Echograms, Proceedings of the NATO Advanced Study Institute on Ultrasonic Diagnostics, Milan, June 1974 Plenum Publishing Co., London.

C.T. Lancée, N. Bom, H.H. Rijndorp (1975) Construction of a Circular Ultrasonic Array with Miniature Elements for Cardiac Application. Proceedings of the 2nd European Congress in Ultrasonics in Medicine, 12-16 May 1975, Excerpta Medica, Amsterdam.

N. Bom, C.T. Lancée, J. Ridder, C. Ligtvoet, J. Roelandt (1976) The Technology of Miniature Acoustic Element Arrays. Proceedings of the Conference on Cardiovascular Imaging and Image Processing. Society of Photo-optical Instrumentation Engineers: 11-15.

C.T. Lancée, N. Bom (1977) Some signal processing aspects in medical ultrasound. In: Aspects of Signal Processing, Proceedings of the NATO Advanced Studies Institute, Portovenere, La Spezia, Italy. G. Tacconi (Ed) Reidel Publishing Co., Dordrecht-Boston: 649-657.

N. Bom, F. Hagemeijer, C.T. Lancée, J. Roelandt, C. Ligtvoet, J.A. Vogel (1977) Two-dimensional Real-Time Echocardiography. In: Recent Advances in Ultrasound and Biomedicine, D. White (Ed): 203-216.

C.M. Ligtvoet, J. Ridder, C.T. Lancée, F. Hagemeijer, W.B. Vletter (1977) A dynamically focused multiscan system. In: Echocardiology, N. Bom (Ed) Martinus Nijhoff Publishers, The Hague-Boston-London: 313-324.

N. Bom, C.T. Lancée (1978) Echocardiografie, Natuurkundige Voordrachten, Nieuwe Reeks 54: 129-138. W.P. van Stockum & Zn, The Hague.

P.D. Verdouw, C.T. Lancée, X.H. Krauss, P.G. Hugenholtz (1978) New invasive techniques in cardiology: multiple sensors. In: Cardiovascular System Dynamics, J. Baan, A. Noordergraaf and J. Raines (Eds). The MIT Press, Cambridge (Mass.)/London: 543-552.

P.G. Hugenholtz, J.R.T. Roelandt, N. Bom, C.T. Lancée (1978) Current status of echocardiology. In: Developments in Cardiovascular Medicine, C.J. Dickinson and J. Marks (Eds.) MTP Press Limited: 15-28.

N. Bom, C.T. Lancée, C.M. Ligtvoet (1979) Improvement of lateral resolution in ultrasonic systems. Acta Med Scand Suppl 627: 41-47.

J. Vogel, N. Bom, J. Ridder, C. Lancée (1979) Transducer design considerations in dynamic focusing, Ultrasound Med & Biol 5: 187-193.

C.T. Lancée (Ed) (1979) Echocardiology, Proceedings of the 3rd Symposium on Echocardiology, Rotterdam. Martinus Nijhoff Publishers, The Hague-Boston-London.

N. Bom, C.T. Lancée (1979) Current Instrumentation. In: Echocardiology, C.T. Lancée (Ed), Martinus Nijhoff Publishers, The Hague-Boston-London: 373-384.

N. Bom, C.T. Lancée (1980) New Techniques. In: Progress in Medical Ultrasound Vol 1, A. Kurjak (Ed) Excerpta Medica, Amsterdam-Oxford-Princeton: 19-33.

R.S. Meltzer, O.E.H. Sartorius, C.T. Lancée, P.W. Serruys, P.D. Verdouw, C.E. Essed, J. Roelandt (1981) Transmission of ultrasonic contrast through the lungs. Ultrasound Med & Biol 7 (4): 377-384.

O.L. Bastiaans, R.S. Meltzer, P.W. Serruys, C.T. Lancée (1981) Verdunningscurves voor echocontrastmateriaal uit 2D-echografie. Ultrasonoor Bulletin: 5-10.

C.T. Lancée, J.A. Blom (1981) M-mode scanning with automatic gain control. In: Echocardiology H. Rijsterborgh, (Ed.) Martinus Nijhoff Publishers, The Hague-Boston-London: 433-441.

N. Bom, C.T. Lancée (1981) New Techniques. In: Progress in Medical Ultrasound 2, A. Kurjak (Ed.). Excerpta Medica, Amsterdam/Oxford/Princeton: 5-17.

N. Bom, C.T. Lancée, C. Ligtvoet, J. Roelandt (1982) Physical Limitations of Echocardiography. Practical Cardiology 8 (3): 133-163.

C.T. Lancée, C.M. Ligtvoet, N. de Jong (1982) On the design and construction of a transesophageal scanner. In: Cardiovascular Diagnosis by Ultrasound, P. Hanrath, W. Bleifeld, J. Souquet (Eds), Martinus Nijhoff Publishers, The Hague-Boston-London: 260-269.

R.S. Meltzer, C.T. Lancée, J. Roelandt (1982) Transmission of echocardiographic contrast through the lungs. In: Contrast Echocardiography, R.S. Meltzer and J. Roelandt (Eds.). Martinus Nijhoff Publishers, The Hague-Boston-London: 304-312.

R.S. Meltzer, C.T. Lancée, G.R. Swart, J. Roelandt (1982) 'Spontaneous' echo contrast on the right side of the heart. J Clin Ultrasound 10: 240-242.

R.S. Meltzer, J. Roelandt, O.L. Bastiaans, L. Piérard, P.W. Serruys, C.T. Lancée (1982) Videodensitometric processing of contrast two-dimensional and echocardiographic data. Ultrasound Med & Biol 8: 509-14.

R.S. Meltzer, B. Diebold, N.K. Valk, D. Blanchard, J.-L. Guermonprez, C.T. Lancée, P. Peronneau, J. Roelandt (1983) Correlation between velocity measurements from Doppler echocardiography and from M-mode contrast echocardiography. Br Heart J 49: 244-249..

C.T. Lancée, J. Souquet, H. Ohigashi, N. Bom (1985) Transducers in medical ultrasound I: Ferro-electric ceramics versus polymer piezoelectric materials. Ultrasonics 23: 138-142.

N. de Jong, C.T. Lancée, W.J. Gussenhoven, N. Bom, C.M. Ligtvoet (1985) Transesophageal Echocardiography. Med & Biol Engineering & Computing 23 (Supp I): 204-205.

N. Bom, C.T. Lancée, J.W. Wladimiroff (1985) Heeft ultrageluid neveneffecten? Ned Tijdschr Geneesk 129 (45): 1150-2154.

N. de Jong, C.T. Lancée, W.J. Gussenhoven, N. Bom, C.M. Ligtvoet (1985) Transoesofagale echocardiografie. Ultrasonoor Bulletin: 28-31.

N. Bom, C.T. Lancée, N. de Jong, C.M. Ligtvoet (1985) Diagnostic ultrasound: History, transducers, artefacts and new applications. In: Acoustical Imaging 14, A.J. Berkhout, J. Ridder, L.F. van der Wal (Eds.) Plenum Press, New York/London: 397-403.

C.T. Lancée, R. Daigle, D.J. Sahn, J.M. Thijssen (1985) Transducers in Medical Ultrasound III: Transducer applications in cardiology. Ultrasonics 23: 199-205.

N. de Jong, N. Bom, C.T. Lancée (1986) Esophageal echocardiography. In: IEEE/Eighth Annual Conference of the Engineering in Medicine and Biology Society, G.V. Kondraske and C.J. Robinson (Eds.): 3-6.

C.T. Lancée, J.M. Vissers, S. Mientki, C.M. Ligtvoet, N. Bom (1987) Influence of amplitude errors on beam-steered phased arrays. Ultrasonics 25: 147-153.

C.T. Lancée, J.M. Vissers, S. Mientki, C.M. Ligtvoet, N. Bom (1987) Influence of phase errors on beam-steered phased arrays. Ultrasonics 25: 154-159.

M.A. Taams, W.J. Gussenhoven, C.T. Lancée (1987) Left artrial vascularized trombus diagnosed by transoesophageal two-dimensional echocardiography. Br Heart J (accepted for publication).

R.J. van Suylen, W.J. Gussenhoven, C.T. Lancée, C.E. Essed, J.R.T.C. Roelandt, M. Simoons, E. Bos (1987) Relatie tussen echocardiografische en anatomische metingen van de linker ventrikel wanddikte. Ultrasonoor Bulletin (accepted for publication).

N. de Jong, A. den Ouden, J.F. Brinkman, R. Niesing, C.T. Lancée, N. Bom (1987) A multiwire saw for the production of ultrasound transducers. J Phys E (Accepted for publication).

C.T. Lancée, N. de Jong, N. Bom (1987) Design and construction of an esophageal phased array probe. Submitted for publication to Med Prog Technol.

C.T. Lancée, H. Rijsterborgh, N. Bom (1987) Monitoring aspects of an ultrasonic esophageal transducer. Submitted for publication to Med Prog Technol.

J.M. Thijssen, W.T. van Beekum, O. Daniëls, C.W. Koch, C.T. Lancée, J.C. Somer, M. de Vlieger, J.W. Wladimiroff (1987) Diagnostic ultrasound equipment: safety and dosimetry. Submitted for publication to Eur J Radiol.